Theoretical Study on Complex Chemical Reaction Systems: Development of Methodology and Its Applications

（複合化学反応系に関する理論的研究：方法論の開発とその適用）

Yuichi Suzuki

Contents

Chapter 1

General Introduction

1.1. Introduction

It is well-known that most phenomena of materials occur through complex transformation mechanisms, generally accompanied with various chemical reactions [1-3]. When focusing on each chemical reaction, it is recognized as a process in which one or more kinds of substances, called reactants, are converted to new kinds of substances with different compositions, called products [1]. From the macroscopic point of view, the process tends to transfer towards a dynamic equilibrium in which both reactants and produces are present but show no further tendency to undergo net change [1-3]. Moreover, it can be understood that most chemical reactions proceed in a reaction mechanism consisting of a number of elementary steps, called elementary reactions, that might occur successively and/or simultaneously [1-3]. Thus, throughout this thesis, I define “complex chemical reaction” as a chemical phenomenon in which an initial state reaches to chemical equilibrium or nonequilibrium steady state by a succession of the elementary reactions.

In modern chemistry, many experimental techniques and methods have been developed to clarify the static chemical properties of substances and the dynamic physicochemical properties of their formation processes in the chemical phenomena (or complex chemical reactions) [1-11]. For investigating the former static properties, there are typical methods such as X-ray photoelectron spectroscopy (XPS), Rutherford

backscattering spectrometry (RBS), transmission electron microscopy (TEM), atomic force microscopy (AFM) and positron annihilation lifetime spectroscopy (PALS) [1-8]. On the other hand, to monitor the latter dynamic properties in time domain, there are typical methods such as flow method, stopped-flow technique, flash photolysis, in situ X-ray diffraction and in situ FTIR reflection spectroscopy [1-3,9-11]. However, in many cases, it would be impossible to completely clarify both properties even by such experimental approaches, thus meaning that an alternative and advanced tool is strongly required.

Under the circumstances, computational simulation has become a powerful methodology [12-17] that is not only complementary to experimental approaches but also essential for investigating the chemical phenomena microscopically. As its basic methodologies, Monte Carlo (MC) method, molecular mechanics (MM) method, molecular dynamics (MD) method and quantum mechanics (QM) method are widely used [18-21]. Based on these methods, many useful computational methodologies such as QM/MM method, Car-Parrinello (CP) MD method, density functional theory (DFT) method and reactive force field (ReaxFF) method have been newly developed to deal with various chemical phenomena [15,22-24]. Even though such methodologies are available, there are few methods capable to simulate complex chemical reactions, explicitly treating the dynamic motion of each atom in the whole molecular system [12-15]. In general, the main problem would be in the limited computational resource, which makes it impossible to realize the computational simulations in full space-time scale comparable to the actual one of real molecular systems.

In this thesis, towards realizing plausible computational treatment of complex chemical reactions, I propose a new method as a practical “atomistic” simulation even

in the limited computational resources. This method consists of a couple of conventional molecular simulation methods of MC and MD techniques, so that I call it the hybrid MC/MD reaction method. Then, the hybrid MC/MD reaction method enables us to construct full atomistic models for any types of chemical components, simulating a succession of the elementary reactions, i.e., complex chemical reaction. In particular, it would be quite meaningful to apply it to typical three chemical reaction systems in which racemization or polymerization reactions occur. In the former system, a stereo-specific characteristic is observed whereas, in the latter two systems, a complex aggregation structure is analyzed. In the hybrid MC/MD reaction simulation, the "atomistic" structural complexity and flexibility of all molecules in those systems can be considered conserved as they are really generated during the real chemical reactions. For that reason, the present method would make it possible to microscopically provide their static and dynamic properties that cannot be observed only by the experimental approaches. Namely, the new possible frontiers must lead to the insight into clearly understanding a whole of unknown chemical phenomena in the atomistic scale.

1.2. Conventional Methods of Molecular Simulation

To introduce a new molecular simulation method, i.e., hybrid MC/MD reaction method, the algorithms of two conventional methods of molecular simulation, i.e., MC and MD methods, are briefly explained [25-27]. Molecular simulation is required to be necessarily compatible with statistical mechanics so that it could adequately determine

macroscopic properties and be used to construct a theoretical model significantly enough.

In an MC method, a number of different trial configurations are generated at random during the simulation. The intermolecular (and intramolecular) interactions in the trial configuration are evaluated, and then probabilities are calculated and used to either accept or reject the configuration change. On the other hand, in an MD method, the equations of motion for the system of molecules are solved. The molecular coordinates and momenta change in accordance with the total intermolecular (and intramolecular) forces for the individual molecules.

Although either MC or MD can be used usually to obtain equilibrium properties, MD simulation enables us to clarify the dynamic properties of the system. Another important distinction between MC and MD methods is that the former involves primarily the calculation of changes in intermolecular energy (including intramolecular one) whereas the latter uses intermolecular (and intramolecular) forces to evolve the system.

1.2.1. Numerical Evaluation of Thermodynamic Quantities

Any thermodynamic quantity $A(\mathbf{r}^N)$ can be described by such a configuration $\mathbf{r}^N$ that is a $3N$ dimensional Cartesian coordinate vector of the N particles (or molecules) in the system, i.e., $\mathbf{r}^N \equiv (\mathbf{r}_1, \mathbf{r}_2, \mathbf{r}_3, \cdots, \mathbf{r}_N)$. The average $\langle A(\mathbf{r}^N) \rangle$ observed macroscopically can be evaluated by the multidimensional integral over the $3N$ degrees of freedom,

$$\left\langle A\left(\mathbf{r}^N\right)\right\rangle = \int A\left(\mathbf{r}^N\right)\rho\left(\mathbf{r}^N\right)\mathrm{d}\mathbf{r}^N \tag{1.1}$$

where $\rho\left(\mathbf{r}^N\right)$ is the probability (density) of obtaining a configuration $\mathbf{r}^N$, which is expressed by the potential energy *E* of the configuration as follows:

$$\rho\left(\mathbf{r}^N\right) = \frac{\exp\left[-\beta E\left(\mathbf{r}^N\right)\right]}{\int \exp\left[-\beta E\left(\mathbf{r}^N\right)\right]\mathrm{d}\mathbf{r}^N} \tag{1.2}$$

where β is defined by $\beta = 1/k_{\mathrm{B}}T$ with the Boltzmann constant k_{B} and temperature *T*. Because these integrals cannot be analytically estimated, the strategy for solution in MC and MD algorithms is to generate a large number of different configurations $\left\{\mathbf{r}_I^N \middle| I = 1,2,\cdots,M\right\}$ where *M* is the total number of configurations generated and to evaluate the integrations as summations over a finite number of configurations. In case that the configuration are randomly generated, Eq. (1.1) is described as

$$\left\langle A\left(\mathbf{r}^N\right)\right\rangle = \frac{\sum_{I=1}^{M} A\left(\mathbf{r}_I^N\right)\exp\left[-\beta E\left(\mathbf{r}_I^N\right)\right]}{\sum_{I=1}^{M}\exp\left[-\beta E\left(\mathbf{r}_I^N\right)\right]} \equiv \frac{1}{M}\sum_{I=1}^{M} A\left(\mathbf{r}_I^N\right). \tag{1.3}$$

In general, it is usual that most of configurations $\mathbf{r}_I^N$ with $E\left(\mathbf{r}_I^N\right)$ result in relatively quite small Boltzmann factors that lead to make very little contribution to the average. It is, therefore, required to generate an extremely large number of configurations in order to obtain statistically significant average properties.

1.2.2. Monte Carlo (MC) Method

Towards effective sampling to evaluate $\left\langle A\left(\mathbf{r}^N\right)\right\rangle$ by using Eq. (1.3), stochastic treatments, i.e., Monte Carlo (MC) treatments, are introduced to obtain the

configurations that make the most significant contribution to $A(\mathbf{r}^N)$. Among these treatments, the sampling method of Metropolis algorithm [25-28] biases the generation of configurations according to a relative probability of $\exp\left[-\beta E(\mathbf{r}^N)\right]$ and counts each of them equally. In contrast, simple MC iterations inefficiently generate those configurations with small probabilities.

Metropolis sampling produces a Markov chain which satisfies the two conditions: (i) the state of each trial depends only on the preceding trial (or the previous state), and (ii) each trial belongs to a finite set of possible states. Metropolis et al. [28] showed that a transition probability matrix π_{ij} ensures Eq. (1.2), obeyed to

$$\begin{cases} \pi_{ij} = C_{ij} & \rho_j/\rho_i \geq 1,\ i \neq j \\ \pi_{ij} = C_{ij}\left(\rho_j/\rho_i\right) & \rho_j/\rho_i < 1,\ i \neq j \end{cases} \tag{1.4}$$

where ρ_i and ρ_i are the probability densities obtained by Eq. (1.2) for states *i* and *j*, respectively, and C_{ij} is the conditional probability of choosing a trial state *j* from the state *i*. Furthermore, the following relational expressions are assumed:

$$\sum_j \pi_{ij} = 1, \tag{1.5}$$

$$\rho_i \pi_{ij} = \rho_j \pi_{ji}, \tag{1.6}$$

and then,

$$\pi_{ij}/\pi_{ji} = \rho_j/\rho_i = \exp\left[-\beta\left(E_j - E_i\right)\right] \equiv \exp\left[-\beta \Delta E_{ij}\right], \tag{1.7}$$

where E_i and E_j are the energies of the states *i* and *j*, respectively.

The procedure in the Metropolis scheme is to generate a trial state and determine the energy difference ΔE_{ij}. If $\Delta E_{ij} < 0$ that is $\rho_j/\rho_i > 1$, the move is accepted,

otherwise, if $\Delta E_{ij} \geq 0$ that is $\rho_j / \rho_i \leq 1$, the move is judged according to a probability of $\rho_j / \rho_i = \exp\left(-\beta \Delta E_{ij}\right)$. In the latter condition, a uniform random number *R* between 0 and 1 is generated and then the move is accepted if $\exp\left(-\beta \Delta E_{ij}\right) \geq R$, otherwise rejected.

In summary, the transition probability of acceptance is typically defined as:

$$W_{i \to j} = \min\left[1,\ \exp\left(-\beta \Delta E_{ij}\right)\right]. \tag{1.8}$$

Thus, by iterative transitions between the states, the Metropolis sampling method enables us to obtain thermodynamic properties or generate different ensembles.

1.2.3. Molecular Dynamics (MD) Method

The force experienced by a particle during displacement in MD algorithm is obtained by Newton's second law of motion. Then, the force $\mathbf{F}_i$ acting on the particle *i* with mass m_i is connected to the following second derivative of Cartesian coordinate vector $\mathbf{r}_i$ of the particle *i* with respect to time *t*:

$$\mathbf{F}_i = m_i \frac{\mathrm{d}^2 \mathbf{r}_i(t)}{\mathrm{d}t^2}. \tag{1.9}$$

In general, the evolution of $\mathbf{r}_i(t)$ with time can be estimated from the Taylor series expansion:

$$\mathbf{r}_i(t + \Delta t) = \mathbf{r}_i(t) + \frac{\mathrm{d}\mathbf{r}_i}{\mathrm{d}t} \Delta t + \frac{1}{2!} \frac{\mathrm{d}^2 \mathbf{r}_i}{\mathrm{d}t^2} \Delta t^2 + \cdots, \tag{1.10}$$

which presents the basis of the 'finite difference' approach that is commonly used to solve ordinary differential equations such as Eq. (1.9). By using Eq. (1.10) in which

Δt^3 and higher are neglected, Eq. (1.9) becomes:

$$\mathbf{r}_i\left(t+\Delta t\right)=\mathbf{r}_i\left(t\right)+\mathbf{v}_i\left(t\right)\Delta t+\frac{\mathbf{F}_i\left(t\right)}{2m_i}\Delta t^2, \tag{1.11}$$

where the second term of RHS in Eq. (1.10) is described by the velocity vector $\mathbf{v}_i\left(t\right)$. Accordingly, the particle's Cartesian coordinates $\mathbf{r}_i\left(t+\Delta t\right)$ at a later time $t+\Delta t$ after the time duration Δt passes can be evaluated by using the information of the Cartesian coordinates, their conjugate velocities and forces at the time *t*.

Subsequently, $\mathbf{F}_i$ is calculated by the first derivative of the potential energy $V\left(\mathbf{r}^N\right)$ depending on $\mathbf{r}^N$ with respect to $\mathbf{r}_i$:

$$\mathbf{F}_i=-\nabla_i V\left(\mathbf{r}^N\right)=-\frac{\partial}{\partial \mathbf{r}_i}V\left(\mathbf{r}^N\right). \tag{1.12}$$

The potential energy describes the interaction energy of the whole system that consists of a number of individual molecules so as to be able to express all the different types of interactions, whichever the intramolecular or intermolecular interaction might be. The former corresponds to the bond, angle and torsional potentials, whereas the latter is related to the repulsion and dispersion (Lennard-Jones potential), and electrostatic interactions among effective charges.

If Eq. (1.9) can be solved even numerically integrated approximately by such as Eq. (1.11), the dynamics of the system can be simulated iteratively by calculating particles' displacements in time interval Δt. Furthermore, an equilibrium thermodynamic quantity similarly as in the MC treatment (subsection 1.2.2) can be estimated by using Eq. (1.9) after the system reaches an equilibrium state. Additionally, some dynamic quantities of the system can also be calculated by MD simulation.

1.3. A New Molecular Simulation Method: Hybrid MC/MD Reaction Method

Each elementary step (or elementary reaction) in a reaction mechanism in complex chemical reaction system is often expressed as a transition between two certain wells defined as stable regions in phase space over an activation barrier [1-3]. Most complex chemical reaction systems spend the overwhelming majority of their time in the stable regions in phase space [15,29,30]. Accordingly, the transition typically rarely occur as infrequent activated events of short durations [15,29,30]. Therefore, the conventional methods of molecular simulation such as MC and MD techniques (subsection 1.2.2 and 1.2.3) cannot be applied straightforwardly to complex chemical reaction systems.

In order to generate plausible states of phase space in chemical equilibrium, it is possible in computationally efficient way to make transitions of the whole system between relatively stable regions in the phase space, and to apply a stochastic approach to judge whether the state after a rare transition occurrence might be adopted. Based on that concept, I utilize both conventional methods, MC and MD methods, to treat complex chemical reaction systems, taking each methodological characteristic into consideration (see subsection 1.2). In MC method, the Metropolis sampling scheme, Eq. (1.8), is introduced to stochastically treat the transitions accompanied with chemical reaction occurrence. On the other hand, in MD method, e.g., Eq. (1.11), a plausible molecular configuration in the stable regions for the reaction occurrence is naturally explored by tracing the dynamical process of the system.

Such hybrid methodology of MC and MD treatments, i.e., hybrid MC/MD reaction method, is able to address the question of the computation of rare event-related

processes occurring in a complex chemical reaction system, keeping the “atomistic” complexity and flexibility of reactive molecules as they really are. This new method of molecular simulation provides an independent alternative class to the commonly applied reaction methods [31-34]. Although creation of a new molecule brings a change in the number of molecules in traditional methods, the present framework does not violate the conservation of the number of atoms. Furthermore, it is not necessary to follow the transition processes accurately from reactants to products with high computational cost because of adopting the present stochastic approach for the transitions for reaction occurrence. The details of the present methodology are shown in chapter 2.

1.4. Thesis Outline

In the present thesis, in order to make it possible to computationally clarify chemical phenomena in complex chemical reaction systems at the atomistic level, I start in chapter 2 to propose a new method, the hybrid MC/MD reaction method, consisting of a couple of MC and MD treatment. Then, it is shown that the method can successfully reproduce some experimental results for four different complex reaction systems in chapter 2, 3, 4 and 5, respectively. In addition, in chapter 5, I propose a theory to estimate an effective time for the system generated stochastically from an initially prepared state to an equilibrium one, using substance concentrations obtained by the hybrid MC/MD reaction simulation.

More precisely, in chapter 2, after introducing the hybrid MC/MD reaction method, I target, for the first demonstration, 2-chlorobutane racemization in *N*,*N*-dimethylformamide (DMF) solution [35-37]. Then, I show how this method would realize, from the optical pure state (100% e.e.) of (*R*)-2chlorobutane molecules, a state

with ~0% e.e. that is the expected purity of (*R*)- to (*S*)-enantiomers of the racemic mixture in chemical equilibrium. In addition, I represent an interesting computational observation and touch a promising possibility of the hybrid MC/MD reaction method in the study of various properties of aggregation structure in chemical reaction systems and their stereo-chemistry.

In chapter 3, I investigate the microscopic characteristic of the aromatic polyamide used as a reverse osmosis (RO) membrane, called FT-30, in industrial materials [38]. The polymer membrane FT-30 is experimentally formed by the two constituent monomers, *m*-phenylenediamine (MPD) and 1,3,5-tricarboxylic acid chloride (TMC) [38]. Starting with the monomer model systems with the different MPD/TMC mixing ratios (1:4, 1:1, 3:2 and 4:1), the four membrane models of the FT-30 by the hybrid MC/MD reaction simulations, are compared with the experimental results [39] to show that the near-surface (NS) and interior active (IA) regions of FT-30 membrane are formed with the MPD/TMC mixing ratio of 1:4 and 1:1, respectively.

In addition to RO membrane used industrially, in chapter 4, I investigate the formation processes and microscopic properties of the solid electrolyte interphase (SEI) film on the anode surfaces in lithium ion batteries (LIBs). The performance of current LIB with liquid electrolytes such as ethylene carbonate (EC) and propylene carbonate (PC) is strongly dependent on the formation of a stable SEI film [40-42]. Thus, I apply the hybrid MC/MD reaction method to the EC- and PC-based electrolyte systems in which some important elementary reactions are assumed to occur. Then, I show a microscopic origin of the stability difference inbetween these SEI films despite the structural similarity of EC and PC.

In chapter 5, on the basis of the theory of chemical kinetics, I examine an interesting trial to introduce a notion of "time" to interpret "MC/MD cycle" in the hybrid MC/MD reaction method as an effective time. The MC/MD cycle is a computational procedure consisting of several steps to deal with chemical reaction. As an example, I take a gas reaction system in which the reversible second-order reaction $H_2+I_2 \rightleftharpoons 2HI$ occurs [1-3]. After showing the realization of chemical equilibrium states of the system consistent to the experimentally report [3], I apply the theory of correspondence between the effective time and the MC/MD cycle to the system, and then estimate the half-life τ of $[H_2]$.

In chapter 6, the general conclusion is provided including future perspectives.

References

[1] R. H. Petrucci, W. S. Harwood, G. E. Herring, J. Madura, GENERAL CHEMISTRY: Principles and Modern Application, 9th ed.; Prentice-Hall, Inc.: New Jersey, 2006.

[2] P. Atkins, J. de Paula, Atkins' Physical Chemistry, 9th ed.; Oxford University Press: Oxford, 2009.

[3] W. J. Moore, BASIC PHYSICAL CHEMISTRY; Prentice-Hall, Inc.: New Jersey, 1983.

[4] C. D. Wagner, W. M. Riggs, L. E. Davis, J. F. Moulder, G. E. Muilenberg, Handbook of X-ray Photoelectron Spectroscopy; Perkin-Elmer: Eden Prairie, Minnesota, 1978.

[5] W. K. Chu, J. W. Mayer, M. A. Nicollet, Backscattering Spectroscopy; Academic Press: New York, 1978.

[6] D. B. Williams, C. B. Carter, Transmission Electron Microscopy; Plenum Press: New York, 1996.

[7] G. Binnig, C. F. Quate, C. Gerber, Phys. Rev. Lett., 56 (1986) 930.

[8] Y.C. Jean, Microchem. J. 42 (1990) 72.

[9] T. Friščić, I. Halasz, P. J. Beldon, A. M. Belenguer, F. Adams, S. A. J. Kimber, V. Honkimäki, R. E. Dinnebier, Nat. Chem. 5 (2013) 66.

[10] A. V. Hesketh, S. Nowicki, K. Baxter, R. L. Stoddard, J. S. McIndoe, Organometallics 34 (2015) 3816.

[11] G. X. Chen, C. F. Xu, X. Q. Huang, J. Y. Ye, L. Gu, G. Li, Z. C. Tang, B. H. Wu, H. Y. Yang, Z. P. Zhao, Z. Y. Zhou, G. Fu, N. F. Zheng, Nat. Mater. 16 (2016) 564.

[12] E. Harder, D. E. Walters, Y. D. Bodnar, R. S. Faibish, B. Roux, J. Phys. Chem. B 113 (2009) 10177.

[13] Y. Luo, E. Harder, R. S. Faibish, B. Roux, J. Membr. Sci. 384 (2011) 1.

[14] K. Moorthi, K. Kamio, J. Ramos, D. N. Theodorou, AIP Conf. Proc. 1518 (2013) 455.

[15] A. C. T. van Duin, S. Dasgupta, F. Lorant, W. A. Goddard III, J. Phys. Chem. A 105 (2001) 9396.

[16] Z. E. Hughes, J. D. J. Gale, Mater. Chem. 20 (2010) 7788.

[17] Z. E. Hughes, J. D. J. Gale, Mater. Chem. 22 (2012) 175.

[18] R. Y. Rubinstein, Simulation and the Monte Carlo method; Wiley: New York, 1981.

[19] U. Burkert, N. L. Allinger, Molecular Mechanics; American Chemical Society: Washington, 1982.

[20] A. Rahman, F. H. Stillinger, J. Chem. Phys. 55 (1971) 169.

[21] R. P. Feynman, A. R. Hibbs, Quantum Mechanics and Path Integrals; McGraw-

Hill: New York, 1964.

[22] A. Warshel, M. Levitt, J. Mol. Biol. 103 (1976) 227.

[23] R. Car, M. Parrinello, Phys. Rev. Lett. 55 (1985) 2471.

[24] R. G. Parr, W. Yang, Density-Functional Theory of Atoms and Molecules; Oxford University Press: Oxford, 1989.

[25] M. P. Allen, D. J. Tildsley, Computer Simulation of Liquids; Clarendon Press: Oxford, 1987.

[26] D. Frenkel, B. Smit, Understanding Molecular Simulations: From Algorithm to Applications; Academic Press: San Diego, 2002.

[27] R. J. Sadus, Molecular Simulation of Fluids, 1st ed., Elsevier, Netherlands, 1999.

[28] N. Metropolis, A. W. Rosenbluth, M. N. Rosenbluth, A. H. Teller, E. Teller, J. Chem. Phys. 21 (1953) 1087.

[29] E. K. Grimmelmann, J. C. Tully, E. Helfand, J. Chem. Phys. 74 (1981) 5300.

[30] E. A. Carter, G. Ciccotti, J. T. Hynes, R. Kapral, Chem. Phys. Lett. 156 (1989) 472.

[31] M. S. Shaw, J. Chem. Phys. 94 (1991) 7550.

[32] W. R. Smith. B. Triska, J. Chem. Phys. 100 (1994) 3019.

[33] J. K. Johnson, A. Z. Panagiotopoulos, K. E. Gubbins, Mol. Phys. 81 (1994) 717.

[34] N. Hansen, S. Jakobtorweihen, F. J. Keil, J. Chem. Phys. 122 (2005) 164705.

[35] K. P. C. Vollhardt, N. E. Schore, Organic Chemistry Structure and Function, 6th ed.; W.H. Freeman & Co: New York, 2006.

[36] M. B. Smith, J. March, March's Advanced Organic Chemistry: Reactions, Mechanisms, and Structure, 6th ed.; Wiley-Interscience: New York, 2007.

[37] M. Imoto, T. Nakaya, Mechanisms of Organic Reactions (Japanese); Tokyo Kagakudojin: Tokyo, 1982.

[38] FILMTEC Reverse Osmosis Membranes Technical Manual, Form No. 609-000710109; Dow Water Solutions: Midland, MI.

[39] O. Coronell, B. J. Marinas, D. G. Cahill, Environ. Sci. Technol. 45 (2011) 4513.

[40] P. B. Balbuena, Y. Wang, Lithium-Ion Batteries: Solid-Electrolyte Interphase; Imperial College Press: London, 2004.

[41] K. Xu, Chem. Rev. 104 (2004) 4303.

[42] Y. Abu-Lebdeh, Nanotechnology for Lithium-Ion Batteries; Splinger: New York, 2013.

Chapter 2

A Hybrid MC/MD Reaction Method with Rare Event-Driving Mechanism: Atomistic Realization of 2-Chlorobutane Racemization Process in DMF solution

2.1. Introduction

It has long been known that in diffusion in solids and chemical reactions, etc., many dynamical systems spend the overwhelming majority of their time in certain well-defined phase space regions [1-3], e.g., 99.9999999% in the initial state of N_2O_4 dissociation reaction at 273 K. The transitions between these stable regions typically occur due to infrequent activated events of short duration [1-3]. With traditional molecular simulations, it is difficult to determine the long-term properties and stereo-chemical characteristics that depend on or originate in such rare events.

A number of simulation methods have been developed to overcome this difficulty, such as generalized ensembles [4], metadynamics [5], transition path sampling [6], and action-based path sampling [7], which can deal with chemical reactions in an automatic or semi-automatic manner. Some have succeeded in performing effective statistical sampling [4] or searches for a minimum energy path for an elementary chemical reaction [5], while others have included dynamical and thermal effects [6,7]. However, there still remains a problem in that several kinds of chemical reactions are compatible in whole

molecular condensed systems, e.g., complex reacting systems. In these systems another issue related to stereochemistry appears, depending on which reactions should occur faster.

A possible computationally efficient way to realize plausible states of phase space in chemical equilibrium is to make the whole system transition between relatively stable regions in the stable phase states that exist divided by transition state regions, and to apply a stochastic approach to judge whether the state after a rare transition occurrence might be adopted. A similar idea was previously introduced to treat gas-phase chemical equilibria [8] and later applied to more complex chemical systems [9-11].

However, this chapter 2 addresses the question of the computation of rare event-related processes occurring in a chemically-reacting system in solution, keeping the "atomistic" complexity and flexibility of reactive molecules as they are. A hybrid Monte Carlo (MC)/molecular dynamics (MD) reaction method with rare event-driving mechanism that would help to develop new possible frontiers in computational chemistry is then presented. This new reaction method provides an independent alternative to the commonly applied reactive techniques [8-11].

The concept of the present hybrid MC/MD reaction method is schematically represented in Figure 2.1. For spatial moves not involving a chemical reaction (or its analogue) in a stable phase space region, we simply execute the usual NVT-MD simulation until some pair of atoms meets the necessary conditions. An MC procedure is then applied to drive the rare event to occur in a manner that is statistical-mechanically reasonable with an MD relaxation process after the spatial move due to chemical reaction.

In this chapter 2, I have applied the hybrid MC/MD reaction method to 2-

chlorobutane racemization in DMF solution assuming the S_N1 mechanism. Starting at the optical pure state (100% e.e.) with all the (*R*)-2-chlorobutane molecules in DMF molecules, it is demonstrated that in the chemical equilibrium after 900 MC/MD cycles, the ratio of (*R*)- to (*S*)-enantiomers becomes almost unity, i.e., racemization (0% e.e.).

2.2. Theoretical Methods and Model System

2.2.1. Total Hamiltonian of a Chemical Reaction System in Molecule Number Representation

For simplicity, I will restrict the current discussion to a simple chemical reaction system in a single pure solvent M that consists of 4 types of elementary chemical reactions,

$$\mathrm{A} \quad \rightleftharpoons \quad \mathrm{B} + \mathrm{C} \quad \rightleftharpoons \quad \mathrm{D}. \tag{2.1}$$

This is because generalization is complicated if not difficult. The "microscopic" or "atomistic" Hamiltonian of the molecular assembly comprising solute and solvent molecules can be described by

$$H = H(N_{\mathrm{A}}, N_{\mathrm{B}}, N_{\mathrm{C}}, N_{\mathrm{D}}; N_{\mathrm{M}}) = H^{\mathrm{S}} + H^{\mathrm{M}} + H^{\mathrm{SS}} + H^{\mathrm{SM}} + H^{\mathrm{MM}} \tag{2.2a}$$

$$= \sum_{i=\mathrm{A}}^{\mathrm{D}} \sum_{\sigma_i=1}^{N_i} H_{\sigma_i}^{\mathrm{S}} + \sum_{\mu=1}^{N_{\mathrm{M}}} H_{\mu}^{\mathrm{M}} + \frac{1}{2} \sum_{i=\mathrm{A}}^{\mathrm{D}} \sum_{j=\mathrm{A}}^{\mathrm{D}} \sum_{\rho_i=1}^{N_i} \sum_{\sigma_j=1}^{N_j} H_{\rho_i\sigma_j}^{\mathrm{SS}} + \sum_{i=\mathrm{A}}^{\mathrm{D}} \sum_{\rho_i=1}^{N_i} \sum_{\mu=1}^{N_{\mathrm{M}}} H_{\rho_i\mu}^{\mathrm{SM}} + \frac{1}{2} \sum_{\mu=1}^{N_{\mathrm{M}}} \sum_{\nu=1}^{N_{\mathrm{M}}} H_{\mu\nu}^{\mathrm{MM}} \tag{2.2b}$$

where the superscripts S and M denote the solute and the solvent, respectively, and *i* and *j* are used for the kinds of solute molecules; ρ_i and σ_j are the serial numbers of the *i*th and *j*th kinds of molecules, respectively, while μ and ν are used for the solvent

molecules. N_i and N_j are the total numbers of solute molecules of kinds *i* and *j*, respectively, and N_{M} is the number of the solvent components. Assuming that molecules A, B, …, M consist of η_{A}, η_{B}, …, η_{M} numbers of atoms, respectively, the conservation of the total number of atoms (i.e., the conservation of mass) stands;

$$\sum_{i=\mathrm{A}}^{\mathrm{D}} N_i \cdot \eta_i + N_{\mathrm{M}} \cdot \eta_{\mathrm{M}} = n \ (=\text{const.}) . \tag{2.3}$$

In the above formulation, it should be noted that such chemical species as ions and radicals, might also be called "molecules" for simplicity.

The whole solution system, expressed by the "atomistic" canonical ensemble with constant NVT, is well described in a state *r* in equilibrium by the Hamiltonian

$$H_r = H_r(N_{\mathrm{A}}, N_{\mathrm{B}}, N_{\mathrm{C}}, N_{\mathrm{D}}; N_{\mathrm{M}}) \equiv H_r(\mathbf{N}_{\mathrm{S}}; N_{\mathrm{M}}) , \tag{2.4}$$

in the molecule number representation $\mathbf{N}_{\mathrm{S}}$ and N_{M} with the representative phase $\mathrm{P}_r(\mathbf{r}_r^{\mathrm{S}}, \mathbf{r}_r^{\mathrm{M}}, \mathbf{p}_r^{\mathrm{S}}, \mathbf{p}_r^{\mathrm{M}})$. Then, if one of the chemical reactions in Eq. (2.1), e.g.,

$$\mathrm{A} \rightarrow \mathrm{B} + \mathrm{C}, \tag{2.5}$$

might occur with just one A molecule creating one B and one C molecule, the whole system then transfers to another state *s* in equilibrium in the different phase space region, expressed well by the representative phase $\mathrm{P}_s(\mathbf{r}_s^{\mathrm{S}}, \mathbf{r}_s^{\mathrm{M}}, \mathbf{p}_s^{\mathrm{S}}, \mathbf{p}_s^{\mathrm{M}})$ with the Hamiltonian

$$H_s = H_s(N'_{\mathrm{A}}, N'_{\mathrm{B}}, N'_{\mathrm{C}}, N'_{\mathrm{D}}; N_{\mathrm{M}}) = H_s(N_{\mathrm{A}} - 1, N_{\mathrm{B}} + 1, N_{\mathrm{C}} + 1, N_{\mathrm{D}}; N_{\mathrm{M}}) \equiv H_s(\mathbf{N}'_{\mathrm{S}}; N_{\mathrm{M}}) \tag{2.6}$$

$$= \sum_{i=\mathrm{A}}^{\mathrm{D}} \sum_{\rho_i=1}^{N'_i} H_{\rho_i}^{\mathrm{S}} + \sum_{\mu=1}^{N_{\mathrm{M}}} H_{\mu}^{\mathrm{M}} + \frac{1}{2} \sum_{i=\mathrm{A}}^{\mathrm{D}} \sum_{j=\mathrm{A}}^{\mathrm{D}} \sum_{\rho_i=1}^{N'_i} \sum_{\sigma_j=1}^{N'_j} H_{\rho_i \sigma_j}^{\mathrm{SS}} + \sum_{i=\mathrm{A}}^{\mathrm{D}} \sum_{\rho_i=1}^{N'_i} \sum_{\mu=1}^{N_{\mathrm{M}}} H_{\rho_i \mu}^{\mathrm{SM}} + \frac{1}{2} \sum_{\mu=1}^{N_{\mathrm{M}}} \sum_{\nu=1}^{N_{\mathrm{M}}} H_{\mu\nu}^{\mathrm{MM}} . \tag{2.7}$$

Here, one should notice that $N'_{\mathrm{A}} = N_{\mathrm{A}} - 1$, $N'_{\mathrm{B}} = N_{\mathrm{B}} + 1$and $N'_{\mathrm{C}} = N_{\mathrm{C}} + 1$. The energy difference ΔH between these states *r* and *s* before and after the reaction occurrence is

$$\Delta H_{rs} = H_s(\mathbf{r}_s^{\mathrm{S}}, \mathbf{r}_s^{\mathrm{M}}, \mathbf{p}_s^{\mathrm{S}}, \mathbf{p}_s^{\mathrm{M}}) - H_r(\mathbf{r}_r^{\mathrm{S}}, \mathbf{r}_r^{\mathrm{M}}, \mathbf{p}_r^{\mathrm{S}}, \mathbf{p}_r^{\mathrm{M}}) . \tag{2.8}$$

As far as the NVT ensemble may be concerned,

$$\Delta H_{rs} = \Delta U_{rs} = U_s(\mathbf{r}_s^{\mathrm{S}}, \mathbf{r}_s^{\mathrm{M}}) - U_r(\mathbf{r}_r^{\mathrm{S}}, \mathbf{r}_r^{\mathrm{M}}) , \tag{2.9}$$

where ΔU_{rs} is the energy difference of reaction and U_r and U_s are the configurational potential energies of the whole system in the states *r* and *s*, respectively. However, the above treatment can be easily extended to other thermodynamic ensembles, with other chemical reactions.

2.2.2. Total "Atomistic" Partition Function of a Chemical Reaction System

In the classical partition function for an "atomistic" canonical ensemble with *S* different kinds of atoms, n_a atoms of kind *a*, and a total of $n = \sum_{a=1}^{S} n_a$ atoms of all kinds, the total "atomistic" partition function [12] becomes in general the "atom" number representation,

$$Q(\mathbf{n}_S, V, T) = \prod_{a=1}^{S} \frac{\Lambda_a^{-3n_a}}{n_a!} \cdot Z(\mathbf{n}_S, V, T) , \tag{2.10}$$

where $\mathbf{n}_S \equiv (n_1, n_2, \cdots, n_a, \cdots, n_S)$ is a vector of non-negative integral numbers. This is unique for each reacting system involved, with the component n_a denoting the number of atoms of the same kind *a*, Λ_a the de Broglie thermal wavelength of the same kind of atom *a*, and $Z(\mathbf{n}_S, V, T)$ the total "atomistic" configuration integral [12] given by

$$Z(\mathbf{n}_S, V, T) = \int \exp\left[-\beta U(\mathbf{n}_S)\right] \prod_{a=1}^{S} \mathrm{d}\mathbf{r}^{n_a} . \tag{2.11}$$

In the atom number representation, such a characteristic of the assembly of atoms as a dynamical system is more emphasized, keeping in mind the "atom type" alteration on the occasion of chemical reaction, while in the molecule number representation the "molecule" idea is regarded as more important from the "chemical" viewpoint [8-11], and sometimes a set of collective coordinates are used instead of the atomistic phase variables $(\mathbf{r}^{\mathrm{S}},\mathbf{r}^{\mathrm{M}},\mathbf{p}^{\mathrm{S}},\mathbf{p}^{\mathrm{M}})$. Since the basic Hamiltonian is, therefore, common to both representations only if the global potential energy function U can be expressed atomistically by $(\mathbf{r}^{\mathrm{S}},\mathbf{r}^{\mathrm{M}})$, the whole partition function can be straightforwardly estimated numerically without approximating it by using a product of molecular partition functions of isolated molecules, such as vibrational or rotational [8-12].

It is in fact common that the partition function for a molecular mixture, within the approximation of separable internal degrees of freedom, can be estimated as a product of separable molecular partition functions of molecular assemblies such as a molecular cluster or solution,

$$Q(\mathbf{N}_S,V,T) = Z(\mathbf{N}_S,V,T)\cdot\prod_{a=1}^{S}\frac{\Lambda_a^{-3N_a}}{N_a!}\cdot q_a^{N_a}\,, \tag{2.12}$$

where q_a's are parts of the partition function, such as vibration and rotation, that correspond to individual molecules. The expressions of the products before and after a chemical reaction then necessarily change according to what kind of molecules appear or disappear. However, Eq. (2.12) is a restriction (e.g. the rigid rotor-harmonic oscillator approximation) of Eq. (2.10) to those atomic coordinates that correspond to the chosen molecular mixture composition. If Eq. (2.10) is introduced for the partition function for an atomistic canonical ensemble, I can relax the above restriction slightly to include any

set of atomic coordinates that corresponds to any set of N_a's which preserves the atomic compositions.

To develop the hybrid MC/MD reaction method, I therefore utilize an "atomistic" canonical distribution function for the whole solution system in a region, e.g., region *r*,

$$P_r^{\mathrm{eq}}(\mathbf{n}_S, V, T) = Q_r^{-1}(\mathbf{n}_S, V, T) \cdot \exp\left[-\beta H_r(\mathbf{n}_S)\right] \tag{2.13a}$$

$$= Z_r^{-1}(\mathbf{n}_S, V, T) \cdot \exp\left[-\beta U_r(\mathbf{n}_S)\right], \tag{2.13b}$$

that is actually ruled by the Hamiltonian Eq. (2.4) in the atom number representation in region *r*, $H_r(\mathbf{n}_S)$ with an appropriate set of atomic potential parameters in region *r*, including a proper set of the atom types suitable for the reactant molecules in region *r*. This strategy is not only nonrestrictive and general but also computationally-tractable.

2.2.3. A Hybrid MC/MD Reaction Method

An MC part of the method can be now executed in the present "atomistic" canonical ensemble if a reasonably likely type of move between nonoverlapping phase space regions before and after a chemical reaction can be found. This can be accomplished by making (/breaking) a chemical bond between a candidate pair of atoms belonging to two different molecules (/a dissociative molecule). (Such extension including intramolecular bond formation or breaking is straightforward). On rearranging these atoms, their original "atom types" in the reactant molecules (/a dissociative molecule) which participate in a chemical reaction are legitimately switched to those ones suitable for the product species, meaning a change of the corresponding atomic potential parameters in the molecular mechanical (MM) force field [13] together with a

proper correction of the "zero" point of energy by the corresponding potential energy of reaction.

It is clear that a Markov chain giving a limiting distribution of $\exp\left[-\beta U\right]$ is then obtained [13, 14] by accepting a reactive move from state *r* to state *s* with the transition probability $W_{r\to s}$ (Figure 2.1) given by

$$W_{r\to s} = \min\left\{1, \exp\left[-\beta \Delta U_{rs}\right]\right\}. \tag{2.14}$$

For this result, I impose the detailed balance (or microscopic reversibility) condition between the states *r* and *s* before and after the reaction

$$p_{r\to s} = p_{s\to r} \tag{2.15}$$

where the *p*'s indicate the unweighted probability of a move, and then finding

$$W_{r\to s} P_r^{\mathrm{eq}} = W_{s\to r} P_s^{\mathrm{eq}}. \tag{2.16}$$

For example, in a reaction such as in Eq. (2.5), one can take for the states *r* and *s* states with the molecular mixture compositions $(\mathbf{N}_{\mathrm{S}}, N_{\mathrm{M}})$ and $(\mathbf{N}'_{\mathrm{S}}, N_{\mathrm{M}})$, respectively; P_r^{eq}, P_s^{eq} and $W_{r\to s}$ can then be regarded as

$$P_r^{\mathrm{eq}} = P_r^{\mathrm{eq}}(\mathbf{r}_r^{\mathbf{N}_{\mathrm{S}}}, \mathbf{r}_r^{N_{\mathrm{M}}}) \quad \left(\equiv P_r^{\mathrm{eq}}(\mathbf{n}_S, V, T)\right), \tag{2.17a}$$

$$P_s^{\mathrm{eq}} = P_s^{\mathrm{eq}}(\mathbf{r}_s^{\mathbf{N}'_{\mathrm{S}}}, \mathbf{r}_s^{N_{\mathrm{M}}}) \quad \left(\equiv P_s^{\mathrm{eq}}(\mathbf{n}_S, V, T)\right) \tag{2.17b}$$

and

$$W_{r\to s} = W(\mathbf{r}_r^{\mathbf{N}_{\mathrm{S}}}, \mathbf{r}_r^{N_{\mathrm{M}}}; \mathbf{r}_s^{\mathbf{N}'_{\mathrm{S}}}, \mathbf{r}_s^{N_{\mathrm{M}}}), \tag{2.18}$$

respectively.

Here, I have shown the hybrid MC/MD reaction method in the case of a single chemical reaction occurring in one phase at specified (*V*, *T*), but its generalization is

straightforward. It is also worth noting that, in the MD part of the hybrid MC/MD reaction approach, I adopt the usual NVT-MD simulation [13,14] for spatial moves in a stable phase space region among *r*, *s* and *t* (Figure 2.1), e.g., in region *r*,

$$\begin{cases} \dfrac{\mathrm{d}\mathbf{r}^{\mathbf{N}_\mathrm{S}}}{\mathrm{d}t} = \dfrac{\partial H}{\partial \mathbf{p}^{\mathbf{N}_\mathrm{S}}} \\ \dfrac{\mathrm{d}\mathbf{p}^{\mathbf{N}_\mathrm{S}}}{\mathrm{d}t} = -\dfrac{\partial H}{\partial \mathbf{r}^{\mathbf{N}_\mathrm{S}}} \end{cases}, \qquad \begin{cases} \dfrac{\mathrm{d}\mathbf{r}^{N_\mathrm{M}}}{\mathrm{d}t} = \dfrac{\partial H}{\partial \mathbf{p}^{N_\mathrm{M}}} \\ \dfrac{\mathrm{d}\mathbf{p}^{N_\mathrm{M}}}{\mathrm{d}t} = -\dfrac{\partial H}{\partial \mathbf{r}^{N_\mathrm{M}}} \end{cases}, \tag{2.19}$$

as far as a certain pair of atoms meets the condition leading to a chemical reaction. An additional MD relaxes the whole system to remove the configurational instability if the approximate local (or regional) potential function is switched after a chemical reactive move. This treatment makes the Metropolis MC algorithm more efficient.

To summarize, the NVT-hybrid MC/MD reaction method consists of a combination of the following types of processes:

1. Equilibrate the whole system through the NVT-MD simulation and select a configuration state *r*.
2. Generate reaction steps with the NVT-MC procedure and NVT-MD simulation, consisting of the following steps:
   (i) Search a pair (/pairs) of “reactive” atoms among reactant molecules with the whole system in a given configuration state *r* according to some criteria for whether possible chemical reactions might plausibly occur. In the present simulation, for bond formation, the criterion for a candidate pair was taken to be whether the interatomic distance is less than the sum of their van der Waals radii. On the other hand, for bond dissociation, a candidate pair of the specific atoms in a molecule is selected among all the molecules that are assumed to be dissociable.

(ii) Randomly select a pair with one of those possible chemical reactions, assuming that each has a corresponding relative weight of selection $R \sim \exp(-\beta E_a)$, where E_a is its energy of activation. In the present simulation, E_a was assumed as the "free" energy of activation that was estimated in advance, i.e., within the continuum model [15] or the free energy gradient method [16, 17] for each chemical reaction.

(iii) Then switch the local (or regional) potential function of the reactant to the product one, keeping the atomic positions unchanged (see also Figure 2.1), and virtually react it to generate a possible configuration state *s*, relaxing the whole system to obtain the state *s* through a short NVT-MD simulation (of 10 ps for the present).

(iv) Compute the energy change Eq. (2.9) and accept (or reject) the reaction step according to the transition probability $W_{r \to s}$ (Eq. (2.14)) under the Metropolis scheme [13,14,18].

3. If the molecular mixture composition might scarcely change, then stop. Otherwise return to process 2.

The convergence of the hybrid MC/MD reaction method is affected by the relative ratios of the three different types of processes, and the optimal choice depends on the system properties. In particular, it is worth noting that E_a can be utilized to stochastically control which chemical reaction would more readily occur, while executing the Metropolis MC algorithm. In fact, this prescription is commonly used in the stochastic MC method. For the Metropolis MC procedure itself, however, *the energy difference of*

reaction ΔU_{rs} (Eq. (2.9)) was simply necessary, because the transition probability $W_{r\to s}$ (Eq. (2.14)) is defined only by the energy difference between the states *r* and *s*.

2.2.4. Model System: 2-Chlorobutane Racemization in DMF Solution

To illustrate the hybrid MC/MD reaction method, I consider the following S_N1 reaction of 2-chlorobutane racemization in *N*,*N*-dimethylformamide (DMF) solution

$$(R)\text{-}C_2H_5CH(CH_3)Cl \rightleftharpoons C_2H_5C^{\oplus}H(CH_3) + Cl^- \rightleftharpoons (S)\text{-}C_2H_5CH(CH_3)Cl \quad (2.20)$$

where (*R*)-$C_2H_5CH(CH_3)Cl$ and (*S*)-$C_2H_5CH(CH_3)Cl$ correspond to A and D in reaction formula (1), respectively, while $C_2H_5C^{\oplus}H(CH_3)$ and Cl^- correspond similarly to B and C, respectively. It is well-known that, since the carbonium ion $C_2H_5C^{\oplus}H(CH_3)$ takes a planar form, both inversion and retention of the original configuration are equally likely, leading to net racemization [19-21]. Further, carbonium ion is a very high-energy species and can only form if its energy is dissipated by solvation, i.e., by complexing with one (or a few) solvent molecule(s). If the ion is stable enough, it will have time to become symmetrically solvated in this way before going on to bond formation, either with solvent or another nucleophile. This gives true racemization [19-21]. In the present model of 2-chlorobutane racemization in DMF solution, I have concentrated on an idealistic S_N1 mechanism through the nucleophilic attack by Cl^- (reaction formula (2.20)) only, without recombination with any other species. This is because the present purpose is to clearly demonstrate the workability of the hybrid MC/MD reaction method as an apparatus of spatial selectivity, installed on the NVT ensemble.

2.3. Results and Discussion

The generalized AMBER force field (GAFF) [22] was used for 2-chlorobutane, 2-butyl cation, chloride ion and DMF molecules. To prepare solution with thermally distributed (*R*)-2-chlorobutane molecules, first, 50 (*R*)-2-chlorobutane molecules were arbitrarily placed and solvated with 350 DMF molecules in a 3D periodic box. Then, a high-temperature (750 K) NVT-MD for 500 ps and a relaxation NPT-MD for 1 ns at the target temperature and pressure (313 K and 1 atm) were executed, yielding a periodic box size of ~36.9×36.9×36.9 $Å^3$. The concentration of (*R*)-2-chlorobutane molecules was ~1.65 mol/L. A production run of the NVT-hybrid MC/MD reaction method at 313 K was then executed for 900 MC/MD cycles. The MD simulation time for relaxation in one MC/MD cycle for a trial of a chemical reaction was set to 10 ps.

The SANDER module of the AMBER 9 package was used to execute all the MD simulations. I used the particle mesh Ewald (PME) procedure to handle long-range electrostatic interactions under periodic boundary conditions. The SHAKE method was used to constrain the hydrogen-heavy atom bond distances and the integration time-step was 1 fs. For NPT- and NVT-MD simulations, a weak coupling algorithm [22] was used to keep the pressure and temperature constant.

Figures 2.2(a) and (b) show typical changes of the potential energy and the temperature of the whole system during the first 10 MC/MD cycles, displaying how they relax into equilibrium [13,14] after MC challenges to chemical reaction occur in each MC/MD cycle, i.e., every 10 ps. One can understand that a sudden increase in potential energy during chemical reaction, if it occurs, dissipates into the surrounding solvent. It can be concluded, therefore, that the hybrid MC/MD reaction method works reasonably well to attain thermal equilibrium in one MC/MD cycle, searching for a

lower potential energy state under the constant temperature scheme. It is worth noting that these kinds of dissipative characteristics of excess energy were often discussed in the 90's from the viewpoint of energy flow during chemical reaction by investigating the relaxation dynamics from transition states [23-26].

The simulation results are presented in Figure 2.3, where the changes of numbers of (*R*)- and (*S*)-2-chlorobutane molecules and 2-butyl cations are shown as functions of the MC/MD cycles. The equilibrium numbers of these molecules, estimated as averages over the last 100 cycles, were 25.3, 24.4 and 0.3, respectively. Thus, racemization could be realized satisfactorily within thermal fluctuation of the numbers of molecules. Moreover, from the chemical viewpoint, this result is consistent with the chemical insight that the amount of 2-butyl cations should be quite small [19, 20]. In fact, the number is either zero or one at most throughout the present MC/MD cycles since a 2-butyl cation may recombine soon or later with a chloride ion that dissociated a little before.

From this observation, one can expect that the racemization would become very slow since 2-butyl cation should keep its stereochemistry. As shown in Figure 2.4, however, there are successive snapshots along the MD trajectory that show a typical stereochemical configurational change between (*R*)- and (*S*)-2-chlorobutane, where the methyl substituent and the hydrogen atom (H6) that are bonding to the asymmetric carbon (C3) rotate as a whole on the axis of the C-C bond between C3 and the carbon at position 2 of the ethyl substituent. As is expected, therefore, the present results clearly indicate that net racemization is easier with less bulky substituents [27]. Although this kind of indication is rarely given for the S_N1 reaction mechanism in common textbooks, both inversion and retention of the original configuration occur [19-21].

Figure 2.5 shows atomistically typical side-by-side stereo-view snapshots of 2-chlorobutane DMF solution in the initial (0 MC/MD cycle) (Figure 2.5(a)) and equilibrium state (897 MC/MD cycle) after racemization was achieved (Figure 2.5(b)). One can understand clearly and pictorially that, starting at the initial optical pure state full of (*R*)-2-chlorobutane molecules, a state is reached with an expected purity of ~0% e.e., where two kinds of (*R*)- to (*S*)-enantiomers of 2-chlorobutane (red and blue) exist in almost equal numbers of ~25. These enantiomers are distributed homogeneously in the solution, together with other species, i.e., one 2-butyl cation (black), one chloride ion (black) and 350 DMF molecules (semitransparent).

2.4. Concluding Remarks

I have proposed and demonstrated, for the first time, an effective hybrid MC/MD reaction method with a rare event-driving mechanism in order to achieve a practical "atomistic" molecular simulation of large-scale chemical reaction systems (~ 1M atoms). This mechanism, which simply drives such rare events as chemical reactions, has enabled to specify the molecular compositions in chemical equilibrium as well as "atomistic" spatial distribution for 2-chlorobutane racemization in *N*,*N*-dimethylformamide (DMF) solution. Starting at the optical pure state (100% e.e.) of (*R*)-2-chlorobutane molecules in DMF molecules, this method has realized a state with ~0% e.e., the expected purity of (*R*)- to (*S*)-enantiomers of the racemic mixture in chemical equilibrium.

The hybrid MC/MD reaction method repeats a combined cycle consisting of a couple of MC and MD treatments. The former stochastically manages such a rare event as activated processes, while the latter simply executes a common dynamical process in

stable phase spaces for naturally searching candidate molecular configurations for reaction occurrence. Although creation of a new molecule brings a change in the number of molecules in traditional methods, the present framework does not violate the conservation of the number of atoms, and there is no need to evaluate the conventional transition probability due to the change in molecular composition. The hybrid MC/MD reaction method enables discussion on the trajectories for the "motion" of a chemically-reacting system and thus makes a rare event more closely resemble a "common" event within some restrictions. In a sense, the present algorithm may also resemble the surface hopping algorithm [28, 29] for treatment of such coupled-"state" dynamics in QM/MM systems.

Since the hybrid MC/MD reaction method is proposed to explore the "rare events" that we theoretical chemists need to tame in order to harvest more "chemical" crops computationally, I feel that an appropriate alternate name would be the "Red Moon" method (from Rare-Event Driving Mechanism Of Our Necessity). By only slightly changing the way that the product state *s* is generated, the framework of the present method can be transferred to chemically-reacting systems using the forces obtained by ab initio electronic structure calculations, including those by the QM/MM methods. Its implementation and applications to more molecular species with more chemical reactions are straightforward with our QM/MM-IF settings [30, 31] and are now being done for polymerization and other reactions (discussed in later chapters 3, 4 and 5). The hybrid MC/MD reaction method described herein is promising for the study of various properties in chemical reaction systems and their stereochemistry.

References

[1] E. K. Grimmelmann, J. C. Tully, E. Helfand, J. Chem. Phys. 74 (1981) 5300.

[2] E. A. Carter, G. Ciccotti, J. T. Hynes, R. Kapral, Chem. Phys. Lett. 156 (1989) 472.

[3] A. C. T. Van Duin, S. Dasgupta, F. Lorant, W. A. Goddard III, J. Phys. Chem. A 105 (2001) 9396.

[4] Y. Okamoto, J. Mol. Graph. Model. 22 (2004) 425.

[5] A. Laio, M. Parrinello, Proc. Nat. Amer. Soc. 99 (2002) 12562.

[6] C. Dellago, P. G. Bolhuis, Top. Curr. Chem. 268 (2007) 291.

[7] For example, H. Fujisaki, M. Shiga, A. Kidera, J. Chem. Phys. 132 (2010) 134101.

[8] M. S. Shaw, J. Chem. Phys. 94 (1991) 7550.

[9] W. R. Smith. B. Triska, J. Chem. Phys. 100 (1994) 3019.

[10] J. K. Johnson, A. Z. Panagiotopoulos, K. E. Gubbins, Mol. Phys. 81 (1994) 717.

[11] N. Hansen, S. Jakobtorweihen, F. J. Keil, J. Chem. Phys. 122 (2005) 164705.

[12] D. A. McQuarie, Statistical Mechanics; Harper & Row: New York, 1976.

[13] M. P. Allen, D. J. Tildesley, Computer Simulation of Liquids; Clarendon: Oxford, 1987.

[14] D. W. Heerman, Computer Simulation Methods in Theoretical Physics, 2nd ed.; Springer: Berlin, 1990.

[15] J. Tomasi, M. Persico, Chem. Rev. 94 (1994) 2027.

[16] N. Okuyama, M. Nagaoka, T. Yamabe, Int. J. Quantum Chem. 70 (1998) 95.

[17] M. Nagaoka, N. Okuyama-Yoshida, T. Yamabe, J. Phys. Chem. A 102 (1998) 8202.

[18] N. Metropolis, A. W. Rosenbluth, M. N. Rosenbluth, A. H. Teller, E. Teller, J. Chem. Phys. 21, (1953) 1087.

[19] K. P. C. Vollhardt, N. E. Schore, Organic Chemistry Structure and Function, 6th ed.; W. H. Freeman & Co: New York, 2006.

[20] M. B. Smith, J. March, March's Advanced Organic Chemistry: Reactions, Mechanisms, and Structure, 6th ed.; Wiley-Interscience: New York, 2007.

[21] M. Imoto, T. Nakaya, Mechanisms of Organic Reactions (Japanese); Tokyo Kagakudojin: Tokyo, 1982.

[22] D. A. Case et al., AMBER 9, University of California, San Francisco, 2006.

[23] M. Nagaoka, Y. Okuno, T. Yamabe, J. Amer. Chem. Soc. 113 (1991) 769.

[24] M. Nagaoka, Y. Okuno, T. Yamabe, J. Phys. Chem. 98 (1994) 12506.

[25] W. P. Keirstead, K. R. Wilson, J. T. Hynes, J. Chem. Phys. 95 (1991) 5256.

[26] M. Strnad, M. T. C. Martins-Costa, C. Millot, I. Tuñón, M. F. Ruiz-López, J. L. Rivail, J. Chem. Phys. 94 (1997) 3643.

[27] D. G. Morris, Stereochemistry; Wiley-RSC: New York, 2002.

[28] J. C. Tully, in: W. H. Miller (Ed.), Dynamics of Molecular Collisions, Part B; Prenum: New York, 1976.

[29] J. Simons, An Introduction to Theoretical Chemistry; Cambridge University Press: Cambridge, 2003.

[30] T. Okamoto, K. Yamada, Y. Koyano, T. Asada, N. Koga, M. Nagaoka, J. Comp. Chem. 32 (2011) 932.

[31] T. Okamoto, T. Ishikawa, Y. Koyano, N. Yamamoto, K. Kuwata, M. Nagaoka, Bull. Chem. Soc. Jpn. 86 (2013) 210.

FIGURES

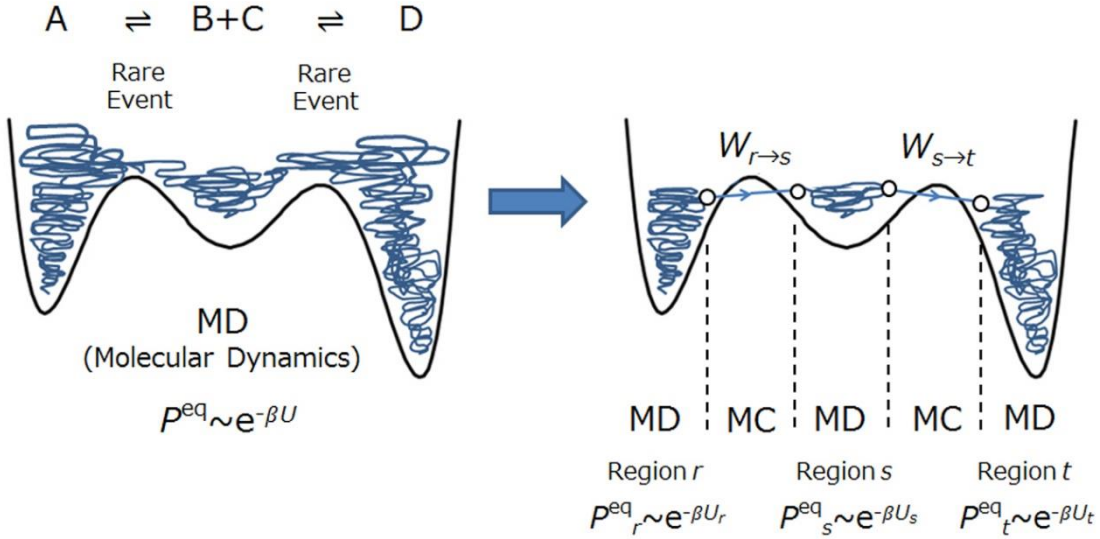

Figure 2.1. Schematic representation of the hybrid MC/MD reaction method. The curly curves represent the molecular dynamical (MD) moves in phase space following the equations of motion, Eq. (19), while the straight lines with arrows represent the Monte Carlo (MC) moves (or transitions) of the system (right figure), whose dynamical moves would be extremely rare events. In the left figure, the configurational distribution in equilibrium P^{eq} is proportional to the exponential factor $\exp[-\beta U]$ where U is the global potential function. The right figure shows regional distributions, e.g., $P^{eq}_r \sim \exp[-\beta U_r]$ in region *r*, etc. The connecting points of the two kinds of moves (open circles) are selected according to the criteria for chemical reaction occurrence (see text). Note that they do not represent real connections since these points correspond to almost identical states in configuration space but not in momentum space and with different configurational gradients. $W_{r\to s}$ and $W_{s\to t}$ are the transition probabilities from state *r* to *s* and from *s* to *t*, respectively.

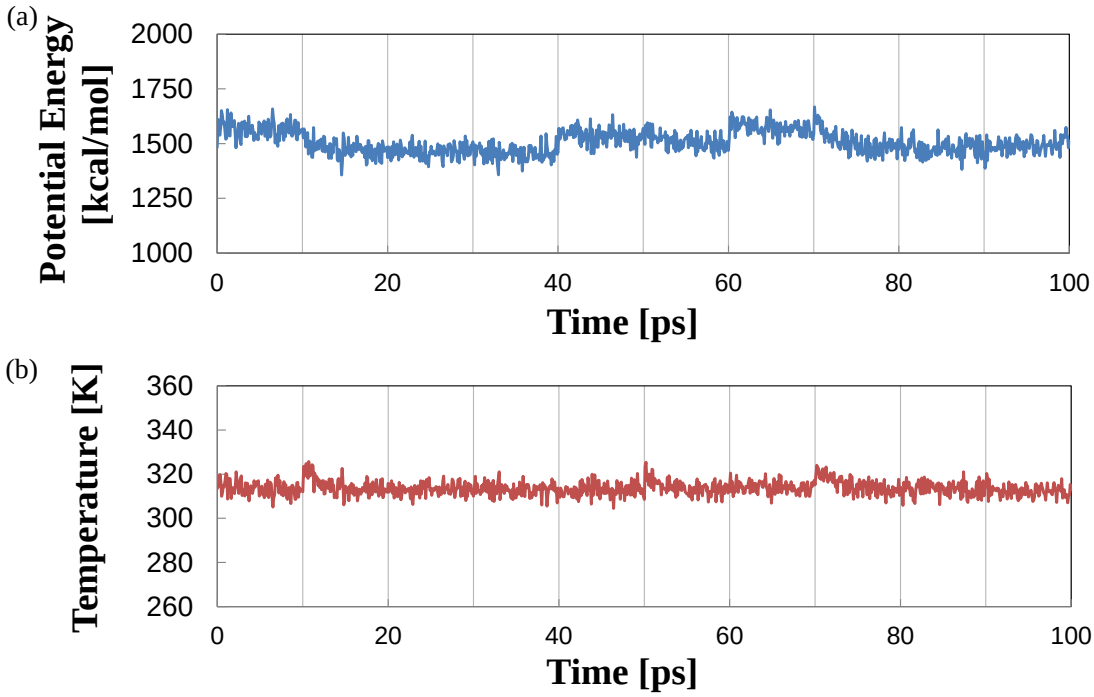

Figure 2.2. Changes in (a) the potential energy and (b) the temperature of the whole system during the first 10 MC/MD cycles of the 2-chlorobutane racemization by the typical hybrid MC/MD reaction simulation.

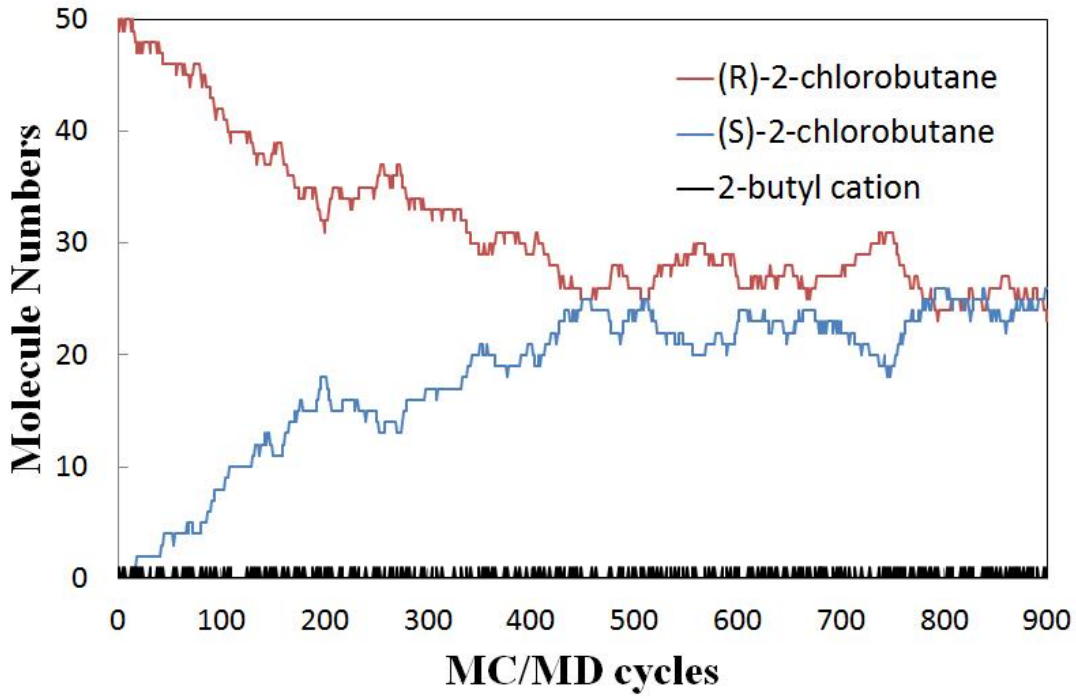

Figure 2.3. Number changes of (*R*)- (red), (*S*)-2-chlorobutane (blue) and 2-butyl cation (black) during the hybrid MC/MD reaction simulations.

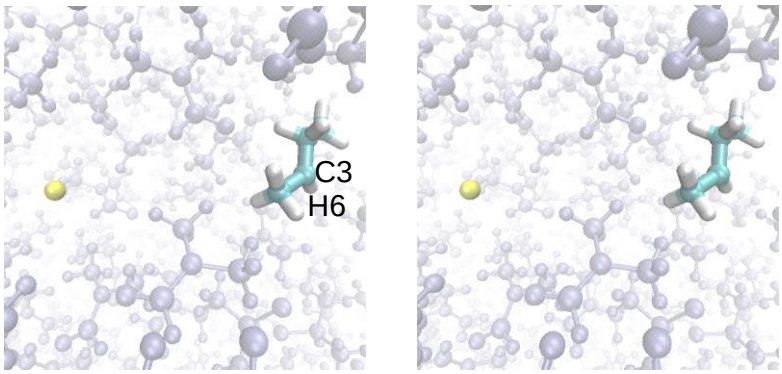

(a) t = 1.6 ps

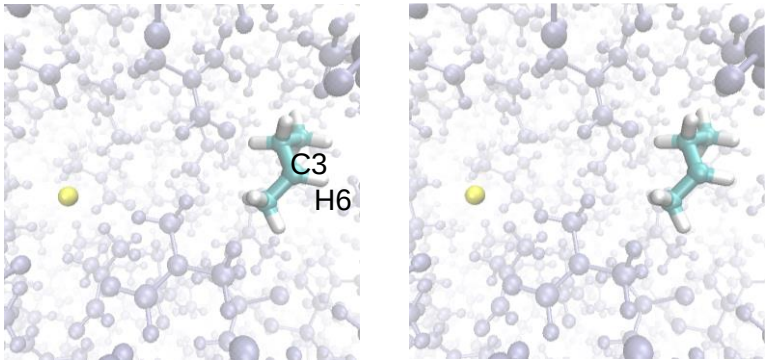

(b) t = 2.0 ps

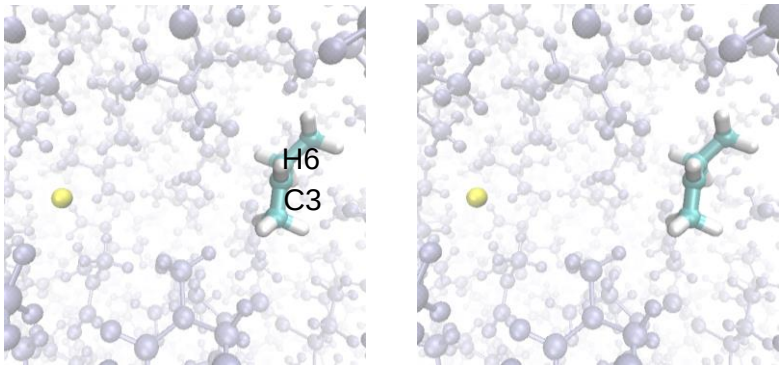

(c) t = 3.0 ps

Figure 2.4. Typical successive side-by-side stereo-view snapshots along the MD trajectory that show the stereochemical configurational change between (*R*)- and (*S*)-2-chlorobutane (in the stick model). Both the methyl substituent and the hydrogen atom (H6) bonding to the asymmetric carbon (C3) rotate as a whole on the axis of the C-C bond between C3 and the carbon at position 2 of the ethyl substituent. Chloride ion are expressed by the yellow balls.

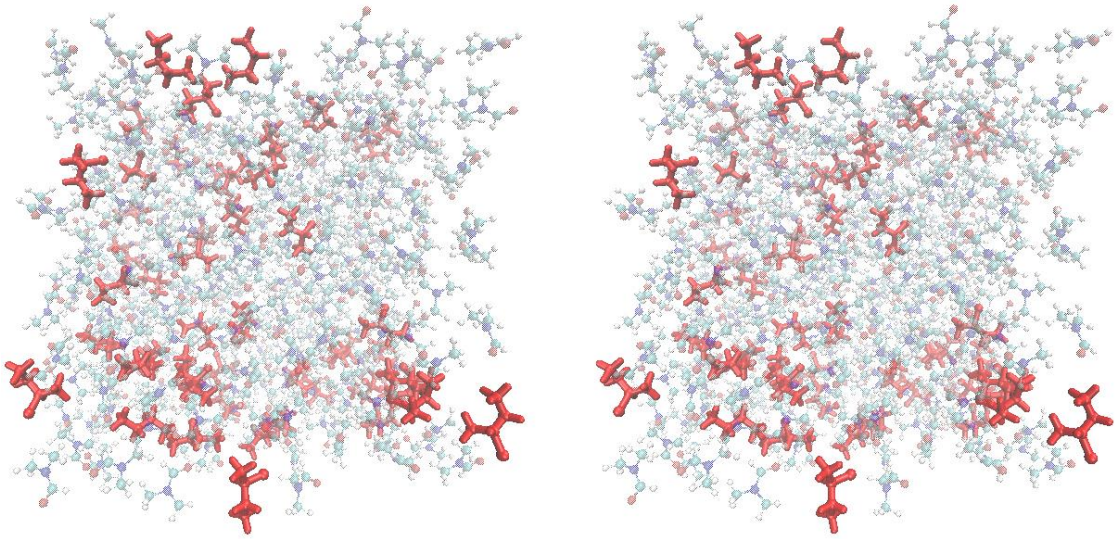

(a) Initial state (MC/MD cycle = 0)

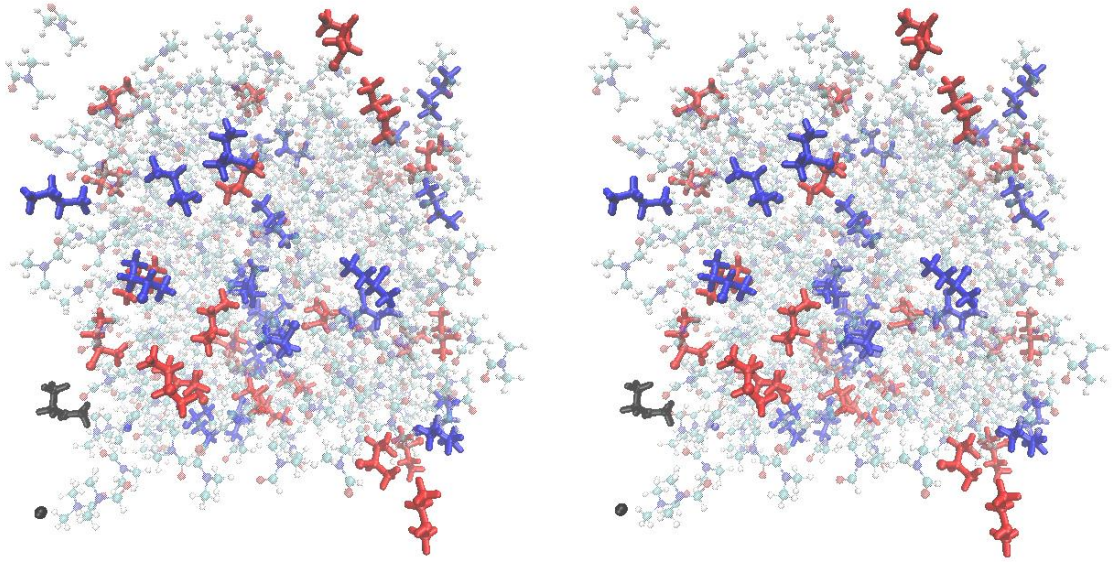

(b) A typical equilibrium state (MC/MD cycle = 897)

Figure 2.5. Side-by-side stereo-view snapshots of (a) the initial and (b) a typical equilibrium configuration of 2-chlorobutane racemic mixture consisting of (*R*)- (red), (*S*)-2-chlorobutane molecules (blue), a 2-butyl cation and a chloride ion (black). Solvent DMF molecules are expressed by the ball-and-stick model (semitransparent).

Chapter 3

Influence of Monomer Mixing Ratio on Membrane Nanostructure in Interfacial Polycondensation: Application of Hybrid MC/MD Reaction Method with Minimum Bond Convention

3.1. Introduction

Polymers are chemical materials composed of a variety of structural units which are connected regularly or irregularly by successive chemical reactions, i.e., polymerization reaction, and are used for various applications as plastics, fibers, coatings, adhesives, rubber and structural materials for packing [1,2]. All substances referred to as polymers or macromolecules are giant molecules with molar masses ranging from several thousand to several million [3], typically showing complex conformations with inhomogeneous distributions of lengths and orientations [1-3].

Among such polymeric materials, the polymer membrane FT-30 is well-known as a useful aromatic polyamide thin film. It is formed experimentally by interfacial polycondensation (IP) reaction between the aqueous and organic phase, in which *m*-phenylenediamine (MPD) and benzene 1,3,5-tricarboxylic acid chloride (TMC) monomers are dissolved, respectively [4]. Moreover, the FT-30 membrane is composed of a number of repeating units of *cross-linked* and *linear* portions[5] with inhomogeneous

spatial rearrangement, as well as general polymers (Figure 3.1 shows (a) MPD and (b) TMC monomers, and the repeating units of their two portions ((c) and (d)) in the FT-30 membrane) [6].

Among industrial applications, the FT-30 membrane has been used for reverse osmosis (RO), which is the most current technique for the desalination and purification of seawater and brackish water. This is a process to obtain feedwater by the filtration of salt ions as impurities through the RO membrane [7]. To improve the performance of the RO membrane, water flux needs to be maximized through an appropriate membrane at high pressure, allowing the water to pass through while the salt ions are largely rejected [7-10].

To experimentally investigate the properties of the FT-30 membrane, methods such as X-ray photoelectron spectroscopy (XPS), Rutherford backscattering spectrometry (RBS), atomic force microscopy (AFM) and positron annihilation lifetime spectroscopy (PALS) are often used [5,6,11]. Although the degree of polymer cross-linking (DPC) and the composition ratios of constituent atoms have been observed by XPS and RBS to be dependent on the depth from the membrane surface [6], the detailed inhomogeneous atomic rearrangement of the membrane has not been clearly characterized [7-9]. For this reason, both the physiochemical mechanisms of the permeation of water and the rejection of salt ions as impurities in the membrane remain imperfectly understood [7-9].

To reveal such physicochemical mechanisms, computational simulation is a powerful methodology [7-10,12,13] that is not only complementary to experimental investigations but also essential for investigating the microscopic structure of inhomogeneous membranes. By constructing a membrane model that correctly

reproduces (/reflects) the microscopic structures of actual polymeric materials, we may understand the microscopic properties of unknown physicochemical phenomena which occur in the interior of the material.

However, in such computational studies [7-10,12,13]. few methods are available to construct and treat inhomogeneous polymers like the FT-30 membrane at the atomistic level. The ones used mainly fall into two categories: (i) one where several polymer chains are initially prepared and then chemical bonds between these chains are made corresponding to the experimental DPC [9,10,14] and (ii) one where the polymer is formed from monomers by reproducing the polymerization reaction [7,8,13]. Although it would seem that the latter method would be more suitable to clarify the microscopic structure of an inhomogeneous polymer membrane, as far as I know, the former method has been utilized more widely than the latter to form polymer membranes in theoretical and computational studies.

I have applied the hybrid Monte Carlo/molecular dynamics (MC/MD) reaction method to the FT-30 membrane [15,16]. This method is a practical and promising "atomistic" molecular simulation approach for large-scale chemical reaction systems such as polymer membranes. In this chapter 3, the method has been modified so that intercellular chemical bonds can be formed over the periodic boundaries between the main cell and the image cells in order to deal with their giant molecules with high molecular weights (Figure 3.2 schematically shows those chemical bonds among "real" atoms only in the main cell (Figure 3.2(a)), i.e., intracellular chemical bonds, and those bonds with additional bonds over the periodic boundaries between the main and image cells (Figure 3.2(b)), i.e., intercellular chemical bonds).

First, under the assumption that the depth dependence of the values observed by

XPS and RBS should emerge due to the difference in the MPD/TMC mixing ratio, I prepared a set of four initial model systems with different four MPD/TMC ratios (1:4, 1:1, 3:2 and 4:1), respectively. Applying the hybrid MC/MD reaction method to these initial model systems, I made a set of bulk membrane models of FT-30 from these monomers assemblies, simulating a succession of amide bond formations (/condensation reactions). From the membrane models thus obtained, I calculated the DPC and the composition ratios of its constituent atoms. Next, the water diffusion through the slab membrane model obtained by modifying the bulk model with the MPD/TMC ratio of 1:1 was simulated to characterize the properties of the water permeability. Then I calculated the mass density of constituent atoms in the membrane and water molecules, and the partition coefficient. Finally, by comparing the present results with the corresponding experimental ones, I investigated the structural characteristics of the membrane at the atomistic level and concluded that the membrane model shows fidelity to the actual membrane.

This chapter 3 is organized as follows. In section 3.2, I explain the hybrid MC/MD reaction method, inter-cellular chemical bonds under the periodic boundary condition, model systems, and computational details, and, in section 3.3, I present the results and discussion. In the last section I offer some concluding remarks.

3.2. Theoretical Methods

3.2.1. The Hybrid MC/MD Reaction Method

To investigate the FT-30 membrane formation, I employed the hybrid MC/MD reaction method (shown in detail in chapter 2) [15,16]. Before executing the simulation, for MPD and TMC monomers, which are elementary constituents of the membrane, atomic potential parameters in the molecular mechanical (MM) force field [17], such as the force constants, Lennard-Jones (LJ) parameters and atomic charges, need to be prepared. When some chemical reaction occurs in the simulation, not only the atomic potential parameters but also the potential function forms (i.e., intramolecular or intermolecular ones) of the reactants are replaced by those suitable to the products.

The hybrid MC/MD reaction method consists of a combination of the following processes (see Figure 2.1):

1. Equilibrate the whole system through classical NVT-MD simulation and obtain an initial configuration state *r*.
2. Generate reaction steps with the NVT-MC procedure and classical NVT-MD simulation, consisting of the following steps:
   (i) Search for a pair (/pairs) of "reactive" atoms among reactant molecules with the whole system in a given configuration state *r* according to some criteria for whether possible chemical reactions might plausibly occur. In the present chapter, the criterion for a *candidate pair* to make an amide bond was taken to be whether the interatomic distance $D_{\text{N-C}}$ between the nitrogen (N) and carbon (C) atoms of an amine and acyl group, respectively, is less than the criteria distance R_c, which is a little larger than the distance estimated by the average of the interatomic distances between N and C atoms at initial states for the whole system in equilibrium (see subsection 3.2.4). As a result,

a set of candidate pairs which can generate the chemical reactions are obtained in a given configuration state *r*.

(ii) Randomly select a pair from among the set of candidate pairs, assuming that each has a corresponding relative weight of selection *R*, which is estimated in advance. If there is no such pair, execute a short NVT-MD simulation instead of the following steps (iii) and (iv) to update the configuration state. In the present chapter, *R* could be taken as a common constant 1, meaning that there is an equal relative probability for any chemical reaction. This is because, for the IP reaction of the membrane, the relative probability for an amide bond formation could be independent of the number of unreacted functional groups of a MPD or TMC monomer. The diffusion of MPD monomers in the aqueous into organic phase would then be more important as a rate-determining step [5,18-22].

(iii) Then switch the atomic potential parameters and potential function forms of the reactant to those of the product, and virtually react it to generate a possible configuration state *s*, relaxing the whole system to obtain the state *s* through a short NVT-MD simulation.

(iv) Compute the energy change of the system ΔU_{rs} (=U_s - U_r) and accept (or reject) the reaction step according to the transition probability $W_{r\to s}$ under the Metropolis scheme [17,23,24]

$$W_{r\to s} = \min\left\{1, \exp\left[-\beta \Delta U_{rs}\right]\right\}. \tag{3.1}$$

In the present chapter, ΔU_{rs} is approximated as follows,

$$\Delta U_{rs} = \Delta U_{rs}^{\mathrm{MM}} + \Delta U_{0}^{\mathrm{reac}}, \tag{3.2}$$

where $\Delta U_{rs}^{\mathrm{MM}}$ is the naïve difference of local potential energies obtained in the MM force field, meaning a change of the corresponding atomic potential parameters and potential function forms together with a proper correction of the "zero" point of energy by the corresponding potential energy of reaction $\Delta U_0^{\mathrm{reac}}$. In the present chapter, because the amide bond is formed by the chemical reaction,

$$\mathrm{C_6H_4\ NH_2\ _2 + C_6H_3\ COCl\ _3 \rightarrow H_2NC_6H_4NHCOC_6H_3\ COCl\ _2 + H^+ + Cl^-} \quad (3.3)$$

this correction is obtained by Eq. (3.4),

$$\Delta U_0^{\mathrm{reac}} = \Delta U_{\mathrm{N\text{-}C}} - \Delta U_{\mathrm{N\text{-}H}} - \Delta U_{\mathrm{C\text{-}Cl}} \quad (3.4)$$

where $\Delta U_{\mathrm{N\text{-}C}}$, $\Delta U_{\mathrm{N\text{-}H}}$ and $\Delta U_{\mathrm{C\text{-}Cl}}$ are the heats of formation of the chemical bonds of N-C, N-H and C-Cl, respectively.

3. If the molecular mixture composition shows little change, then stop. Otherwise return to process 2.

The cycle consisting of the three different types of processes is called an "MC/MD cycle" hereafter. During the present MC/MD simulation, when an amide bond was made, the hydrogen atom of amino groups and the chlorine atom of acid chloride groups were both deleted from the model system because these atoms should flow out into the solutions in the experimental treatment [25]. For the same reason, I similarly deleted these monomers from the model system after polymerization reaction was completed.

3.2.2. Intercellular Chemical Bonds under the Periodic Boundary Condition—Minimum Bond Convention

In the hybrid MC/MD reaction method, the periodic boundary condition (PBC) was used as in the common treatment of MD simulation [17]. Under the PBC for a cubic main cell, which is the unit cell including *real atoms*, the cell is surrounded by 26 replicas that are in contact with it. Each of these 26 image cells includes their *image atoms*. However, the naive realization of the *standard* PBC in the hybrid MC/MD reaction method restricts the polymer extension into the main cell only because chemical bonds are created in between real atoms only in the main cell (Figure 3.2(a)), i.e., *intracellular* chemical bonds, not including those bonds between real and image atoms belonging to the main and adjacent image cells, respectively. However, if we could consider additional chemical bonds over the periodic boundaries between the main and image cells (Figure 3.2(b)), i.e., *intercellular* chemical bonds, it should be possible to obtain a more realistic description of the polymer structure by realizing effectively longer polymer chains with high molecular weights.

For that purpose, I adopted a modified treatment to create a more realistic polymer model which has chemical bonds among atoms in the main cell and image cells under the PBC approximation. In the treatment, I introduce a convention that allows two atoms belonging not only to the main cell but also to the main cell and an image cell to be able to form a chemical bond. These are *candidate pairs* of atoms for a chemical bond in the MC/MD cycle (cf. step 2-(i)). After the minimum image convention (MIC) [17], I named this the minimum bond convention (MBC). This MBC makes it possible to

exclude the discontinuity of the polymer network between the adjacent cells and to construct a more realistic polymer model extending to a sufficiently large dimension (see Figure 3.2(b)).

To realize the MBC in the MC/MD cycles, we collect as sets of possible candidate pairs for chemical bonds (see subsection 3.2.1) such pairs of real atoms *i* and *j*, and pairs of *i* and an image atom *j'* in one of the other 26 image cells (see Figure 3.2) that fulfill the following conditions with respect to the interatomic distances R_{ij} and $R_{ij'}$,

$$R_{ij} = \sqrt{\Delta x_{ij}^2 + \Delta y_{ij}^2 + \Delta z_{ij}^2} \le R_c \left(< L/2\right) \tag{3.5}$$

and

$$R_{ij'} = \sqrt{\Delta x_{ij'}^2 + \Delta y_{ij'}^2 + \Delta z_{ij'}^2} \le R_c \tag{3.6}$$

respectively. In Eqs. (3.5) and (3.6),

$$\begin{cases} \Delta x_{ij} = \left| x_i - x_j \right| \\ \Delta y_{ij} = \left| y_i - y_j \right| \\ \Delta z_{ij} = \left| z_i - z_j \right| \end{cases} \tag{3.7}$$

and

$$\begin{cases} \Delta x_{ij'} = \left| x_i - x_{j'} \right| \\ \Delta y_{ij'} = \left| y_i - y_{j'} \right| \\ \Delta z_{ij'} = \left| z_i - z_{j'} \right| \end{cases}, \tag{3.8}$$

where the positional vectors of real atoms *i* and *j* are denoted $\mathbf{x}_i = \left(x_i, y_i, z_i\right)$ and $\mathbf{x}_j = \left(x_j, y_j, z_j\right)$ with

$$0 \le x_i, y_i, z_i \le L, \quad \left(i = 1, 2, \cdots, N\right) \tag{3.9}$$

and

$$0 \le x_j, y_j, z_j \le L, \quad (j = 1, 2, \cdots, N) \tag{3.10}$$

where L and N are each side length of the cubic unit cell and the total number of atoms in a cell, respectively. The positional vector of image atom j' is $\mathbf{x}_{j'} = (x_{j'}, y_{j'}, z_{j'})$, and then $\mathbf{x}_j$ and $\mathbf{x}_{j'}$ are related as follows,

$$\begin{cases} x_{j'} = x_j \pm L \\ y_{j'} = y_j \pm L. \\ z_{j'} = z_j \pm L \end{cases} \quad \text{(double sign correspond)} \tag{3.11}$$

With the present MBC, we are able to plausibly form a unique polymer model.

Moreover, it is significant to note that all the chemical processes can be treated equally homogeneously during the polymerization reaction, even if a candidate pair of atoms for a chemical bond might appear either near the center or on the edge of the main cell.

3.2.3. Model Systems

3.2.3.1. Bulk Model

Four types of model systems were prepared numerically with the four different initial MPD/TMC ratios 1:4, 1:1, 3:2 and 4:1. The numbers of MPD and TMC monomers in the main cells were 100 and 400, 250 and 250, 300 and 200, and 400 and 100, which correspond to the MPD/TMC ratios 1:4, 1:1, 3:2 and 4:1, respectively. A cubic unit cell (L =48.7 Å for all the ratios) was used for the main cell. The monomer numbers with MPD/TMC ratio 1:1 and the size of the unit cell were chosen according to a previous theoretical study under the NVT condition at the temperature 340 K [7]. With the other MPD/TMC ratios, 1:4, 3:2 and 4:1, the total monomer numbers were the

same as with the ratio 1:1 under the same condition for the temperature and size of the unit cell. The polymerization reaction simulations were performed in vacuum without explicit water and organic solvent molecules [7]. To get rid of the model dependence due to the inhomogeneity of those membranes, five bulk membrane models were made from the different initial structures in each of the four ratios.

3.2.3.2. Slab Model

The properties of the water permeability were investigated through the diffusion of water molecules into a slab membrane with the MPD/TMC ratio 1:1. To prepare the slab membrane model, I disconnected the bulk membrane models at the two boundary surfaces (e.g., z =0, L) and cut the intercellular amide bonds between the "real" nitrogen (/carbon) and "image" carbon (/nitrogen) atoms and then added hydrogen and chlorine atoms to the nitrogen and the carbon ones. Specifically, I cut only those amide bonds that exist across the two boundary surfaces of the membrane where the water phases would be faced. Further, I rearranged two bulk water areas so as to sandwich the slab membrane model in the same z axial direction. Finally, this rectangular system, shown in Figure 3.3, was constructed with the same length of 48.7 Å for x and y axial directions and an extended length of 146.1 Å for the z axial direction. To accomplish better spatial averaging of the inhomogeneous membrane, three independent slab models were made by using each of three Cartesian axes x, y and z of the bulk membrane models.

3.2.4. Computational Details

The force field parameter set, i.e., the generalized amber force field (GAFF) [26] with ANTECHAMBER module of AMBER 9 program [27], was used for all the

molecules in the present systems. Atomic point charges were determined using AM1-BCC partial charges [28], averaged for equivalent atoms in each MPD and TMC monomer. The initial conformation of each monomer was built by the LEaP module of the AMBER 9 program. All of the MD simulations were performed with the SANDER module of AMBER 9 under the NVT conditions, using the Berendsen algorithm to control the system temperature [29]. Trajectories were numerically integrated by the velocity Verlet method with a time step of 1.0 fs. The electrostatic interactions were treated by the particle-mesh Ewald (PME) method [30]. Covalent bonds involving hydrogen atoms were constrained by the SHAKE method [31]. The cutoff distance for the LJ interaction was set to 8.0 Å. During the hybrid MC/MD reaction simulation, if some new bond was created by a "real" atom *i* with an "image" atom *j*' in an adjacent neighboring cell (Figure 3.2(b)), i.e., an intercellular chemical bond, the potential energies (corresponding to U_r in step 2-(iv) in subsection 3.2.1) of the binding interaction between the "real" atom *i* and "image" atom *j*', and the other interactions involving their atoms, could be practically calculated as a function of their spatial coordinates. As shown in Eq. (3.11), the latter coordinates are obtained from those of the corresponding "real" atom *j* (Figure 3.2).

The hybrid MC/MD reaction algorithm was implemented in some modules in the AMBER 9 program. The MD simulation time for relaxation in one MC/MD cycle for a trial of amide bond formation was set to 4 ps, keeping the temperature at 340 K. The total MC/MD cycles were 2000, altering the distance criteria $D_{\text{N-C}}$ for amide bond formation from 3.25 Å to 3.50 Å at 1000 cycles in order to accelerate the diffusion of polymer chains generated by polymerization reaction. According to the experimental values corresponding to the corrections in Eq. (3.4), I used the heats of formation of the

chemical bonds, $\Delta U_{\text{N-C}}$ =85.56 kcal/mol (evaluated at 0 K), $\Delta U_{\text{N-H}}$ =101.10 kcal/mol (evaluated at 298.15 K) and $\Delta U_{\text{C-Cl}}$ =81.74 kcal/mol (evaluated at 0 K) [32]. For the MD simulations of the water permeability, three independent slab model systems were prepared by slicing the bulk model in parallel in three different planes, *x*-*y*, *y*-*z* and *z*-*x*, and were equilibrated with additional water regions for 30 ns at 300 K in the NVT ensemble.

3.3. Results and Discussion

3.3.1. Formation Process of Amide Bonds and Polymerized Membrane

Figure 3.4 shows the number changes in amide bonds for the bulk membrane models with four different MPD/TMC ratios, 1:4, 1:1, 3:2 and 4:1, during the hybrid MC/MD reaction simulations. The curves were obtained as the averages of five bulk membrane models simulated from the different initial structures in each the four ratios. For all four ratios, it was found that the formation of amide bonds was almost finished by 500 MC/MD cycles at the latest. After that, while amide bonds seemed to be scarcely created for the ratios 1:4 and 4:1, those numbers for 1:1 and 3:2 increased very slowly to converge to 500 at 2000 MC/MD cycles. Accordingly, it can be recognized that each of the four systems reached an equilibrium state, meaning that the 2000 MC/MD cycles should be enough to complete the polymerized membrane formation.

Table 3.1 shows the calculated results of the numbers of amide bonds in the bulk membrane models with four different MPD/TMC ratios at 2000 MC/MD cycles, and

their corresponding potential maximum. Those numbers in the bulk membrane models with the MPD/TMC ratios of 1:4 and 4:1 were, on average, 199 ± 1 and 298 ± 1, respectively, and correspond reasonably well to the potential maximum numbers of 200 and 300 in the ratios 1:4 and 4:1, respectively. This is because if either the number of MPD or TMC monomers is larger in the reaction mechanism of the present IP, the mutual steric hindrance among the produced polymer chains would not occur due to the relative difference in the numbers of monomers. In fact, these remaining monomers with relatively higher diffusivity than polymers are able to easily approach the counter functional groups, i.e., the amine or acyl chloride groups, in the nascent polymers. Accordingly, it is concluded that MPD or TMC monomers in these ratios can make amide bonds until each potential maximum number is attained in the hybrid MC/MD reaction simulation.

On the other hand, in the bulk membrane models with the MPD/TMC ratios 1:1 and 3:2, the calculated numbers of amide bonds were, on average, 479 ± 10 and 502 ± 6, respectively (Table 3.1). However, the potential maximum numbers with the ratios 1:1 and 3:2 are 500 and 600, respectively. Thus, it was found that neither of the calculated numbers of amide bonds in the ratios reached their corresponding potential maximums, especially with the ratio 3:2, leading to large differences between the calculated and potential maximum numbers. This is likely because the steric hindrance becomes significantly large among the polymer chains with various lengths, and few monomers remain in the whole system (see Figure 3.5). Thus, it can be expected that the steric hindrance in the polycondensation reaction must be treated effectively in the newly developed hybrid MC/MD reaction simulation for polymers.

Figures 3.5(a) to (h) show eight typical structural snapshots during the

polymerization process by the hybrid MC/MD reaction stimulation where the polymer chains elongate gradually by forming additional amide bonds to finally become the bulk membrane model with the MPD/TMC ratio 1:1. From these snapshots, we can recognize that, as the polycondensation reaction proceeds, the numbers of short polymer chains that consist of less than 50 monomers increase until the 500 MC/MD cycles, and their lengths become longer by forming additional amide bonds bridging between such shorter polymer chains. In a typical bulk membrane model for the MPD/TMC ratio 1:1, it was observed that the membrane finally consisted of three long polymer chains with 311, 56 and 24 monomer units, and other shorter chains including 1 MPD and 17 TMC monomers. In a previous theoretical study, the molecular weight polydispersity of the membrane categorized as a random-branched polymer was analytically understood [33]. In that analysis it was found that as DPC (the degree of the polymer cross-linking) becomes higher, the number of the polymer chains decreases. Because the former three longer chains have relatively higher DPC than the latter ones, the present results may be considered sufficiently comparable with the analytical ones.

In addition, Figure 3.5(i) shows the distribution of the TMC moieties of the cross-linked and linear junctions at the same final membrane configuration (Figure 3.5(h)) obtained by the hybrid MC/MD reaction simulation. In Figure 3.5(i), those TMC moieties with three amide bonds and two amide bonds are shown in red and blue, as the cross-linked and linear junctions, respectively, and were found to be not uniformly distributed in this length scale, leading to the inhomogeneous property of the FT-30 membrane.

Figure 3.6 shows side-by-side stereoview snapshots of the bulk membrane models with four different MPD/TMC ratios, 1:4, 1:1, 3:2 and 4:1, at the 2000 MC/MD cycle.

The bulk membrane models are expressed by smooth molecular surface, using the proven radius of 1.40 Å for water molecules (MPD and TMC monomers not shown). In the bulk membrane models with the ratios 1:1 and 3:2, it was found that there are very many dense spaces consisting of polymer aggregates where the polymer network is densely formed, while there are few sparse spaces, i.e., aggregate pores. Because this theoretical observation is consistent with an experimental report [5], the present computational analysis should become helpful for experimentally exploring such polymer aggregates and aggregate pores. It may be also expected that my membrane models obtained by the hybrid MC/MD reaction simulations reasonably reproduce the actual properties of the porous and inhomogeneous membrane of FT-30 [5,6].

To estimate numerically the ratios of occupancy of such aggregate pores in the bulk membrane models, I calculated the fractional accessible volume (FAV), which corresponds to the ratio of the free volume to the total one [34]. In the present calculations, such free volume was defined as the accessible spaces probed by a hard sphere with the van del Waals radius of a water molecule (1.40 Å). As a result, the averaged FAV values in the bulk membrane models with the MPD/TMC ratios 1:1 and 3:2 were estimated to be 0.08 ± 0.01 and 0.13 ± 0.00, respectively, which are considerably smaller than those of the ratios 1:4 and 4:1 (0.28 ± 0.01 and 0.31 ± 0.00). The free volumes of the former were found to be larger than those of the latter. Therefore, the spatial regions with such relatively small free volume in the membrane should be responsible for the performance of RO.

3.3.2. Microscopic Clarification of the MPD/TMC Mixing Ratios for the Interfacial Polycondensation Reaction Process

Table 3.2 shows the present results of DPC (the degree of polymer cross-linking) and the composition ratios of carbon, oxygen and nitrogen of FT-30 membrane, and the corresponding experimental results. The present values were calculated with each of the four MPD/TMC ratios, 1:4, 1:1, 3:2 and 4:1, and were obtained as the averages of 5 bulk membrane models simulated from the different initial structures with each of the four ratios. It was found that the present results of the MPD/TMC ratios 1:4 and 1:1 show good agreement with the corresponding experimental results obtained by XPS and RBS, respectively [6].

When we take into account the actual mechanism of the IP reaction and experimental treatment of water permeation, it may be considered that unreacted acid chloride groups in the FT-30 membrane are converted into carboxylic groups in the experimental situation [5,6]. Therefore, I regarded the chlorine atoms of acid chloride groups as the oxygen atoms of carboxylic groups for the estimation of the present results. It may also be considered that the remaining monomers of MPD and TMC in the FT-30 membrane essentially flow out. Therefore, these monomers were deleted from the model systems and not included.

To examine the significance of the present simulations, I reconsider the reaction mechanism of the IP in detail. As shown in Figure 3.7, an FT-30 membrane is experimentally formed by IP reaction between the aqueous and organic phase in which MPD and TMC monomers are dissolved, respectively [4]. It is known that there is a

rate-determining step in the IP reaction, which is the diffusion of MPD monomers in the aqueous phase into the organic one [5,18-22]. In fact, this polymerization reaction is promoted by the formation of amide bonds between MPD and TMC monomers, the former diffusing into the organic phase and encountering the latter [5,18-22]. It can be expected, therefore, that the concentration of MPD monomers in the organic phase should become gradually lower in the *z* axial direction (see Figure 3.7).

On the other hand, experimental observations [6,35] have shown that the structure of an FT-30 membrane is divided into two regions: (i) the near-surface active (NSA) region (from the surface of the membrane to ~25 nm depth [35]) consisting of the coating layer and partial active layer and (ii) the interior active (IA) region (from 25 nm to ~141 nm depth [35]) consisting of the active layer including most of the membrane structure (see Figure 3.7). The difference in structural properties between these regions has been observed in some experiments [6,35,36]. Experimental studies by Coronell et al. [6], showed that XPS can be used to characterize the properties of the NSA region in the FT-30 membrane, while RBS can be used to quantify the volume-averaged characteristics of the IA region.

From the results shown in Table 3.2, the reaction mechanism of the IP, and the properties of the experimental method, I determine the MPD/TMC mixing ratio for the FT-30 membrane formation process. It seems that that the NSA region would be formed at the boundary surface between the IA region and the organic phase (see Figure 3.7). In addition, the number density of MPD monomer in the NSA region should be lower than that of TMC monomer due to decrease in the MPD concentration in the organic phase in the *z* axial direction. It is also expected that the number density of TMC monomer in the NSA region would be high because of contact with the organic phase.

On the other hand, because the IA region can be formed at the interface where MPD and TMC monomers are mixed in the same amounts, their number densities in the region should be equal. From the above results, it can be concluded that the IA region in the FT-30 membrane is formed from the initial states with the MPD/TMC mixing ratio 1:1, and then the NSA region is formed with the MPD/TMC mixing ratio 1:4 at the boundary surface between the IA region and the organic phase.

3.3.3. Water Permeability and Fidelity of the Membrane Model

From both the snapshots in Figure 3.6 and the FAV values in subsection 3.3.1, it was found that the bulk membrane models with the MPD/TMC ratios 1:1 and 3:2 have relatively small free volumes in the membranes. From Table 3.2 in subsection 3.3.2, it can be understood that the membrane model with the ratio 1:1 represents the IA region in the FT-30 membrane. On the other hand, because the major part of the FT-30 membrane that salt ions and water permeates into is the IA region, it must be important to investigate the properties of the water permeability using the membrane model with the ratio 1:1 [6]. I therefore made a model system consisting of a slab membrane model sliced out from the MPD/TMC ratio 1:1 bulk model with modification of the amide bond cleavages, and bulk water rearranged on both sides of the slab model as explained in subsection 3.2.3.2 (see Figure 3.3). I then performed a water diffusion (/permeation) simulation through the slab model.

The properties of the water permeability were investigated, and Figure 3.8 shows the number density profile of water molecules in the membrane interior region and bulk

water model. The abscissa of Figure 3.8 is the *z* coordinate originating at the central position of all the atoms forming the whole slab model. The total mass density of constituent atoms in the membrane and the water molecules within a region of ±24.35 Å (corresponding to the total width 48.7 Å of the slab membrane model) (Figure 3.8) was 1.39 g/cm^3, which is in good agreement with the experimental value of the hydrated FT-30 membrane (1.38 g/cm^3) [37].

I further calculated the partition coefficient *K* determined in the following equation (3.12) as another physical quantity for clarifying the properties of the water permeability,

$$K = \frac{\rho_{\mathrm{mbrn}}}{\rho_{\mathrm{bulk}}} \tag{3.12}$$

where ρ_{mbrn} and ρ_{bulk} are the water number densities in the membrane interior region and in bulk water model at equilibrium state, respectively. To estimate the ρ_{mbrn} value, I newly determined a membrane interior region within ±10 Å to prevent the influence of the membrane structure where the intercellular amide bonds were cut artificially. Both ρ_{mbrn} and ρ_{bulk} values were estimated by averaging the number densities in the membrane interior region and in the two regions from +35 Å to +55 Å and from -55 Å to -35 Å, in Figure 3.8, respectively.

As a result, I obtained the partition coefficient *K* of 0.275, which is in good agreement with both the experimental value of 0.29 [37] and the recent theoretical ones (0.21 and 0.30) [7,8]. The former theoretical value of 0.21 was calculated for the same system size as the present one, while the latter value of 0.30 was done for a system that is 8 times larger. From this observation, the present result may be considered to be sufficiently reasonable and therefore the hybrid MC/MD reaction method with an extension to realize the formation of intercellular amide bonds between *real* and *image*

atoms should work very effectively to reproduce the experimental properties in such simulation models with smaller system sizes.

In addition, it is meaningful to note that the present results were obtained by the averages of 15 model systems (=5×3, see subsection 3.2.3), and the standard error of partition coefficient K was ±0.018 (sufficiently small) and, therefore, K can be said to be nearly independent of the initial configurations in the water diffusion simulations through the slab membrane models.

The simulation results for water diffusion through the slab membrane models should be significantly affected by the spatial arrangement in the IA region. However, it was found that not only the DPC and the composition ratios shown in Table 3.2 but also the water number density of the hydrated membrane and the partition coefficient K corresponded to the experimental values quantitatively. Finally, it should be mentioned that the membrane model formed by the hybrid MC/MD reaction method is used to fully reproduce the actual inhomogeneous spatial arrangement of the FT-30 membrane.

3.4. Conclusion Remarks

In this chapter 3, I have discussed the properties of an aromatic polyamide membrane, called the FT-30, that was computationally prepared, investigating the structural characteristics of the membrane at the atomistic level. For that purpose, I performed an atomistic molecular simulation with a hybrid MC/MD reaction method which I have been developing recently to treat complex chemical reaction systems. Using the initial model systems with four different ratios of the constituent MPD and TMC monomers, 1:4, 1:1, 3:2, 4:1, I successfully made polyamide membrane models of FT-30 from the assemblies of these monomers, simulating a succession of amide bond

formations (/condensation reactions). This could be done thanks to the successful extension of the normal hybrid MC/MD reaction method to those polymer systems where such intercellular chemical bonds between *real atoms* in the main cell and *image atoms* in the image cells can be formed over the periodic boundaries, constructing a more realistic polymer model extending to a sufficiently large dimension without discontinuity of the polymer network between adjacent cells. (I propose naming this treatment the *minimum bond convention* (MBC) after the minimum image convention (MIC) [17] in traditional molecular simulation.) Then, by comparing the present results of the degree of polymer cross-linking (DPC) and the composition ratios of constituent atoms in the FT-30 membrane with the corresponding experimental results [6], I clarified the MPD/TMC mixing ratios in the near-surface active (NSA) and interior active (IA) regions, which were explained in connection to the membrane formation mechanism in the interfacial polycondensation (IP) reaction.

Further, to investigate the water permeability through the membrane, I executed water diffusion simulations using the slab membrane model with the MPD/TMC ratio 1:1. This is because the permeability is determined by the proper diffusion through the major part of the membrane, whose MPD/TMC mixing ratio was found to be 1:1 from the comparison of the simulation results with the experimental ones [6]. In fact, to prepare the slab membrane model, I cleaved intercellular amide bonds between *real atoms* and *image atoms* along one of the orthogonal coordinate axes of the bulk membrane model. I obtained the slab membrane model after additive chlorine and hydrogen atoms were suitably bonded to the resulting monovalent carbon and nitrogen atoms. Then, I generated the target model system by arranging the bulk water on both sides of the slab model along the same coordinate axis.

My calculated results of the total mass density of the hydrated membrane and the partition coefficient *K* obtained through the water diffusion simulations showed good agreement with the corresponding experimental results [37], although the calculated results should be significantly affected by the inhomogeneous arrangement of the membrane. Consequently, it was confirmed that my membrane model constructed by the present method was reproduced with sufficient fidelity to the actual membrane.

Although the model systems in this study should be uniformly prepared in the unit cell (48.7×48.7×48.7 $Å^3$), this size is in fact insufficient in dealing with the targeted system corresponding to the actual material, even if the PBC might be applied legitimately. Therefore, the model systems obtained by performing the hybrid MC/MD reaction simulation can be considered identical to a partial sampling of the equilibrium structure at chemical equilibrium state. Nevertheless, because both the scale sizes of the actual NSA and IA regions are 1 order of magnitude larger than the present simulation box, the present model systems of aromatic polyamide membranes may be regarded as local equilibrium structures in their regions. Thus, it is meaningful to note that application of the present method to the FT-30 membrane formation was successful and the membranes obtained could be used to simulate a stable spatial structure in the local equilibrium state under a nonequilibrium stationary state of permeation.

In the future, by performing saltwater diffusion simulation through an RO membrane such FT-30 prepared by the present method, I will evaluate the free energy profiles of both water and salt ions for the membrane systems. In this way, I would like to reveal the microscopic reasons for physicochemical phenomena that are not well understood, i.e., how water can permeate membranes with a high flux while salt ions are largely rejected. The method I have developed—atomistic reaction simulation using

the hybrid MC/MD reaction method—may be a unique approach complementary to experiments that will support the design of new materials with high performance as RO membranes.

References

[1] F. Davis, J. Polymer Chemistry; Oxford University Press, Inc.: New York, 2004.

[2] E. Charles, Carraher, Jr. Seymour/Carraher's Polymer Chemistry, 7th ed.; CRC Press: Boca Raton, 2008.

[3] J. M. G. Cowie, V. Arrighi, Polymers: Chemistry and Physics of Modern Materials; CRC Press: Boca Raton, 2007.

[4] FILMTEC Reverse Osmosis Membranes Technical Manual, Form No. 609-000710109; Dow Water Solutions: Midland, MI.

[5] S. H. Kim, S. Y. Kwak, T. Suzuki, Environ. Sci. Technol. 39 (2005) 1764.

[6] O. Coronell, B. J. Marinas, D. G. Cahill, Environ. Sci. Technol. 45 (2011) 4513.

[7] E. Harder, D. E. Walters, Y. D. Bodnar, R. S. Faibish, B. Roux, J. Phys. Chem. B 113 (2009) 10177.

[8] Y. Luo, E. Harder, R. S. Faibish, B. Roux, J. Membr. Sci. 384 (2011) 1.

[9] Z. E. Hughes, J. D. Gale, J. Mater. Chem. 20 (2010) 7788.

[10] Z. E. Hughes, J. D. Gale, J. Mater. Chem. 22 (2012) 175.

[11] O. Coronell, M. I. Gonzalez, B. J. Marinas, D. G. Cahill, Environ. Sci. Technol. 44 (2010) 6808.

[12] H. Ebro, Y. M. Kim, J. H. Kim, J. Membr. Sci. 438 (2013) 112.

[13] K. Moorthi, K. Kamio, J. Ramos, D. N. Theodorou, AIP Conf. Proc. 1518 (2013) 455.

[14] M. Zhang, F. Yuen, P. Choi, Macromolecules 39 (2006) 8517.

[15] M. Nagaoka, Y. Suzuki, T. Okamoto, N. Takenaka, Chem. Phys. Lett. 583 (2013) 80.

[16] N. Takenaka, Y. Suzuki, H. Sakai, M. Nagaoka, J. Phys. Chem. C 118 (2014) 10874.

[17] M. P. Allen, D. J. Tildsley, Computer Simulation of Liquids; Clarendon Press: Oxford, 1987.

[18] V. Freger, Langmuir, 19 (2003) 4791.

[19] V. Enkelmann, G. Wegner, Makromol. Chem. 177 (1976) 3177.

[20] L. J. J. M. Janssen, K. te Nijenhuis, J. Membr. Sci. 65 (1992) 59.

[21] S. K. Karode, S. S. Kulkarni, A. K. Suresh, R. A. Mashelkar, Chem. Eng. Sci. 52 (1997) 3243.

[22] J. Ji, J. M. Dickson, R. F. Childs, B. E. McCarry, Macromolecules 33 (2000) 624.

[23] D. W. Heerman, Computer Simulation Methods in Theoretical Physics, 2nd ed.; Springer: Berlin, 1990.

[24] N. Metropolis, A. W. Rosenbluth, M. N. Rosenbluth, A. H. Teller, E. Teller, J.

Chem. Phys. 21 (1953) 1087.

[25] S. Qiu, L. Wu, L. Zhang, H. Chen, C. Gao, J. Appl. Polym. Sci. 112 (2009) 2066.

[26] J. Wang, R. M. Wolf, J. W. Caldwell, P. A. Kollman, D. A. Case, J. Comp. Chem. 25 (2004) 1157.

[27] D. A. Case et al., AMBER 9, University of California, San Francisco, 2006.

[28] A. Jakalian, D. B. Jack, C. L. Bayly, J. Comput. Chem. 23 (2002**)** 1623.

[29] H. J. C. Berendsen, J. P. M. Postma, W. F. van Gunsteren, A. DiNola, J. R. Haak, J. Chem. Phys. 81 (1984) 3684.

[30] T. Darden, D. York, L. Pedersen, J. Chem. Phys. 98 (1993) 10089.

[31] J. P. Ryckaert, G. Ciccotti, H. J. C. Berendsen, J. Comput. Phys. 23 (1977) 327.

[32] The Chemical Society of Japan, Kagaku Binran, 5th ed.; Maruzen: Tokyo, 1993.

[33] Y. Matsushita, T. Sato, T. Kanaya, K. Ito, H. Watanabe, K. Tanaka, T. Shimomura, T. Inoue, Structures and Physical Properties of Polymers; Kodansha Press: Tokyo, 2013.

[34] D. Hofmann, M. Entrialgo-Castano, A. Lerbret, M. Heuchel, Y. Yampolskii, Macromolecules 36 (2003) 8528.

[35] O. Coronell, B. J. Marinas, X. Zhang, D. G. Cahill, Environ. Sci. Technol. 42 (2008) 5260.

[36] C. Y. Tang, Y.-N. Kwon, J. O. Leckie, J. Membr. Sci. 287 (2007) 146.

[37] B. Mi, D. G. Cahill, B. J. Marinas, J. Membr. Sci. 291 (2007) 77.

FIGURES

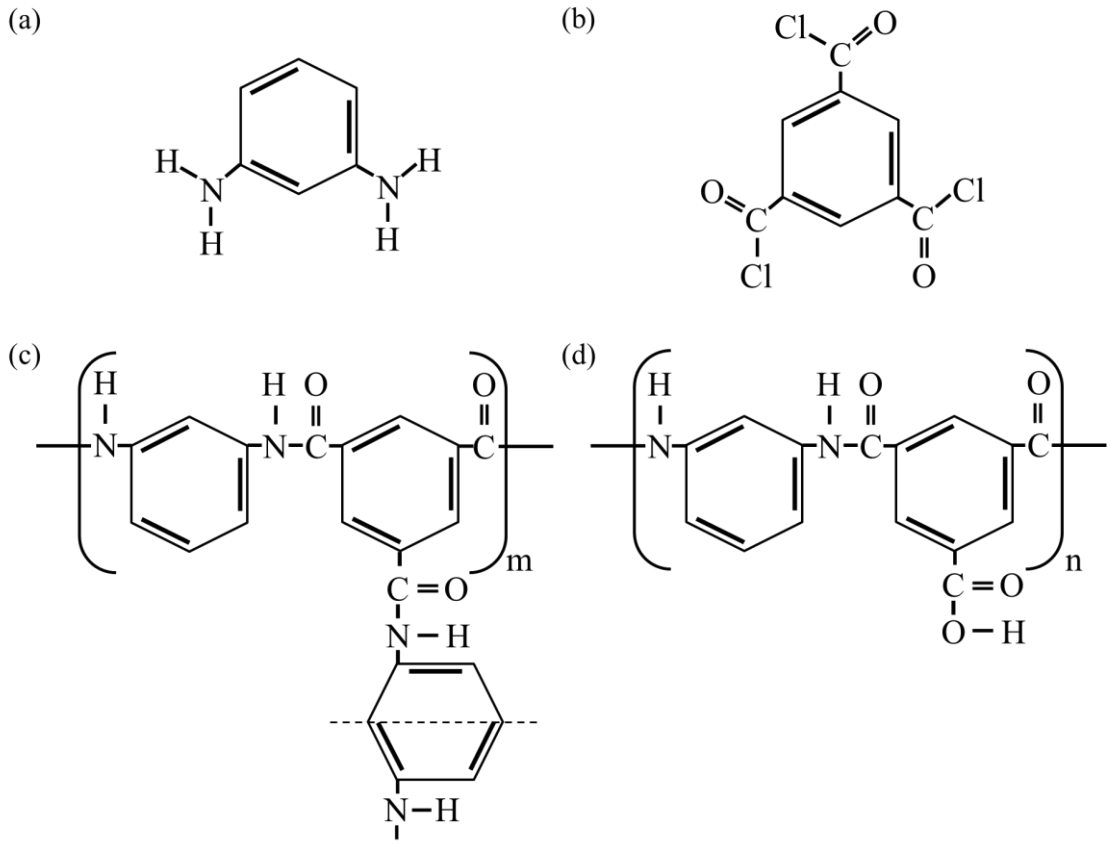

Figure 3.1. Monomers of (a) MPD (meta-phenylenediamine) and (b) TMC (benzene 1,3,5- tricarboxylic acid chloride), and the repeating units of (c) the cross-linked and (d) the linear portions in the FT-30 membrane.

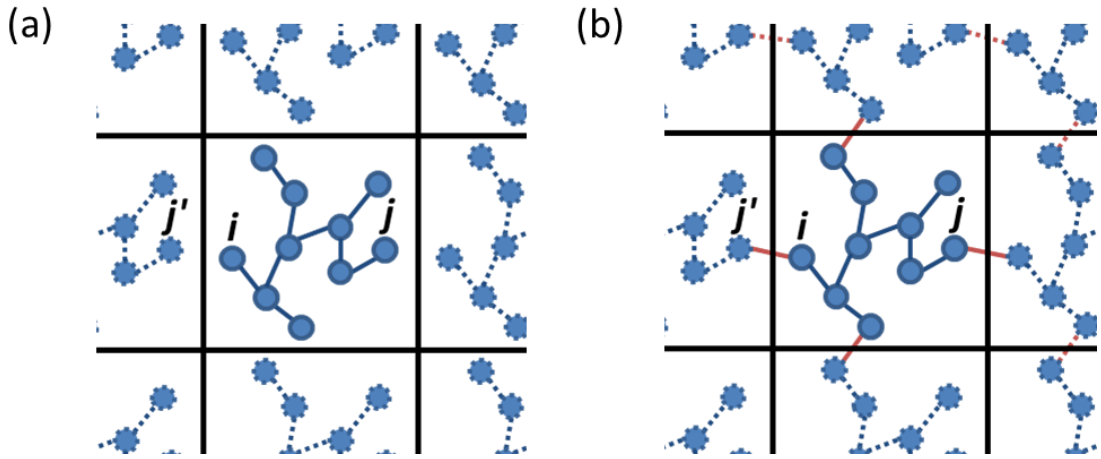

Figure 3.2. Schematic view of (a) chemical bonds among "real" atoms only in the main cell, i.e., intracellular chemical bonds, and (b) those bonds with additional bonds over the periodic boundaries between the main and image cells, i.e., intercellular chemical bonds.

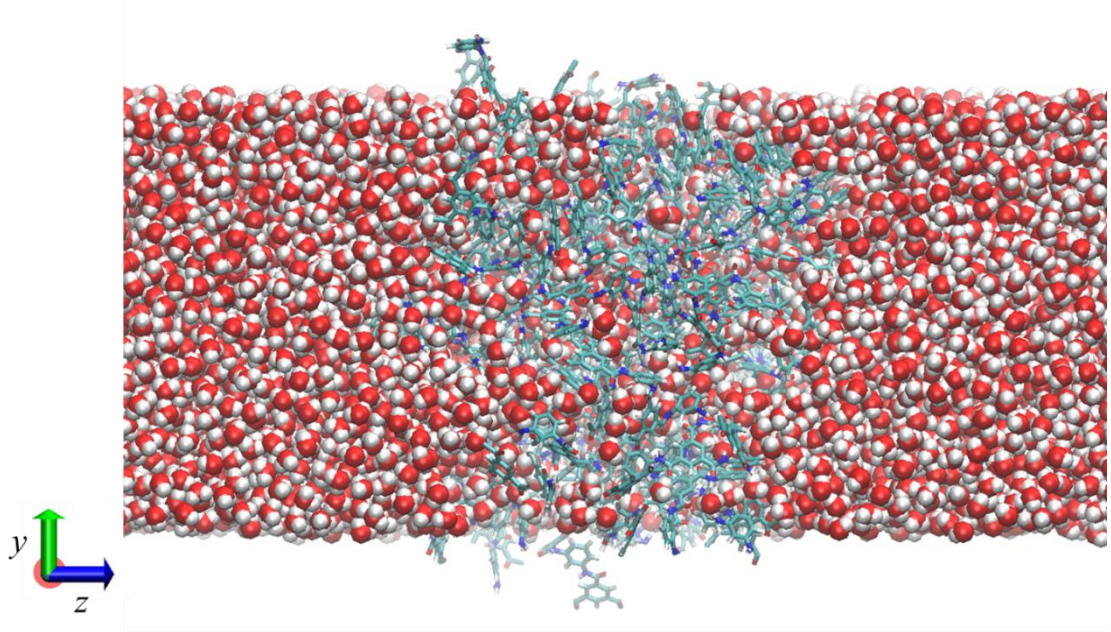

Figure 3.3. A typical snapshot of the equilibrium state of the model system consisting of the slab membrane model and bulk water arranged on the both sides of the slab model. The slab membrane model and all water molecules are expressed by ball and stick and sphere models, respectively.

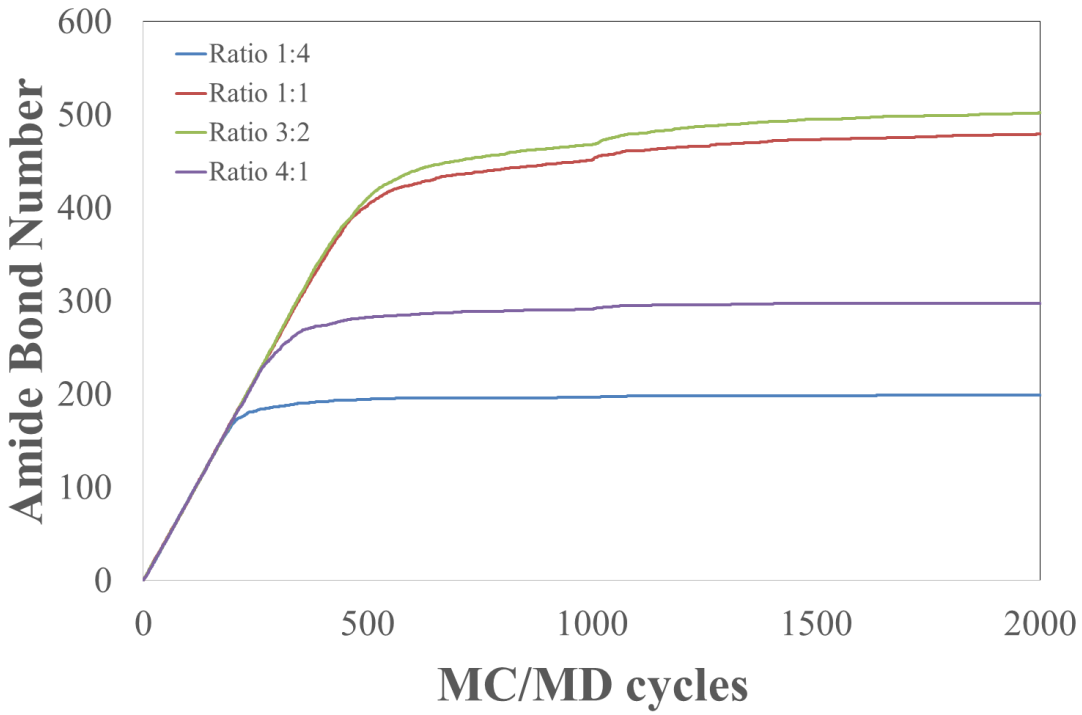

Figure 3.4. Number changes of amide bonds for the bulk membrane models with four different MPD/TMC ratios, 1:4, 1:1, 3:2 and 4:1, during the hybrid MC/MD reaction simulations. The curves were obtained as the averages of five bulk membrane models simulated from the different initial structures in each of the four ratios.

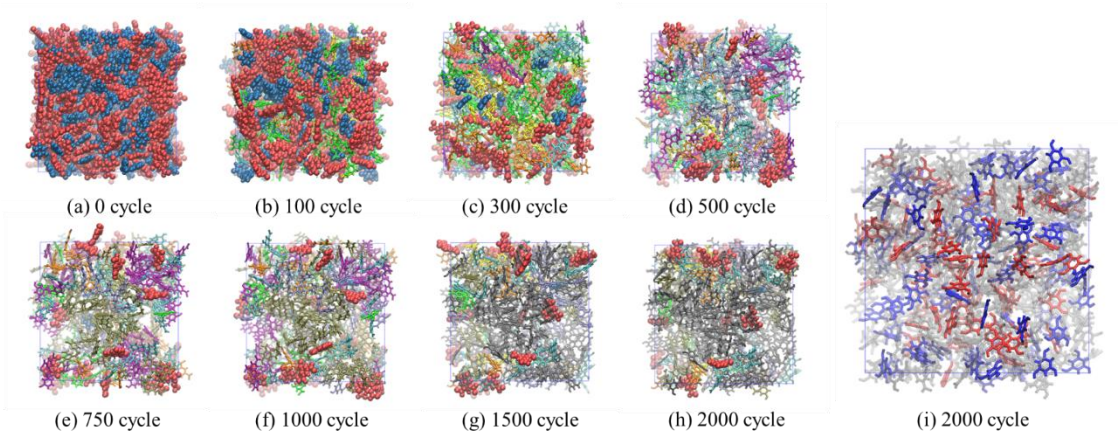

Figure 3.5. Eight typical structural snapshots during the polymerization process by the hybrid MC/MD reaction stimulation where the polymer chains elongate gradually by forming additional amide bonds to finally become the bulk membrane model with the MPD/TMC ratio 1:1; (a) 0 MC/MD cycle, (b) 100 MC/MD cycles, (c) 300 MC/MD cycles, (d) 500 MC/MD cycles, (e) 750 MC/MD cycles, (f) 1000 MC/MD cycles, (g) 1500 MC/MD cycles, (h) 2000 MC/MD cycles (blue, MPD monomers; red, TMC monomers; green, dimers; orange, trimers; yellow, tetramers; light blue, 5-10 monomer units; purple, 11-20 monomer units; bluish purple, 21-50 monomer units; ocher, 51-100 monomer units; brown, 101-250 monomer units; black, 251-500 monomer units). One snapshot distribution of TMC moieties as the cross-linked and linear junctions; (i) 2000 MC/MD cycles (at the same structural configuration as that of (h)) (red, 3-amide-bonds-formed TMC (cross-linked junction); blue, 2-amide-bonds-formed TMC (linear junction); semitransparent black, MPD and TMC monomers, and all polymer chains).

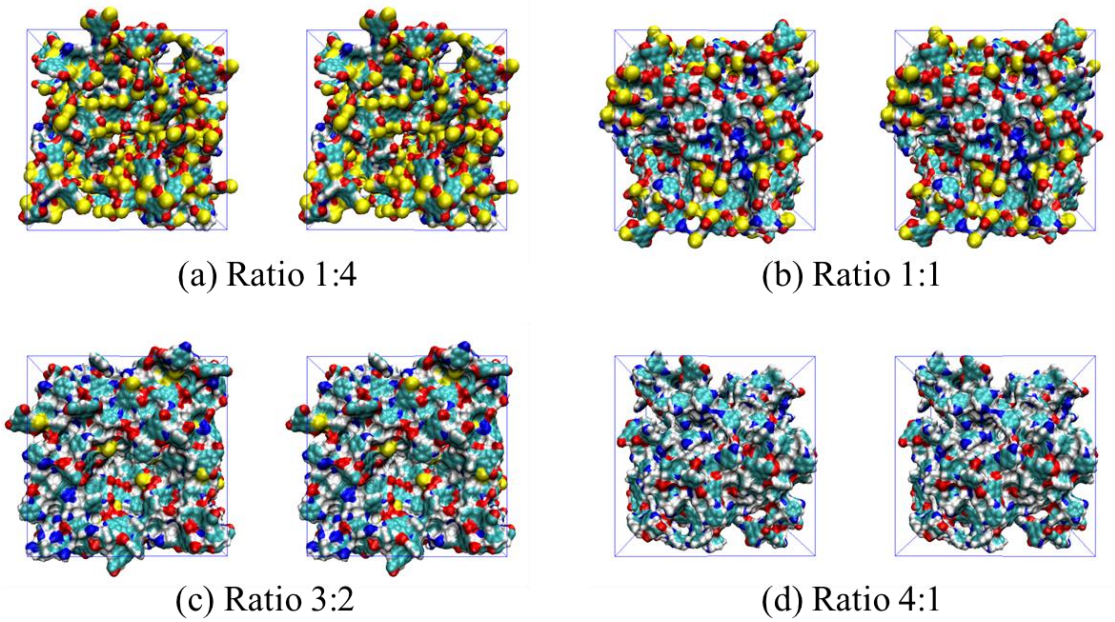

Figure 3.6. Side-by-side stereoview snapshots of the bulk membrane models with four different MPD/TMC ratios at 2000 MC/MD cycles; (a) ratio 1:4, (b) ratio 1:1, (c) ratio 3:2, (d) ratio 4:1. The bulk membrane models are expressed by the smooth molecular surface, using the probe radius 1.4 Å of a water molecule (MPD and TMC monomers not shown) (white, hydrogen atom; cyan, carbon atom; blue, nitrogen atom; red, oxygen atom; yellow, chlorine atom).

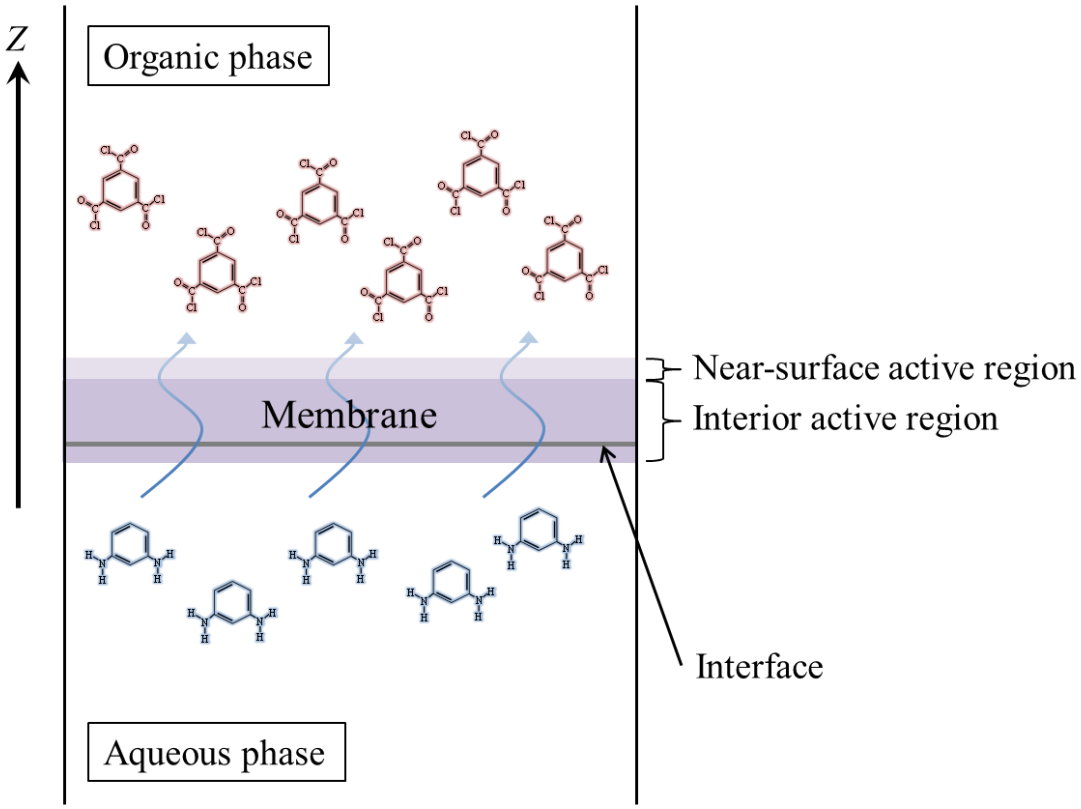

Figure 3.7. Schematic representation of the reaction mechanism of the interfacial polycondensation in the experimental treatment to produce FT-30 membrane.

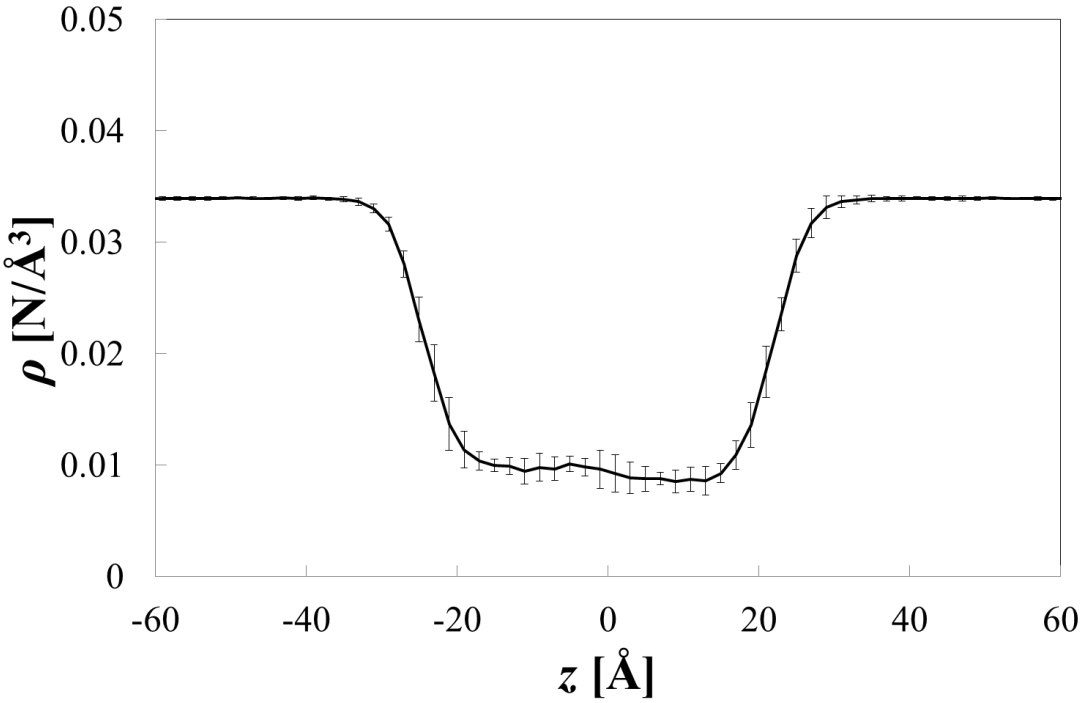

Figure 3.8. Number density of the water molecule profile in the region of the slab membrane and bulk water as a function of *z* coordinate originating at the central position of all the atoms forming the whole slab model.

TABLES

Table 3.1. Calculated Results of the Numbers of Amide Bonds in the Bulk Membrane Models with Four Different MPD/TMC Ratios, 1:4, 1:1, 3:2 and 4:1, at 2000 MC/MD Cycles, and Their Corresponding Potential Maximums.

	ratio 1:4	ratio 1:1	ratio 3:2	ratio 4:1
number calculated	199 ± 1[a]	479 ± 10[a]	502 ± 6[a]	298 ± 1[a]
potential maximum number	200	500	600	300

[a]The calculated results were obtained as the averages of five sample models.

Table 3.2. Computational Values of the Degree of Polymer Cross-linking (DPC); the Composition Ratios of Carbon, Oxygen and Nitrogen; and Their Experimental Values in the FT-30 Membrane.

	present[a]				expt[b]	
	ratio 1:4	ratio 1:1	ratio 3:2	ratio 4:1	XPS	RBS
DPC	94.3 ± 0.3	96.9 ± 0.2	99.0 ± 0.1	100.0 ± 0.0	91.7 ± 3.9	96.2 ± 0.2
%C	67.8 ± 0.1	71.6 ± 0.2	73.6 ± 0.1	74.9 ± 0.0	71.0 ± 1.6	71.0 ± 1.2
%O	25.7 ± 0.3	18.6 ± 0.3	14.2 ± 0.1	9.4 ± 0.0	26.2 ± 1.7	17.4 ± 0.4
%N	6.5 ± 0.1	9.9 ± 0.1	12.2 ± 0.0	15.6 ± 0.1	2.8 ± 1.7	11.5 ± 0.6

[a]The calculated results were obtained as the averages of five sample models. [b]The experimental results were obtained by XPS and RBS.[6]

Chapter 4

On Electrolyte-Dependent Formation of Solid Electrolyte Interphase Film in Lithium-Ion Batteries: Strong Sensitivity to Small Structural Difference of Electrolyte Molecules

4.1. Introduction

Rechargeable lithium-ion batteries (LIBs) play a vital role in our daily life as the prominent power sources for various electronic devices. The performance of current LIB with liquid electrolytes, e.g., ethylene carbonate (EC) and propylene carbonate (PC), is strongly dependent on the formation of a stable solid electrolyte interphase (SEI) film on the electrode surfaces, which is formed as a result of reduction or oxidation of the electrolyte solvents and lithium salts [1-3]. In particular, on the anode surface during the initial lithiation cycle, a number of reaction products of electrolyte reduction form a thin SEI film, which should realistically protect the electrolyte from further reductive decomposition during the subsequent cycles. At the same time, such an SEI film enables only Li^+ cations to exchange between the anode and electrolyte in the charge-discharge cycles. To build the high-performance LIB, it is, therefore, crucial to understand the microscopic formation processes and structures of the SEI film because its characteristic is directly related to the life time of the batteries.

It is generally accepted that the SEI film contains inorganic salts (e.g., Li_2CO_3, LiF), organic ones (e.g., $ROCO_2Li$) [1-3] and its inner layer is primarily comprised of inorganic salts, while the outer layer is thought to be done largely of organic ones [4-6]. Among the organic solvents, PC is attractive as a nonaqueous electrolyte owing to its wide liquid temperature range. For example, PC is known to be more efficient than other solvents in the sodium-ion batteries (NIB) with the hard-carbon electrode, which have been recently attracted special attention due to the increase in the cost of Li [7]. However, when pure PC-based electrolyte is used in the LIB with the graphite anode, no effective SEI film is formed on the graphite surface despite the close structural similarity between EC and PC [1,2]. In fact, according to some experimental studies, it is generally believed that this can be attributed to the gas evolution upon decomposition of solvents and the co-intercalation of PC molecules with larger molecular sizes [1,2]. However, it is still difficult to identify the microscopic origins only by experiments since we lack the techniques to directly observe the transient processes of the SEI film formation on the graphite anode surface in the LIB.

Under the circumstances, some theoretical studies have provided the important insight into the elementary reaction processes [8-13] and initial stage (~ps) in the SEI film formation [14-17]. The quantum chemical (QC) calculations have focused on the elementary reactions in the SEI film formation by using the dielectric continuum model (DCM), which approximately assume the bulk liquid regions [8-11]. The reduced EC (/PC) molecules have a negative charge and can be expected to be associated with a Li^+ cation, yielding the complex denoted as the Li^+/close-EC^- (/-PC^-) radical. The cyclic radical is then thought to undergo a ring-opening reaction forming Li^+/open-EC^- (/-PC^-) one, which is significantly lower in energy than the close form. Such free energy of

activation in the EC-based electrolyte was quantitatively estimated to be ~4.8 kcal/mol by using the ab initio molecular dynamics (AIMD) method with blue-moon ensemble technique, and thus, the one-electron (1e) reduction process could be quite fast [12].

Then, the Li^+/open-EC^- (/-PC^-) radicals would form the dilithium butylene dicarbonate, i.e., Li_2BDC (/2,3-dimethyllithium butylene dicarbonate, i.e., Li_2DMBDC), which have been proposed as one of the major components in the anode SEI film [1,2] resulting from combination reactions of pairs of them via the radical polymerization [8,10,13]. From the viewpoint of the free energies of reaction, Li_2BDC (/Li_2DMBDC) was found to be most favorable although the free energy of activation has not been provided [8,10]. However, according to the gas-phase simulation with the reaction force field (ReaxFF) that those parameters are adjusted so as to reproduce the QC calculations, the energy of activation of Li_2BDC via the radical polymerization of Li^+/open-EC^- radicals was estimated to be ~3.5 kcal/mol, which is rather smaller than those of other polymerization reactions [13].

While providing useful predictions, such QC calculations necessarily ignore the presence of the electrodes. However, with the development of computational technology, the AIMD method has been recently applied to simulate chemical reactions on several explicit electrode surface [14-16] Leung and co-workers have investigated the decomposition mechanism of the EC solvent and concluded that the fast e^- transfer and EC electrochemical reactions occur to form either CO + $OC_2H_4O^{2-}$ or C_2H_4 + CO_3^{2-} via the two-electron (2e) reductions at the initial stage of SEI film formation when the fully lithiated graphite (LiG) [18] was employed [14]. Furthermore, according to the AIMD studies by Ganesh and co-worker, it was found that the PF_6^- salt anions are also doubly reduced on the LiG, and decompose into PF_3 gases and LiF complexes [16]. These

computational results strongly support the experimental predictions that the electrolyte solvents and lithium salts are reduced on the graphite anode surface, forming the main components of the SEI films [1-3]. Such AIMD studies are therefore indispensable to investigate microscopically elementary reaction processes of electrolyte solvents and lithium salts on the explicit electrode surface, since they are not easy to be observed solely by the experiments.

As indicated by the previous QC studies, there is nothing but very small difference in the energy diagrams of the elementary reaction processes involved in the SEI film formation between the EC- and PC-based electrolytes [8,10]. To theoretically understand why those SEI films are so different, therefore, more long-term atomistic reaction simulations must be done, considering a necessary and sufficient set of multiple elementary reaction processes simultaneously. In fact, it is true that the AIMD method can provide quite accurate computational predictions. However, the time-scale relevant to the SEI film formation, unfortunately, should be considerably longer in experimental observations than that which the AIMD method can reach under the current computational development. Under the circumstances, I have recently proposed a new atomistic reaction simulation method, i.e., the hybrid Monte Carlo (MC)/molecular dynamics (MD) reaction method (or the Red Moon method), in order to deal with the long-term characteristics of the sub-micro scale structure produced by successive complex chemical reaction processes (discussed in detail in chapter 2) [19]. Its major goal is to understand the reaction mechanism in complex chemical reaction systems from the viewpoint with a little larger and longer space-time scale, considering complementarily the inevitable microscopic information of such elementary reaction processes obtained by the QC and AIMD studies.

In this chapter 4, to investigate the microscopic differences in the SEI film formation between the EC- and PC-based electrolytes on the graphite anode, I have performed the atomistic reaction simulations via the hybrid MC/MD reaction method. First, I have demonstrated the SEI film formation processes in both the EC- and PC-based electrolytes. Then, I have investigated the density distributions and compositions of constituent molecules in the resulting SEI films, and finally discussed the atomistic structural differences between the EC- and PC-based SEI films. I explain both the hybrid MC/MD reaction method and computational models in section 4.2, and provide the results and discussion in section 4.3 and the conclusion in section 4.4.

4.2 Methods

4.2.1 Model Systems

The present atomistic reaction simulations were executed in ~1.1 mol/L $LiPF_6$ EC- and PC-based electrolyte with the graphite anode, whose model simulation system is shown in Figure 4.1. The graphite surface was modeled by a pile of graphene sheets, i.e., ten layers of carbon atoms. The interlayer distance was kept 3.7 Å, corresponding to the separation in the LiG [18]. For simplicity, the graphite anode was fixed at present during the atomistic hybrid MC/MD reaction simulations, and the intercalation of Li^+ into the graphite was restricted by adding the potential to focus only on the SEI film formation on the graphite anode surface. A vacuum region is assumed adjacent to the electrolyte according to the previous computational treatment for the ionic liquid with the charged graphite surface [20]. To describe the electric potential difference between

the electrolyte and graphite anode, the simulations were performed with the negatively charged graphite [20]. A single point charge was placed at the center of each carbon atom on the graphite surface, and its magnitude is adjusted so that the electric potential difference becomes ~2.0 V in the initial system. The total charge is -2 e, which corresponds to -2.5 μC/cm^2. Accordingly, the system was neutralized by adding positive ions (Li^+) into the bulk electrolyte. As a result, the EC-based electrolyte consist of 850 EC molecules, 69 Li^+ cations and 67 PF_6^- anions, while in the PC-based one, there are 850 PC molecules, 87 Li^+ cations and 85 PF_6^- anions in a rectangular simulation cell with linear dimensions 34.08 Å × 37.00 Å × 300.0 Å, respectively.

4.2.2. The Hybrid MC/MD Reaction Method

To investigate the SEI film formation on the graphite anode, I have employed the hybrid MC/MD reaction method (discussed in detail in chapter 2) [19]. In the present chapter, I have considered the reaction scheme in Figure 4.1, consisting of a list of elementary reaction processes necessary and sufficient to simulate the SEI film formation. These processes were introduced based on the previous experiments [1,2] and theoretical studies [8-17], where both reactions of the reduction and polymerization are included. Before executing the simulation, for all the molecules in the reaction scheme, we need to prepare the atomic potential parameters in the molecular mechanical (MM) force field [21], e.g., the force constants, Lennard-Jones parameters and atomic charges. In the simulation, when the chemical reaction occurs, not only the atomic potential parameters but also the potential function forms (i.e., intramolecular or intermolecular ones) of the reactant are replaced by those of the product.

The hybrid MC/MD reaction method consists of a combination of the following types of processes (see Figure 2.1):

1. Equilibrate the whole system through the classical NVT-MD simulation and select an initial configuration state *r*.
2. Generate reaction steps with the NVT-MC procedure and classical NVT-MD simulation, consisting of the following steps:
   (i) Search a pair (/pairs) of "reactive" atoms among reactant molecules with the whole system in a given configuration state *r* according to some criteria for whether possible chemical reactions might plausibly occur. In the present chapter, the criterion for a candidate pair was taken to be whether the interatomic distance is less than the sum of their van der Waals (vdW) radii. As a result, a set of candidate pairs which are able to generate the chemical reactions are obtained in a given configuration state *r*.
   (ii) Randomly select a pair from among the set of candidate ones, assuming that each has a corresponding relative weight of selection *R*, which is estimated in advance [19]. If there is not such a pair, execute a short NVT-MD simulation instead of the following step (iii) and (iv) to update the configuration state. In the present chapter, *R* was able to be taken a common constant 1, meaning to the equal relative probability, for any chemical reactions. This is because the free energies of activation of the elementary reactions in the EC-based electrolyte was almost the same as those in the PC-based one [8,10].
   (iii) Then switch the atomic potential parameters and potential function forms of the reactant to the product ones, and virtually react it to generate a possible

configuration state *s*, relaxing the whole system to obtain the state *s* through a short NVT-MD simulation.

(iv) Compute the energy change of the system ΔU_{rs} (= U_s - U_r) and accept (or reject) the reaction step according to the transition probability $W_{r\to s}$ under the Metropolis scheme [21-23],

$$W_{r\to s} = \min\left\{1, \exp\left[-\beta \Delta U_{rs}\right]\right\}. \tag{4.1}$$

In the present chapter, ΔU_{rs} is approximately estimated as follows,

$$\Delta U_{rs} = \Delta U_{rs}^{\mathrm{MM}} + \Delta U_0^{\mathrm{reac}}, \tag{4.2}$$

where $\Delta U_{rs}^{\mathrm{MM}}$ is the naïve difference of local potential energies obtained in the MM force field, meaning a change of the corresponding atomic potential parameters and potential function forms together with a proper correction of the "zero" point of energy by the corresponding potential energy of reaction $\Delta U_0^{\mathrm{reac}}$. Table 4.1 lists $\Delta U_0^{\mathrm{reac}}$ for the present elementary chemical reaction processes in gas phase at B3LYP/6-31+G(d) level of theory [11].

3. If the molecular mixture composition might scarcely change, then stop. Otherwise return to process 2.

The cycle consisting of the three different types of processes is called an "MC/MD cycle" hereafter. In the present simulations, any EC (/PC) molecules, LiEC (/LiPC) complexes and PF_6^- anions are regarded candidate reactants of the reduction reaction when they get closer to the graphite anode surface, meaning that each distance of closest approach between their constituent atoms and some carbon atoms on the graphite anode surface becomes within the critical distance (the sum of vdW radii) in each MC/MD

cycle. On the other hand, a pair of LiEC (/LiPC) complexes also becomes the candidate reactants of the radical polymerization reaction when their radical carbon atoms get close to each other within the critical distance (the sum of vdW radii). Then, only one among the candidate reactants is randomly selected to generate a chemical reaction through the NVT-MC procedure in each MC/MD cycle. For example, an EC (/PC) molecule can become an open form of radial anion, i.e., EC^- ($/PC^-$), virtually injected each by one electron. It should be noted that the charge transfer due to the reduction reaction is simply represented by changing the atomic potential parameters (i.e., atomic charges) of reactant to product ones, adding at the same time the corresponding potential energy of reaction evaluated by the QM calculation. Such an EC^- ($/PC^-$) anion (initially uncoordinated to Li^+) can become a LiEC (/LiPC) complex by their binding to Li^+ cations. Additionally, a LiEC (/LiPC) complex can decompose to form a gaseous C_2H_4 ($/C_3H_6$) molecule and a stable Li_2CO_3 complex, virtually injected each by another electron. At the same time, a pair of LiEC (/LiPC) complexes can become a Li_2BDC ($/Li_2DMBDC$) dimer via their radical polymerization. On the other hand, a PF_6^- anion can decompose to form a gaseous PF_3 molecule and three LiF complexes, virtually injected each by two electrons.

As is the case in real chemical reacting systems, each chemical reaction process in the reaction scheme is randomly repeated by natural selection via the hybrid MC/MD reaction method, so as to assure that the SEI films would be microscopically formed spontaneously. Since these processes are randomly selected among the possible ones in each MC/MD cycle, their frequencies of appearance should be determined naturally in proportion to the instantaneous concentration of the reactant molecules during the SEI film formation process. The natural introduction of such concentration dependence into

the reaction simulations must be essential to reproduce realistically the SEI film formation, including the multiple elementary reaction processes simultaneously.

4.2.3. Computational Details

The generalized AMBER force field (GAFF) [24] was used for the electrolyte and reaction products, with the exclusion of the PF_6^- anion. The force field of the PF_6^- anion was obtained by reference to the previous theoretical study [25]. The atomic point charges are obtained with the RESP method at the B3LYP/6-31+G(d) level of theory. In this case, the charges of the electrolyte solvent (EC and PC) molecules were legitimately scaled (the scaling parameter 0.8) so as to reproduce the experimental dipole moments [2]. The mass densities of the pure EC and PC solvent without the graphite electrode were 1.31 and 1.21 g/cm^3 by the NPT-MD simulations at 1 atm, being in quite good agreement with the experimental values 1.30 and 1.21 g/cm^3 [2], respectively. In addition, those calculated diffusion constants at 298 K were 4.9×10^{-10} and 3.7×10^{-10} cm^2/s in pure EC and PC solvent, which are in good agreements with the experimental values 8.0×10^{-10} cm^2/s (at 313 K) [26] and 4.9×10^{-10} cm^2/s (at 298 K) [27], respectively.

The SANDER module of AMBER 9 package [28] was used to execute all the atomistic simulations. The SHAKE method was used to constrain the hydrogen-heavy atom bond distances and the integration time-step was 1 fs. The temperature was maintained at 298 K with the Berendsen thermostat. Then, a production run of the hybrid MC/MD reaction simulation was executed for 2000 MC/MD cycles. The MD simulation time for relaxation in one MC/MD cycle for a trial of chemical reaction, was set to 4 ps. To check the initial structure dependence, the present simulations were performed by

using a set of 10 different initial configurations, and those standard errors were estimated with the two-sided 95 % confidence interval (in Figures 4.4 and 4.5, Tables 4.2 and 4.3).

Whenever the electrolyte solvents and lithium salts were reduced, to neutralize the whole system, the same number of Li^+ cations as that of injected electrons was additionally placed randomly in the vacuum region. Then, to accelerate the ion diffusion, I have executed the additional 20 ps MD simulation with a smaller electrostatic interaction (the scaling parameter 0.1), and relaxed the whole system for 20 ps under the normal electrostatic interaction, fixing all the reaction product structures as a whole. In this case, the space that the electrolyte molecules are able to move was limited by the constrained potential to avoid evaporating into the vacuum region.

4.3. Results and Discussion

4.3.1. Formation Processes of the SEI films

In Figures 4.2 and 4.3, shown are each 5 typical snapshots of the changes of the aggregation states of reaction products in the EC- and PC-based electrolyte, respectively, displaying how the constituents of electrolyte solutions develop into the SEI films during the hybrid MC/MD reaction simulations. As shown in Figure 4.2, LiEC complexes (blue and yellow) were continually produced via the reduction of solvent EC molecules on the graphite surface until the reaction products grow up to the stable SEI film. During their growth, they were further reduced on the graphite surface, and dissociated to form C_2H_4 gases (gray) and Li_2CO_3 complexes (blue and red). At the same time, they formed Li_2BDC dimers (blue and green) via their radical polymerization.

Additionally, it was also shown that a few PF_6^- anions were reduced to form PF_3 gases (orange) and LiF complexes (blue and pink) on the graphite surface. Finally, these reaction products are linked to one another through ion-bonding with the sharing Li^+ cations (blue), and formed the stable SEI film. However, in the PC-based electrolyte, some fragments of the reaction products were found to drift away into the bulk region of the electrolyte solution during the SEI film formation process (see Figure 4.3). It is plausible that the difference between the solvent EC and PC molecules is mainly due to the existence of the methyl group. Its existence in solvent PC molecules and the PC-originating reaction products, therefore, should prevent them from clumping together to make the SEI film formation processes unstabilized, enhancing the products drifting into the bulk region of the electrolyte solution.

Then, Figure 4.4 shows the changes in the number per unit area of the graphite surface, i.e., the surface number density ρ_n^S, of the reaction products obtained by averaging over different 10 initial configurations in the EC- and PC-based electrolyte (Figures 4.4(a) and 4.4(b)), where the abscissa is taken as the number of the MC/MD cycles in the present atomistic reaction simulation. In these figures, each point in the curves shows the average value over the 40 MC/MD cycles. In both electrolytes, accompanying the initial consumption of the solvent EC (/PC) molecules (purple curves), the numbers of LiEC (/LiPC) molecules (yellow curves) increased drastically and showed the maximum at the MC/MD cycles 600-700 in the SEI film formation process. Then, the Li_2CO_3 complexes (red curves), C_2H_4 ($/C_3H_6$) gases (gray curves) and Li_2BDC ($/Li_2DMBDC$) dimers (green curves) were succeedingly produced by consuming the LiEC (/LiPC) complexes previously formed. Finally, the composition ratio of the molecular mixture of the reaction products became almost unchanged in the

final stage of the formation process, i.e., in larger MC/MD cycles than 1600. In this case, the standard errors obtained by the 10 simulations with different 10 initial configurations were sufficiently small. It is clearly said, therefore, that the differences in the surface number density changes between the EC- and PC-based electrolytes are statistically significant.

Compared the surface number density changes of reaction products in the EC-based electrolyte (Figure 4.4(a)) with those in the PC-based one (Figure 4.4(b)), the surface number density of dimers, i.e., Li_2BDC, in the EC-based electrolyte was found to considerably increase in comparison to that in the PC-based one, i.e., Li_2DMBDC. On the other hand, such differences of the surface number densities of the Li_2CO_3 complexes and C_2H_4 (/C_3H_6) gases became rather small. However, PF_6^- anions were scarcely reduced during the formation process although the production of LiF complexes slightly increased in the EC-based electrolyte owing to the smaller molecular size of EC. This is partially because the concentration of PF_6^- anions is considerably lower, and partially because it is so difficult that they might get closer to the negatively charged graphite surface.

4.3.2. Density Distributions and Compositions of Constituent Molecules in the SEI films

Figure 4.5 show the mass density distributions ρ_m of reaction products in the final stage (2000 MC/MD cycles). It was clarified that the large amount of Li_2CO_3 complexes lied closer to the anode while those of organic ones, i.e., LiEC, Li_2BDC (/LiPC, Li_2DMBDC) did farther away. This feature is essentially consistent with such

experimental result that the inorganic salts such as Li_2CO_3 are more abundant near the anode surface than the organic ones [4-6]. The thickness of the SEI film obtained was almost 65 Å and was of the same order reported experimentally [6]. It is interesting to notice that Li_2CO_3 complexes were distributed rather widely and diffusely over in the whole SEI film. The primary cause is the fact that they become junctions which bind a plurality of couples of the organic salts, stabilizing the SEI film. In addition, the mass density of dimers in the EC-based SEI film (Figure 4.5(a)) was found to be larger than that in the PC-based one (Figure 4.5(b)), indicating that there is a denser network among the organic salts in the EC-based SEI film. On the other hand, it is suggested that the network formation in the PC-based SEI film should be insufficient since there was not a dominant peak but rather broad distribution of dimers.

In Table 4.2 and 4.3, shown are the average number and mass densities of stable reaction products obtained by using the different 10 initial configurations in the EC- and PC-based SEI films, respectively. I regarded the length z = 65 Å as the maximum extensions of these SEI films since it is the largest distance from the electrode surface (z = 0 Å) in both EC- and PC-based SEI films (see Figure 4.5). In both electrolytes, the standard errors of number and mass densities were sufficiently small and, therefore, the compositions in the stable SEI films can be said nearly independent of the initial configurations in the hybrid MC/MD reaction simulations. In particular, in the EC-based electrolyte, the number density of dimers (Li_2BDC) was found to be 1.73×10^{-3} $Å^{-3}$, and drastically increased in comparison to the value of the dimers (Li_2DMBDC) 0.99×10^{-3} $Å^{-3}$ in the PC-based one. Accordingly, the ratio of the organic salts in the EC-based SEI film (~62 %) became considerably large in comparison to that in the PC-based one

(~46 %). Such significant increase of the organic salts should enhance the network formation in the EC-based SEI film.

Then, I have also shown in Tables 4.2 and 4.3 the desorption ratios, which are estimated as the percentages of the reaction products outside the SEI film ($z > 65$ Å). Typically in Figure 4.3, some reaction products actually drifted away into the bulk region of the electrolyte solution during the SEI film formation processes. It was found that the desorption ratios of the inorganic and organic salts in the PC-based electrolyte are very high (~21.6 %) while those in the EC-based one are quite low (< 1 %). This observation clearly shows that the existence of methyl groups in solvent PC molecules and their reaction products prevent the stable aggregation of reaction products. Such frequent desorption should bring about the destabilization of the PC-based SEI film [1,2]. On the other hand, the desorption ratio of the gases was found to decrease in the PC-based SEI film due to the larger size of PC molecules and their reaction products. As a result, the amount of the gases relatively increased in comparison to that in the EC-based SEI film. If the intercalation of these gaseous molecules into the graphite anode might have been considered explicitly in the simulations, their excess should have really enhanced the destruction of the graphite anode in the PC-based electrolyte [29,30].

4.3.3. Atomistic Structures of the SEI film -Electrolyte Protection and Li^+ Transportability-

The SEI film should have two significant roles in the LIB, i.e., (1) the protection of electrolyte from further succeeding reduction on the anode surface, and (2) the transportability of Li^+ cations between the anode and electrolyte. From these functional

aspects, I have investigated the atomistic structural differences between the EC- and PC-based SEI films obtained via the present simulations. Figures 4.6 shows the typical snapshots of the SEI films and electrolytes near the graphite anode surfaces, where the left panels show the side views, while the middle and right ones the front views of the interface structures ($0 \leq z \leq 20$ Å) in the SEI films in two different ways of visualization. Those SEI films include the LiEC (/LiPC), Li_2BDC (/Li_2DMBDC), Li_2CO_3 and LiF complexes. As shown in the side views, the electrolyte solvent molecules (purple) were found to considerably penetrate into the inside of the SEI films so that their number gradually decreased as they get closer to the graphite anode surface. In particular, the interface structures of the SEI film (see the left panel of Figure 4.6(a)) must be very important for the protection of the electrolyte from the reduction since the reaction products were especially abundant within this region (see Figure 4.5).

As a result, the EC-based SEI film was found to serve ECs as a protective covering to prevent them from approaching the anode surface (see the left panel of Figure 4.6(a)). This is owing to the dense interface structures of the EC-based SEI film (see the middle panel of Figure 4.6(a)). At the same time, it is very important that there are still some connective cavities existing in the EC-based SEI film which have sufficient sizes for the passing of Li^+ cations (~2.3 Å in diameter). Namely, the EC-based SEI film would enable Li^+ cations to transport between the graphite anode and electrolyte, protecting the electrolyte from further reductive decomposition on the surface. In contrast, in the PC-based SEI film, it was evident that there are a few solvent PC molecules in the vicinity of graphite anode surface, their entering through the SEI film (see the left panel of Figure 4.6(b)). This shows that the protection of the electrolyte is insufficient in the PC-based SEI film.

According to the comparison of the front views, this is because that the size of cavities in the interface structure of the PC-based SEI film was apparently larger than that in the EC-based one (see the two middle panels of Figure 4.6). This characteristic difference was observed in common in all the ten sets of snapshots obtained similarly by those atomistic simulations starting with ten sets of different initial conditions (see Figure S4.1 and S4.2 in Supporting Information). To estimate numerically such cavity sizes in the interface structures of the SEI films, I have calculated the fractional accessible volume (FAV) [31], which is the ratio of the cavity volume to the total one. In the present calculations, such cavities were defined as the accessible spaces probed by the spheres with the van der Waals radius of Li^+ cation (1.137 Å). As a result, the averaged FAV in the interface structure of the PC-based SEI films was estimated to be 0.40, which is considerably large in comparison to that in the EC-based one (0.30).

To clarify the microscopic origin of the difference in interface structures between the EC- and PC-based SEI films, I have shown in right panels in Figure 4.6 the front views of the interface structures in the SEI films using both the stick and the ball model at the same time. It was understood in general that such constitutional residues as the polar $-CO_3$ groups (red) of the organic salts (in the stick model) surround or enclose the Li_2CO_3 complexes (blue and red in the ball model (full vdW radii), while the remaining nonpolar $-C_2H_4$ (or $-C_3H_6$) groups (green in the stick model) mainly form the cavities in the interface structures of the SEI films. In particular, in the EC-based SEI film, there was the dense network via the complex formation of inorganic and organic salts in the interface structure (see the right panel of Figure 4.6(a)), while, in the PC-based one, some clusters were formed due to polar residues ($-CO_3$) of the organic salts, coordinating to the Li_2CO_3 complexes (see the right panel of Figure 4.6(b)). This is considered

because that the methyl groups of the solvent PC molecules and their reaction products should enhance the aggregation of the Li^+ cations and Li_2CO_3 complexes, preventing the organic salts from clumping together (see the general feature of those snapshots in Figure S4.3 and S4.4 in Supporting Information). It is such unfavorable separation of inorganic salts from organic ones in the PC-based SEI film that should decrease its durability under any mechanical impact, e.g., the collision of Li^+ cations and electrolyte solvents.

4.4. Concluding Remarks

In this chapter, to investigate the microscopic structures in the electrolyte-dependent SEI film formation on the graphite anode, I performed the atomistic reaction simulations using my recently developed hybrid MC/MD reaction method [19]. I was able to demonstrate the SEI film formation process microscopically by the present atomistic reaction simulation and reproduced successfully a number of structural characteristics of the SEI film reported experimentally, keeping the atomistic spatial heterogeneity. Then, it was clarified theoretically, for the first time, that the EC-based SEI film has sufficient function to protect the electrolyte from the excess reduction on the graphite surface and, at the same time, there were still some connective cavities in the interface structures of the SEI film which Li^+ cations are allowed to pass through. In contrast, such protection was found insufficient in the PC-based SEI film due to the presence of methyl groups of solvent PC molecules and their reaction products, which prevents the organic salts from their aggregating. Considering that the potential energy differences in the elementary chemical reactions between the EC- and PC-based electrolytes were very small (see Table 4.1), it must be essentially important that the

long-term SEI film formation is highly influenced by such a small structural difference between EC and PC, whether the methyl group exists or not.

The clarified strong sensitivity of the SEI film formation to the electrolyte solvents would show the difficulty to design the electrolytes and electrode materials for the LIBs only by experiments. In other words, we need the detailed information of atomistic structures of the SEI film presented here via the theoretical study because it must provide a number of important guides to design them from the aspect of the microscopic molecular structure. On the other hand, to improve the performance of the LIB, it is also crucial to find proper additives, e.g., vinylene carbonate (VC) and fluoroethylene carbonate (FEC) to the electrolyte which would help to generate the efficient SEI films. From the theoretical viewpoint, the effects of such additives on the microscopic reaction processes associated with the SEI film formation have been investigated continuously with the QC calculations [1,9,10,32] and AIMD simulations [12,32]. On the basis of such inevitable information, in the next study, I am going to apply the present computational approach to investigate the additives that are valid from the viewpoint of optimizing electrolytes and stabilizing SEI films that are more effective in blocking electron transport while maintaining high ion mobility.

References

[1] P. B. Balbuena, Y. Wang, Lithium-Ion Batteries: Solid-Electrolyte Interphase; Imperial College Press: London, 2004.

[2] K. Xu, Chem. Rev. 104 (2004) 4303.

[3] Y. Abu-Lebdeh, Nanotechnology for Lithium-Ion Batteries; Splinger: New York, 2013.

[4] D. Aurbach, Y. Ein-Ely, A. J. Zaban, Electrochem. Soc. 1994, 141, L1.

[5] D. Aurbach, A. Zaban, A. Schecheter, Y. Ein-Ely, E. Zinigrad, B. Markovsky, J. Electrochem. Soc. 142 (1995) 2873.

[6] E. Peled, D. Golodnitsky, G. Ardel, J. Electrochem. Soc. 144 (1997) L208.

[7] S. Komaba, W. Murata, T. Ishikawa, N. Yabuuchi, T. Ozeki, T. Nakayama, A. Ogata, K. Gotoh, K. Fujiwara, Adv. Funct. Mater. 21 (2011) 3859.

[8] Y. Wang, S. Nakamura, M. Ue, P. B. Balubuena, J. Am. Chem. Soc. 123 (2001) 11708.

[9] Y. Wang, S. Nakamura, K. Tasaki, P. B. Balubuena, J. Am. Chem. Soc. 124 (2002) 4408.

[10] Y. Wang, P. B. Balbuena, J. Phys. Chem. B 106 (2002) 4486.

[11] J. M. Vollmer, L. A. Curtiss, D. R. Vissers, K. Amine, J. Electrochem. Soc. 151 (2004) A178.

[12] K. Ushirogata, K. Sodeyama, Y. Okuno, Y. Tateyama, J. Am. Chem. Soc. 135 (2013) 11967.

[13] D. Bedrov, G. D. Smith, A. C. T. van Duin, J. Phys. Chem. A 116 (2012) 2978.

[14] K. Leung, J. Budzien, J. Phys. Chem. Chem. Phys. 12 (2010) 6583.

[15] K. Leung, Y. Qi, K. R. Zavadil, Y. S. Jung, A. C. Dillon, A. S. Cavanagh, S.-H. Lee, S. M. George, J. Am. Chem. Soc. 133 (2011) 14741.

[16] P. Ganesh, P. R. C. Kent, D. Jiang, J. Phys. Chem. C 116 (2012) 24476.

[17] S. P. Kim, A. C. T. van Duin, V. B. Shenoy, J. Power Sources 196 (2011) 8590.

[18] X. Y. Song, K. Kinoshita, T. D. Tran, J. Electrochem. Soc. 143 (1996) L120.

[19] M. Nagaoka, Y. Suzuki, T. Okamoto, N. Takenaka, Chem. Phys. Lett. 583 (2013) 80.

[20] S. A. Kislenko, I. S. Samoylov, R. H. Amorov, Phys. Chem. Chem. Phys. 11 (2009) 5584.

[21] M. P. Allen, D. Tildsley, J. Computer Simulation of Liquids; Clarendon Press: Oxford, 1987.

[22] D. W. Heerman, Computer Simulation Methods in Theoretical Physics, 2nd ed.; Splinger-Verlag: Berlin, 1990.

[23] N. Metropolis, A. W. Rosenbluth, M. N. Rosenbluth, A. H. Teller, E. J. Teller, Chem. Phys. 21 (1953) 1087.

[24] J. Wang, R. M. Wolf, J. W. Caldwell, P. A. Kollman, D. A. Case, J. Comp. Chem. 25 (2004) 1157.

[25] Z. Liu, S. Huang, W. Wang, J. Phys. Chem. B 108 (2004) 12978.

[26] K. Kondo, M. Sano, A. Hiwara, T. Omi, M. Fujita, A. Kuwae, M. Iida, K. Mogi, H. Yokoyama, J. Chem. Phys. B 104 (2000) 5040.

[27] K. Hayamizu, Y. Aihara, S. Arai, C. G. Martinez, J. Phys. Chem. B 103 (1999) 519.

[28] D. A. Case, et al. AMBER 9; University of California: San Francisco, 2006.

[29] R. Fong, U. von Sacken, J. R. Dahn, J. Electrochem. Soc. 137 (1990) 2009.

[30] Z. X. Shu, R. S. McMillan, J. J. Murray, J. Electrochem. Soc. 140 (1993) 922.

[31] D. Hofmann, M. Entrialgo-Castano, A. Lerbret, M. Heuchel, Y. Yampolskii, Macromolecules 36 (2003) 8528.

[32] K. Leung, S. B. Rempe, M. E. Foster, Y. Ma, J. M. M. de la Hoz, N. Sai, P. B. Balbuena, J. Electrochem. Soc. 161 (2014) A213.

FIGURES

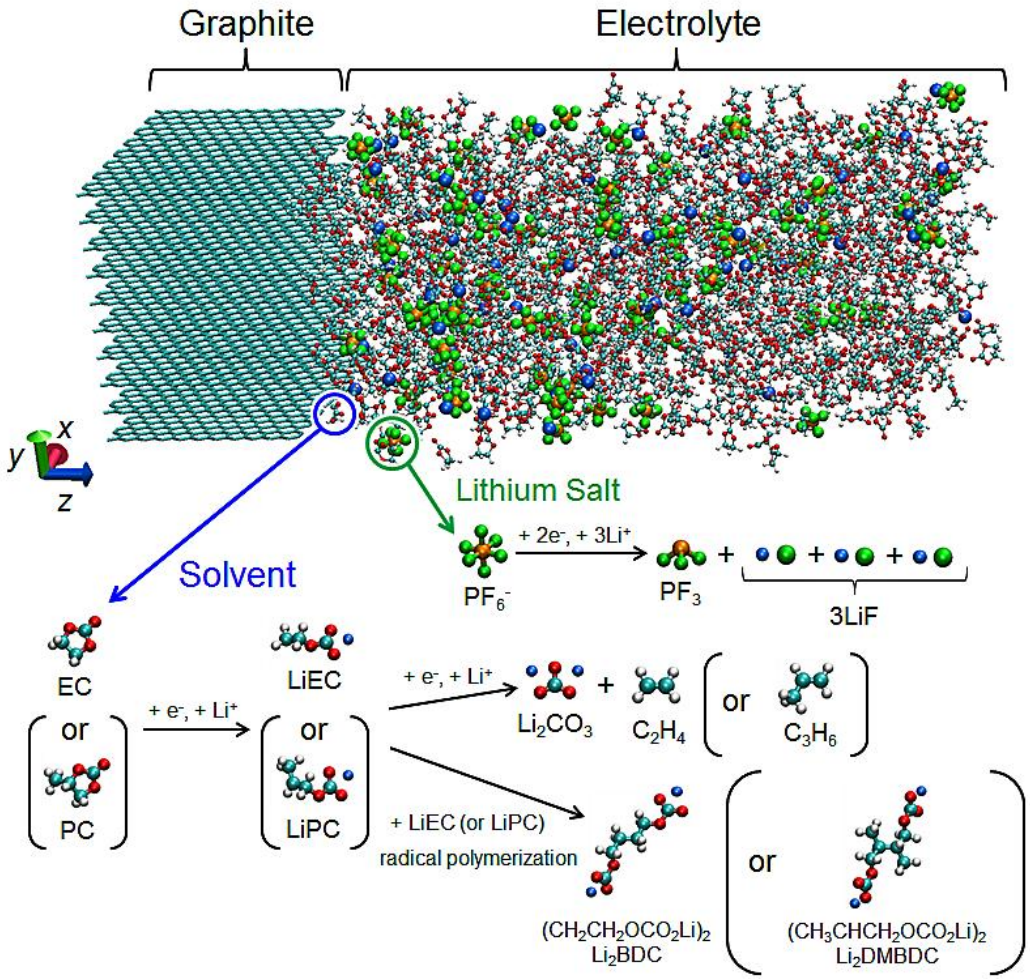

Figure 4.1. Model simulation system and the reaction scheme (cyan: carbon, red: oxygen, white: hydrogen, orange: phosphorus, green: fluorine, blue: Li^+). The origin of *z* coordinate is taken at the position of the carbon atoms on the graphite anode surface in contact with the electrolyte.

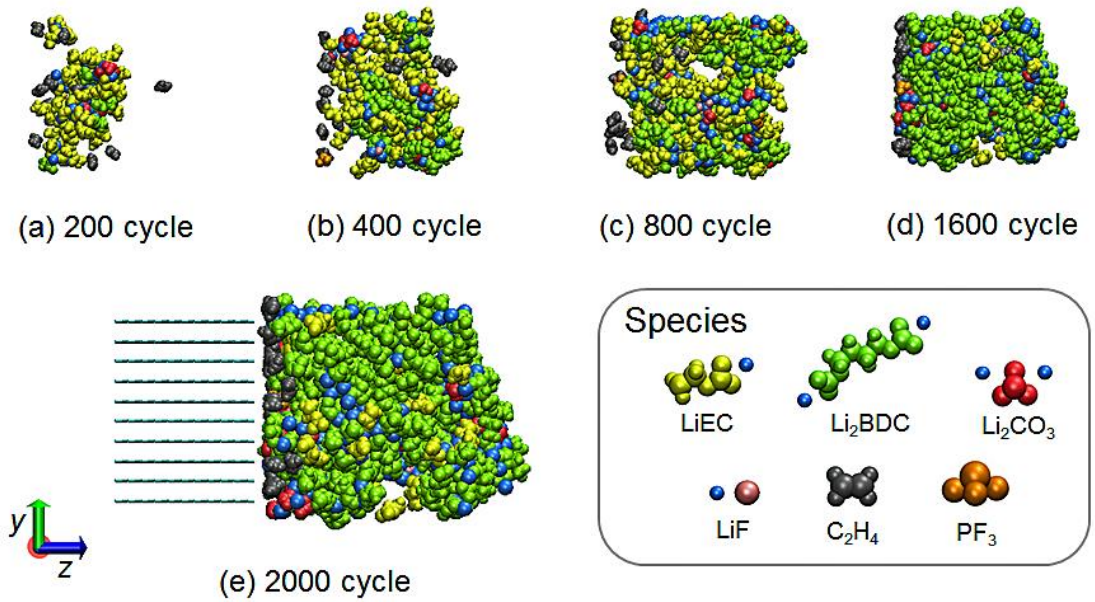

Figure 4.2. The SEI film formation process in the EC-based electrolyte. 5 typical snapshots of the changes of the aggregation states of reaction products during the hybrid MC/MD reaction simulation (Bulk EC not shown.) in the (a) 200 MC/MD cycle, (b) 400 MC/MD cycle, (c) 800 MC/MD cycle, (d) 1600 MC/MD cycle and (e) 2000 MC/MD cycle.

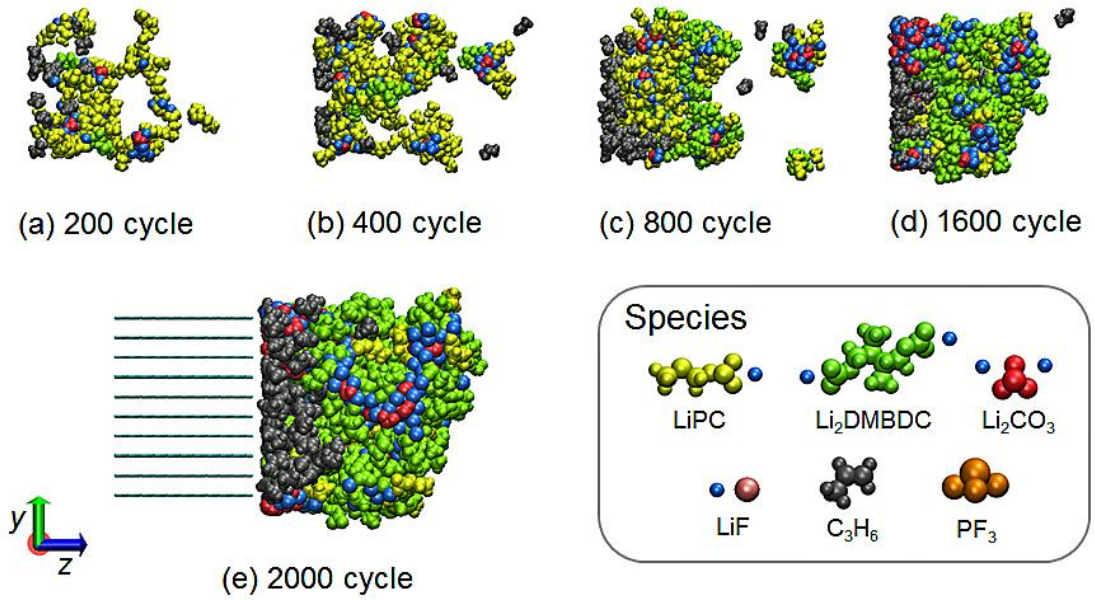

Figure 4.3. Typical snapshots of the SEI films and electrolytes ((a) EC-based and (b) PC-based SEI film) (green: SEI film, blue: Li^+, gray: PF_3, C_2H_4 or C_3H_6, purple: EC or PC, orange: PF_6^-), where the left panels show the side views, while the middle and right ones the front views of the interface structures in the SEI films (visualized in the depth $0 \leq z \leq 20$ Å of the view from the side of bulk electrolyte). In the right panels, inorganic salts (Li_2CO_3, LiF) are depicted by the ball model (full vdW radii) (red: CO_3^{2-}, F^-, blue: Li^+), while organic ones (LiEC, Li_2BDC or LiPC, Li_2DMBDC) by the stick model (green: $-C_2H_4$ or $-C_3H_6$, red: $-CO_3$).

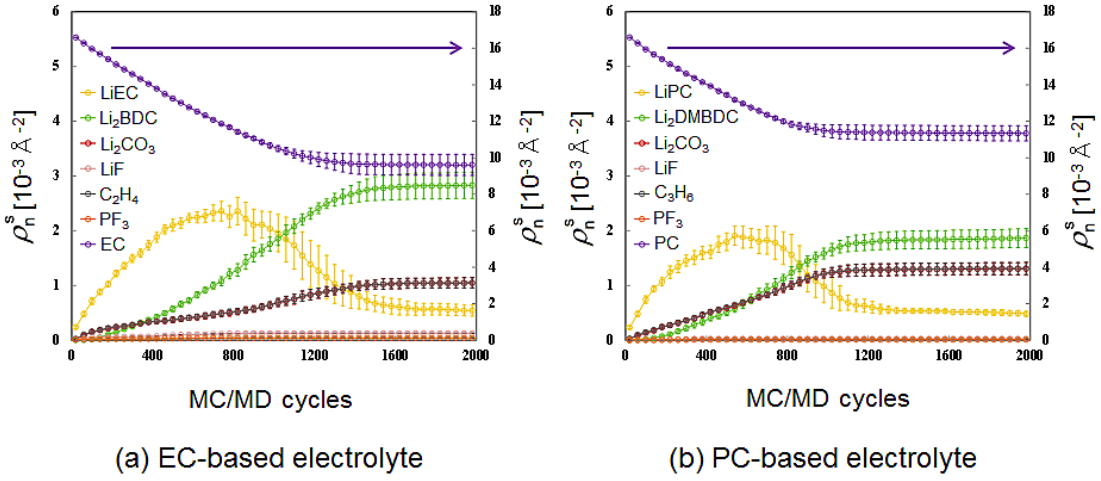

Figure 4.4. Changes in the surface number densities ρ_n^S of the solvent molecules and reaction products during the SEI film formation processes with respect to the MC/MD cycles in the atomistic reaction simulations in (a) EC-based and (b) PC-based electrolyte.

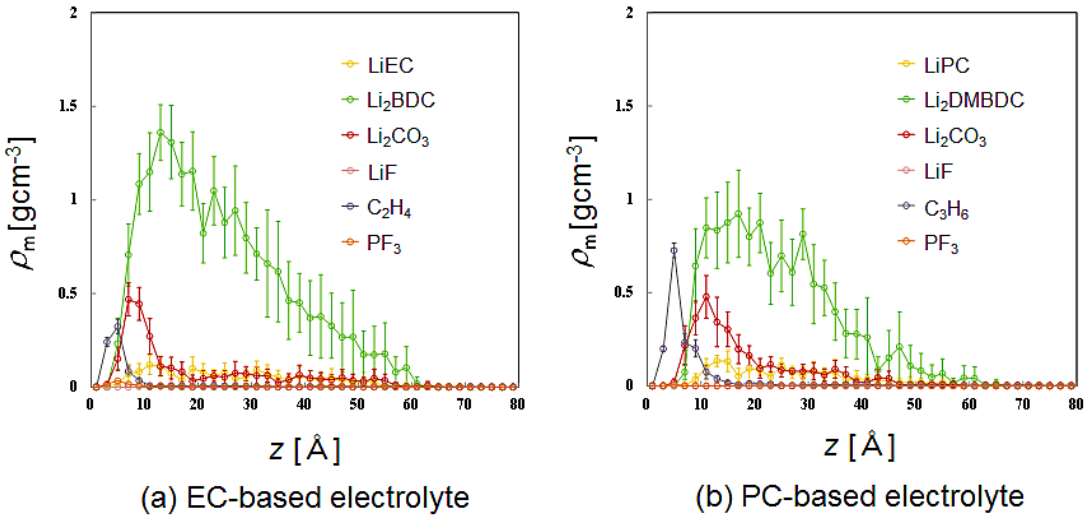

Figure 4.5. Mass density distributions ρ_m of the reaction products in the final stages (2000 MC/MD cycles) in the present atomistic reaction simulations in (a) EC-based and (b) PC-based electrolyte.

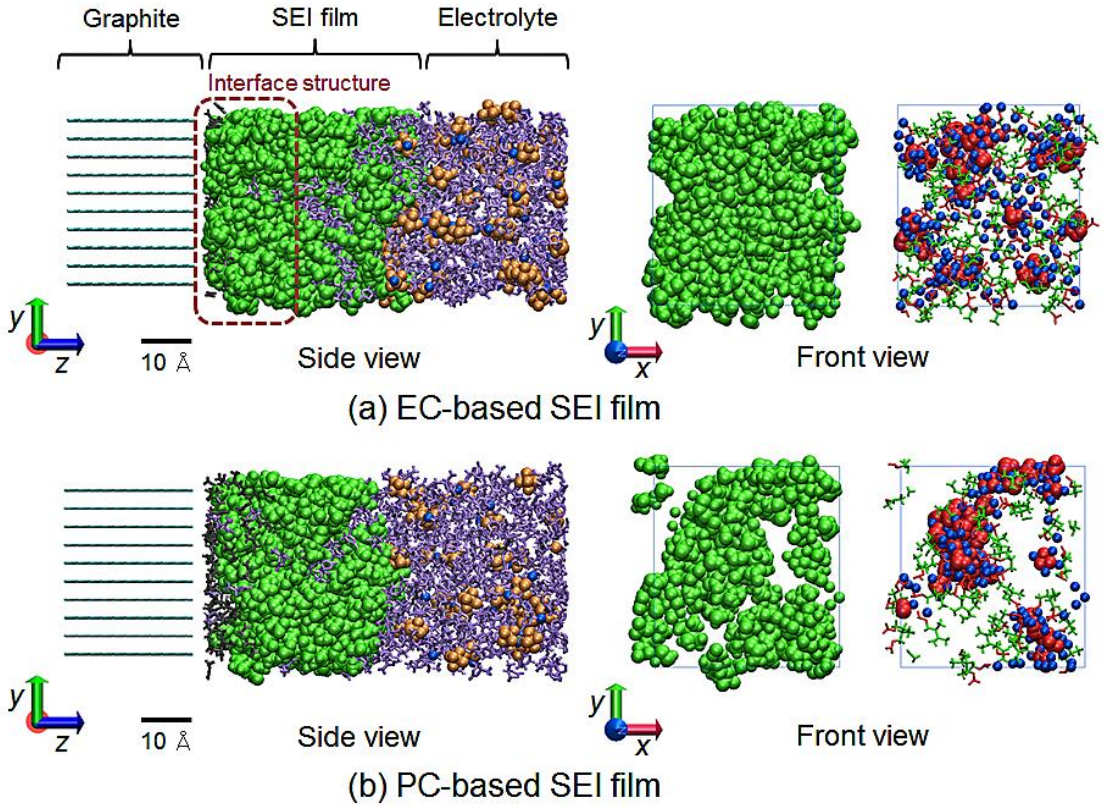

Figure 4.6. Typical snapshots of the SEI films and electrolytes ((a) EC-based and (b) PC-based SEI film) (green: SEI film, blue: Li^+, gray: PF_3, C_2H_4 or C_3H_6, purple: EC or PC, orange: PF_6^-), where the left panels show the side views, while the middle and right ones the front views of the interface structures in the SEI films (visualized in the depth $0 \leq z \leq 20$ Å of the view from the side of bulk electrolyte). In the right panels, inorganic salts (Li_2CO_3, LiF) are depicted by the ball model (full vdW radii) (red: CO_3^{2-}, F^-, blue: Li^+), while organic ones (LiEC, Li_2BDC or LiPC, Li_2DMBDC) by the stick model (green: $-C_2H_4$ or $-C_3H_6$, red: $-CO_3$).

TABLES

Table 4.1. Potential Energy Differences of Reaction ΔU_0^{reac} in Gas Phase at the B3LYP/6-31+G(d) Level of Theory.

Chemical reaction process	ΔU_0^{reac} [kcal/mol]
$EC + e^- + Li^+ \rightarrow LiEC$	-169.8
$PC + e^- + Li^+ \rightarrow LiPC$	-168.9
$LiEC + LiEC \rightarrow Li_2BDC$	-88.5
$LiPC + LiPC \rightarrow Li_2DMBDC$	-76.0
$LiEC + e^- + Li^+ \rightarrow C_2H_4 + Li_2CO_3$	-224.6
$LiPC + e^- + Li^+ \rightarrow C_3H_6 + Li_2CO_3$	-224.4
$PF_6^- + 2e^- + 3Li^+ \rightarrow PF_3 + 3LiF$	-88.8

Table 4.2. Number and Mass Densities of Stable Reaction Products in the EC-based SEI Film and the Desorption Ratio of the Reaction Products from the SEI Film.

species				
type	formula	Number density [10^{-3} Å^{-3}]	Mass density [gcm^{-3}]	Desorption ratio [%]
organic salts	LiEC	0.30 ± 0.09 (9.04 %)	0.047 ± 0.015	0.54
	Li_2BDC	1.73 ± 0.14 (52.91 %)	0.550 ± 0.045	
inorganic salts	Li_2CO_3	0.64 ± 0.06 (19.61 %)	0.079 ± 0.007	0.19
	LiF	0.065 (1.97 %)	0.0028	
gases	C_2H_4	0.52 ± 0.05 (15.85 %)	0.024 ± 0.002	19.3
	PF_3	0.020 (0.62 %)	0.003	

Table 4.3. Number and Mass Densities of Stable Reaction Products in the PC-based SEI Film and the Desorption Ratio of the Reaction Products from the SEI Film.

species		Number density [10^{-3} Å^{-3}]	Mass density [gcm^{-3}]	Desorption ratio [%]
type	formula			
organic salts	LiPC	0.24 ± 0.03 (8.81 %)	0.043 ± 0.006	14.61
	Li_2DMBDC	0.99 ± 0.11 (36.68 %)	0.360 ± 0.038	
inorganic salts	Li_2CO_3	0.75 ± 0.05 (27.56 %)	0.092 ± 0.007	6.99
	LiF	0.011 (0.41 %)	0.00048	
gases	C_3H_6	0.72 ± 0.05 (26.46 %)	0.050 ± 0.004	10.69
	PF_3	0.0024 (0.09 %)	0.00036	

Supporting Information

Figures S4.1 and S4.2 show the snapshots of the interface structures of the EC- and PC-based SEI films, which are obtained from the different 10 initial configurations, respectively. Figures S4.3 and S4.4 show those of the EC- and PC-based SEI films using both the stick and the ball model at the same time, respectively.

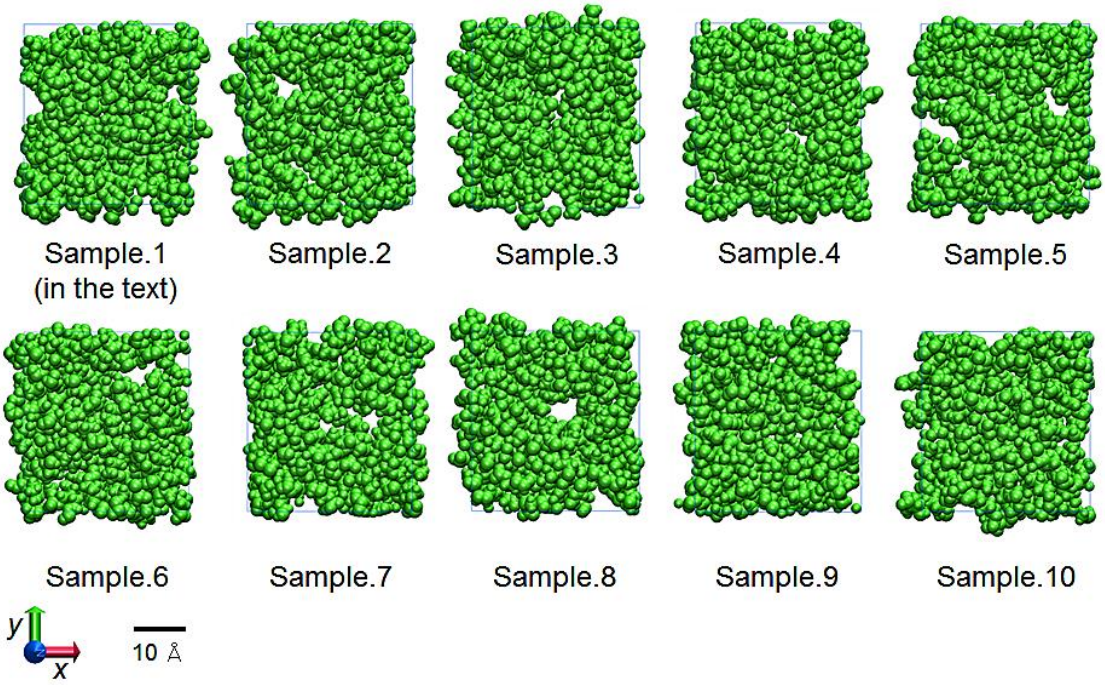

Figure S4.1. Front view snapshots of the interface structures of the EC-based SEI film (visualized in the depth $0 \leq z \leq 20$ Å of the view from the side of bulk electrolyte). These structures are obtained from the different 10 initial configurations, where the sample 1 is shown in the middle panel of Figure 4.6(a).

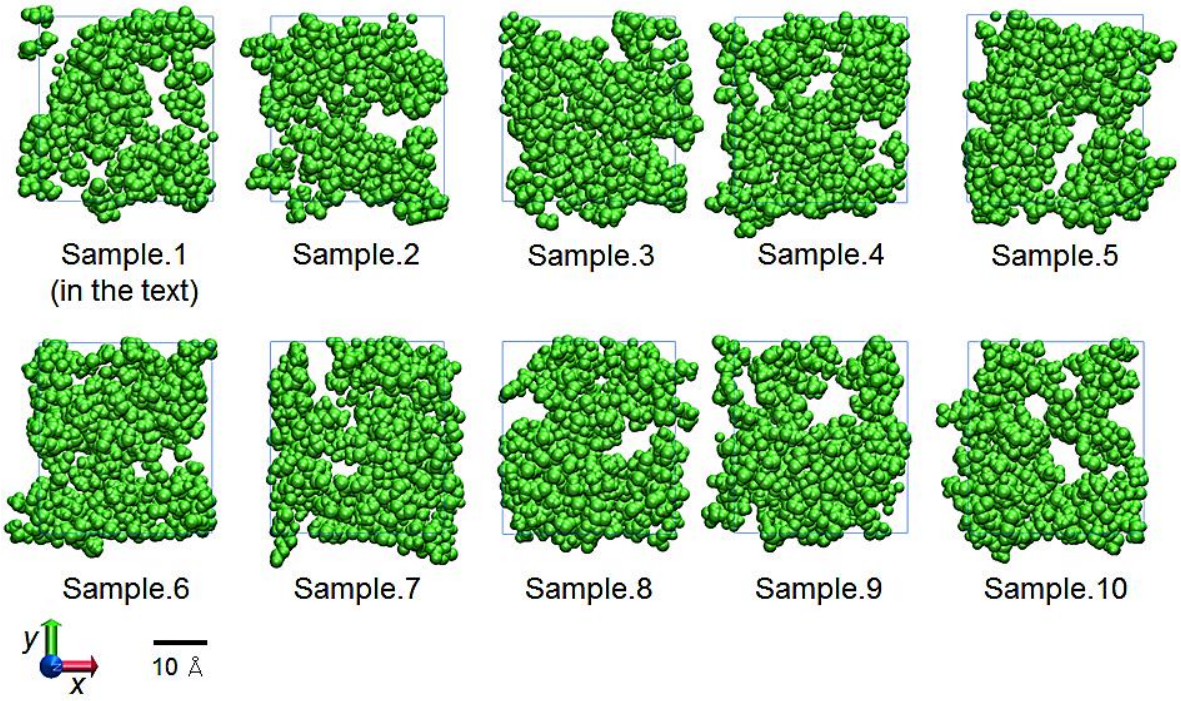

Figure S4.2. Front view snapshots of the interface structures of the PC-based SEI film (visualized in the depth $0 \leq z \leq 20$ Å of the view from the side of bulk electrolyte). These structures are obtained from the different 10 initial configurations, where the sample 1 is shown in the middle panel of Figure 4.6(b).

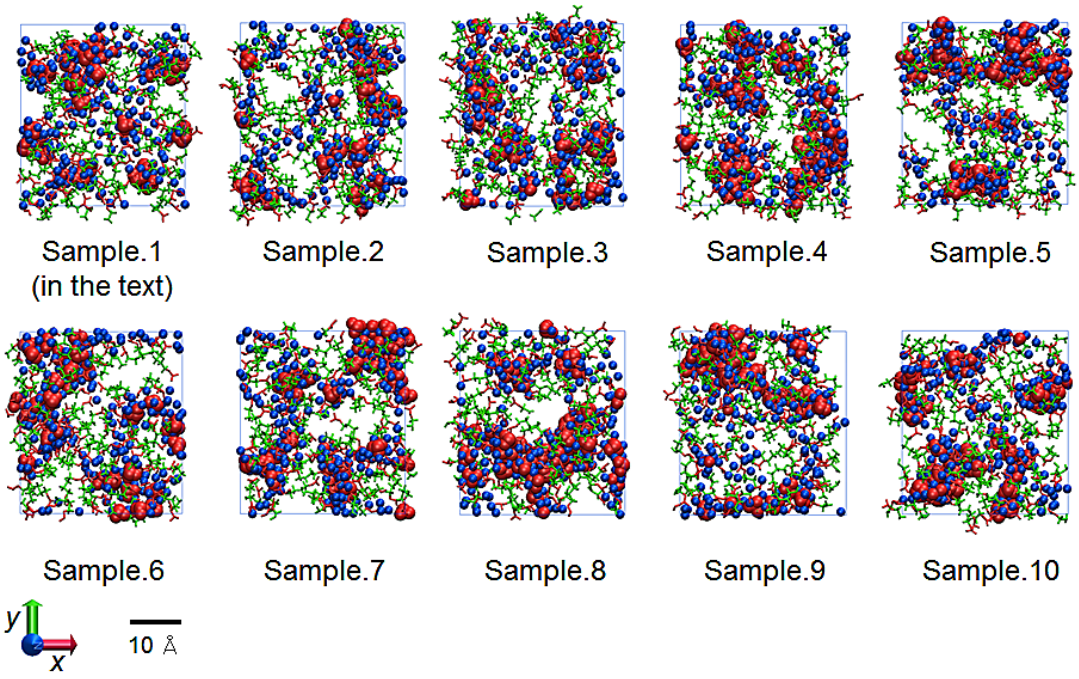

Figure S4.3. Front view snapshots of the interface structures of the EC-based SEI film (visualized in the depth $0 \leq z \leq 20$ Å of the view from the side of bulk electrolyte). These structures are obtained from the different 10 initial configurations, where the sample 1 is shown in the right panel of Figure 4.6(a).

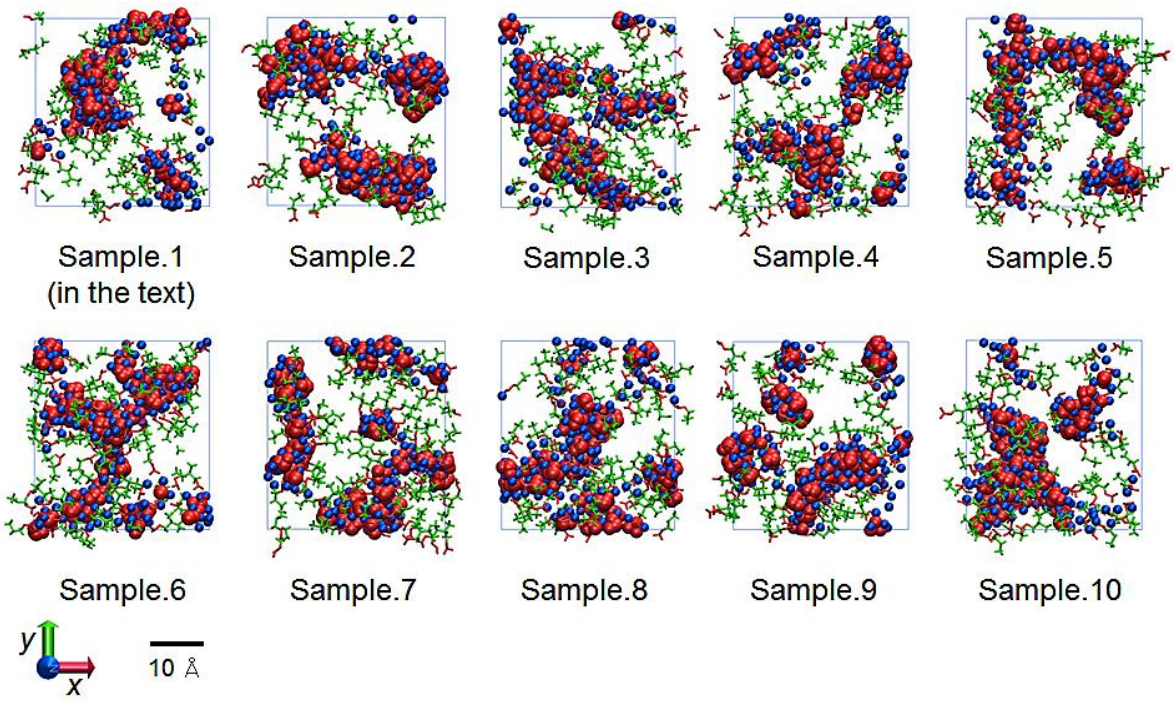

Figure S4.4. Front view snapshots of the interface structures of the PC-based SEI film (visualized in the depth $0 \leq z \leq 20$ Å of the view from the side of bulk electrolyte). These structures are obtained from the different 10 initial configurations, where the sample 1 is shown in the right panel of Figure 4.6(b).

Chapter 5

Time Interpretation of MC/MD Cycle in Chemical Reaction Process of Hybrid MC/MD Reaction Method: Application to Reversible Second-Order Reaction System, $H_2 + I_2 \rightleftharpoons 2HI$

5.1. Introduction

A chemical reaction is a process in which one set of substances, called reactants, is converted to a new set of substances, called products [1]. The process reaches a state of dynamic equilibrium in which both reactants and products are present but have no further tendency to undergo net change [1]. Moreover, most chemical reactions occur in a sequence of elementary steps, called elementary reactions, which describe any molecular events that significantly alter a molecule's energy or structure or produce a new molecule [1-3]. On understanding such chemical reaction process consisting of the sequence of the elementary reactions, it is essentially important to study the rate of the chemical reaction based on the principles of chemical kinetics [1-3].

In relation, it has been well-known that the reaction rate depends on the concentrations of reactants (and products), and can be expressed in terms of complex differential equations known as "rate laws" [1-3]. If the solution of these equations can be obtained, even if it might be numerically, it would be helpful and could allow us to predict the accurate concentrations of their components at any time after the start of

reaction occurrence [1-3]. However, the rate laws of the chemical reactions are elucidated only by the experiments, so that the construction of the rate laws from proposed elementary reactions and its comparison with experiment can lead to reveal a reaction mechanism, i.e., chemical reaction process [2].

To determine the rate of the chemical reaction, it is necessary to measure changes in concentration or its alternative quantities over time in reaction progress [1-3]. Actually, the methods and techniques such as flow method, stopped-flow technique, flash photolysis, *in situ* X-ray diffraction and *in situ* FTIR reflection spectroscopy have been used in experiments for a real-time analysis [1-6]. However, instantaneous and microscopic structures of a whole system have not been observed even by these experimental approaches. If such insight into clearly understanding chemical phenomena is obtained, it could be realized to optimize reaction mechanisms by appropriate conditions of such as the pressure, the temperature, and especially the presence of a catalyst and an additive [1-3].

Under the circumstances, molecular simulation has been a powerful methodology that is not only complementary to experimental investigations but also essential for the chemical phenomena microscopically [8-12]. However, in such computational methodologies [8-12], there are few methods that can treat the model chemical reaction systems sufficiently comparable to such systems with the actual space-time scale. To overcome the issue, I have developed the hybrid Monte Carlo/molecular dynamics (MC/MD) reaction method [13-16], and its extension of theoretical methodology is still in progress. This method can simulate chemical reaction processes by a cycle consisting of several steps, called “MC/MD cycle” (explained in subsection 5.2.1), dealing with all the atoms and the microscopic structures for the systems [13-16]. Actually, I have

already succeeded in applying it to the complex formation (/chemical reaction) processes of the 2-cholorobutan racemization in DMF solution [13], aromatic polyamide membrane used as reverse osmosis [14] and solid electrolyte interphase film on the anode surface in secondary batteries [15,16].

However, it has not yet been explained how the MC/MD cycle could be physically interpreted although the progress of the chemical reaction processes has been shown along the MC/MD cycle base in the previous chapter 2, 3 and 4, and studies [13-16]. Therefore, in this chapter, to understand the microscopic changes of molecular structures and orientations over time for chemical reaction systems, I propose a theory to interpret an MC/MD cycle as an effective time based on chemical kinetics. For demonstration, I applied the theoretical method to a reversible second-order system in gas phase consisting of the molecular hydrogen, molecular iodide and hydrogen iodide molecule, shown as $H_2+I_2 \rightleftharpoons 2HI$. Then, for the present system, I estimate the effective time as a function of MC/MD cycle with the concentrations of their components obtained by the present simulation.

This chapter 5 is organized as follows. In section 5.2, I explain the hybrid MC/MD reaction method and the theory for the time interpretation of the MC/MD cycle, and, in section 5.3, I describe the target reaction system $H_2+I_2 \rightleftharpoons 2HI$, its computational treatment and computational details. In section 5.4, I present results and discussion, and, in the last section, I finally provide some concluding remarks.

5.2. Theoretical Method

5.2.1. The Hybrid MC/MD Reaction Method

To apply the hybrid MC/MD reaction method [13-16], considering both experimental and theoretical results, we first assume a reaction mechanism which consists of a set of chemical reactions R_1, R_2, …, i.e., chemical reaction process. Then, we provide them their corresponding activation energies $\Delta E_{\mathrm{a}}^{\mathrm{R_1}}$, $\Delta E_{\mathrm{a}}^{\mathrm{R_2}}$, … . Each activation energy is obtained properly as the "free" energy of activation that is estimated in advance, within the continuum model [17], the free energy gradient method [18, 19] or some experimental methods for each chemical reaction.

The method consists of a combination of the following types of processes:

1. Equilibrate the whole system through the classical NVT-MD simulation and obtain an initial configuration state *r*.
2. Generate reaction steps with the NVT-MC procedure and classical NVT-MD simulation, consisting of the following steps:
   (i) Search a pair (/pairs) of "reactive" atoms among reactant molecules with the whole system in a given configuration state *r* according to some criteria for whether possible chemical reactions R_1, R_2, … might occur. In the previous chapter 2 and 4, and studies [13-16], the criterion for (a/) *candidate pair (/pairs)* among their molecules have been simply taken to be whether the interatomic distance is less than the sum of their van der Waals (vdW) radii. However, in the present treatment, I determine the criterial distances for the present H_2-I_2 system on the basis of chemical kinetics (discussed in detail in subsection 5.3.2). As a result, a set of the number of candidate pairs for each chemical reaction $\left\{N_{\mathrm{cand}}^{\mathrm{R_1}}, N_{\mathrm{cand}}^{\mathrm{R_2}}, \cdots\right\}$ that is able to generate the chemical reactions is obtained in a given configuration state *r*.

(ii) Randomly select a chemical reaction R_i among R_1, R_2, … according to their corresponding relative weights of selection w^{R_1}, w^{R_2}, … , where a relative weight w^{R_i} for R_i is expressed by the product of $N_{\text{cand}}^{R_i}$ and $\exp\left(-\beta\Delta E_{\text{a}}^{R_i}\right)$ as follows,

$$w^{R_i} = N_{\text{cand}}^{R_i} \exp\left(-\beta\Delta E_{\text{a}}^{R_i}\right). \tag{5.1}$$

Then, randomly select (a/) candidate pair (/pairs) among the candidate pairs for R_i. If there are no pairs for any chemical reactions, execute a short NVT-MD simulation instead of the following step (iii) and (iv) to update the configuration state.

(iii) Switch the atomic potential parameters and potential function forms of the reactant atoms to the product ones, and virtually react them to generate a possible configuration state *s*, relaxing the whole system to obtain the state *s* through a short NVT-MD simulation.

(iv) Compute the energy change of the system $\Delta U_{rs} (= U_s - U_r)$ and accept (or reject) the reaction step according to the transition probability $W_{r\to s}$ under the Metropolis scheme [20-22],

$$W_{r\to s} = \min\left\{1, \exp\left[-\beta\Delta U_{rs}\right]\right\}. \tag{5.2}$$

In the present chapter, ΔU_{rs} is approximately estimated as follows,

$$\Delta U_{rs} = \Delta U_{rs}^{\text{MM}} + \Delta U_0^{\text{reac}}, \tag{5.3}$$

where $\Delta U_{rs}^{\text{MM}}$ is the naïve difference of total potential energies obtained in the MM force field, meaning a change of the corresponding atomic potential parameters and potential function forms together with a proper correction of the "zero" point of energy by the corresponding potential energy of reaction

$\Delta U_0^{\mathrm{reac}}$. In the present chapter, since the reactant of molecular hydrogen and molecular iodine and the product of hydrogen iodide, are reversibly formed by the chemical reaction,

$$\mathrm{H_2 + I_2 \rightleftharpoons 2HI}. \tag{5.4}$$

I assumed that both forward and backward reactions occur simply in one-step reaction mechanism. Then, the correction is obtained as

$$\Delta U_0^{\mathrm{reac}} = \Delta E_a^{\mathrm{b}} - \Delta E_a^{\mathrm{f}}, \tag{5.5}$$

where ΔE_a^{f} and ΔE_a^{b} are the activation energies of both reactions, respectively (obtained by the Arrhenius plot with the experimental values in subsection 5.3.2).

3. If the molecular mixture composition might scarcely change, then stop. Otherwise return to process 2.

The cycle consisting of the three different types of processes is called an "MC/MD cycle". By repeating the MC/MD cycle, we can stochastically realize a succession of various types of chemical reaction many times even if they occur competitively, and simulate reasonably dynamics of the whole system [13-16].

As for those parameters in the method, it can be considered that "the number of candidate pairs for a chemical reaction R_i, $N_{\mathrm{cand}}^{\mathrm{R}_i}$," is proportional to "a product of the frequency factor and a product of algebraic powers of the individual concentrations of reactant molecules, i.e., $A[\mathrm{A}]^a[\mathrm{B}]^b \cdots$," (the principles of chemical kinetics) [1-3]. On the other hand, "the exponential factor for R_i, $\exp\left(-\beta \Delta E_{\mathrm{a}}^{\mathrm{R}_i}\right)$," can correspond to "the exponential factor in the reaction rate equation of Arrhenius-type, $\exp(-\beta \Delta E_{\mathrm{a}})$, where ΔE_{a} is an activation energy," [1-3]. The former association between "$N_{\mathrm{cand}}^{\mathrm{R}_i}$" and

"$A[\mathrm{A}]^{a}[\mathrm{B}]^{b}\cdots$" intends to determine a criterion for R_i, as $N_{\mathrm{cand}}^{R_i}$ reproduces the actual frequency considering the concentrations [A], [B], … for a target reaction system. Hence, R_i can be selected among R_1, R_2, … according to its relative weight of selection w^{R_i}, as w^{R_i} relatively corresponds to its actual reaction rate v^{R_i} with the other competitive reactions at equilibrium states for the system.

In the present chapter, to reproduce the equilibrium state for the present H_2-I_2 system, I have employed the hybrid MC/MD reaction method [13-16]. Before executing the simulation, for all molecules in the system, we need to prepare the atomic potential parameters in the molecular mechanical (MM) force field [20], e.g., the force constants, Lennard-Jones (LJ) parameters and atomic electric charges. In the simulation, when some chemical reaction occurs, not only the atomic potential parameters but also the potential function forms (i.e., intramolecular or intermolecular ones) of the reactants are replaced by those suitable to the products.

5.2.2. MC/MD Cycle as the Effective Time

For applying the hybrid MC/MD reaction method, I first assume that a set of chemical reactions R_1, R_2, … occurs in a target reaction system. Then, if chemical components involved in the simultaneous equations of those chemical reactions are denoted as A, B, … , the concentrations of all the components [A], [B], … are obtained as a function of the MC/MD cycle from an initial state to the final one of the reaction system. Accordingly, in order to interpret the MC/MD cycle as an effective time, we propose to estimate a change in time corresponding to a change in a concentration of a certain component within the relaxation process of its concentration.

In general, we may assume that the instantaneous rate of consumption (or formation) of the component A at a given time can be expressed as a function of the time *t*, a set of the rate constants k^{R_1}, k^{R_2}, … and the concentrations of all the components [A], [B], … in the overall chemical equations for all of R_1, R_2, … as follows,

$$\frac{\mathrm{d[A]}}{\mathrm{d}t} = f_{\mathrm{A}}\left(t, k^{R_1}, k^{R_2}, \cdots, [\mathrm{A}], [\mathrm{B}], \cdots\right). \tag{5.6}$$

One can solve this equation for an infinitesimal time d*t*, and then it can be described as the difference equation with the difference time Δt_{A} for A,

$$\Delta t_{\mathrm{A}} = \frac{\Delta[\mathrm{A}]}{f_{\mathrm{A}}\left(t, k^{R_1}, k^{R_2}, \cdots, [\mathrm{A}], [\mathrm{B}], \cdots\right)}. \tag{5.7}$$

In Table 5.1, among all the components, only the concentrations of A with respect to sample number (=S_1, S_2, …) and MC/MD cycle (=0, 1, …) are shown. For instance, the concentration of A for the sample number S_i at the *k*th MC/MD cycle is shown as $[\mathrm{A}]_k^{S_i}$. Then, the average concentration $\langle[\mathrm{A}]_k\rangle$ is obtained by averaging $[\mathrm{A}]_k^{S_i}$ over all the samples at the same *k*th MC/MD cycle, and the same operation provides the average concentrations of the other components, $\langle[\mathrm{B}]_k\rangle$, … . Moreover, the differential concentration of A between the *k*th and *k*-1th MC/MD cycles is calculated as $\Delta\langle[\mathrm{A}]_k\rangle (= \langle[\mathrm{A}]_k\rangle - \langle[\mathrm{A}]_{k-1}\rangle)$. In Table 5.1, the sets of $\{\langle[\mathrm{A}]_k\rangle\}$ and $\{\Delta\langle[\mathrm{A}]_k\rangle\}$ with the MC/MD cycle for $\langle[\mathrm{A}]_k\rangle$ and $\Delta\langle[\mathrm{A}]_k\rangle$ are also shown.

Next, by substituting $\langle[\mathrm{A}]_k\rangle$, $\langle[\mathrm{B}]_k\rangle$, … and $\Delta\langle[\mathrm{A}]_k\rangle$ for their corresponding parameters in Eq. (5.7), the differential time between the *k*th and *k*-1th MC/MD cycles, $\Delta t_{\mathrm{A},k}$ (its set $\{\Delta t_{\mathrm{A},k}\}$ shown in Table 5.1), is estimated by

$$\Delta t_{\mathrm{A},k} = \frac{\Delta\langle[\mathrm{A}]_k\rangle}{f_{\mathrm{A}}\left(t, k^{R_1}, k^{R_2}, \cdots, \langle[\mathrm{A}]_k\rangle, \langle[\mathrm{B}]_k\rangle, \cdots\right)}. \tag{5.8}$$

Finally, by summing $\Delta t_{\mathrm{A},k}$, from k equals one to N_{eq}, which is the MC/MD cycle when the concentration of A reaches an equilibrium concentration, the time while a process of an initial concentration of A becoming an equilibrium one, t_{eq}, is obtained,

$$t_{\mathrm{eq}} = \sum_{k=1}^{N_{\mathrm{eq}}} \Delta t_{\mathrm{A},k} \ . \tag{5.9}$$

If the relaxation process of the concentration of A corresponds to the overall one for the target reaction system, the relaxation time or time to reach chemical equilibrium state from an initial one for the whole system is estimated by using the equation.

In addition, by the same operation of summing $\Delta t_{\mathrm{A},k}$, from k equals one to N_τ, which is the MC/MD cycle when $[\mathrm{A}]_0 (= \langle [\mathrm{A}]_0 \rangle)$ becomes its half (shown as $\langle [\mathrm{A}]_{N_\tau} \rangle$ in Table 5.1), half-life τ is calculated (shown in Table 5.1),

$$\tau = \sum_{k=1}^{N_\tau} \Delta t_{\mathrm{A},k} \ , \tag{5.10}$$

where N_τ and τ satisfy the following relational expression

$$\frac{\left\langle [\mathrm{A}]_{N_\tau} \right\rangle}{\left\langle [\mathrm{A}]_0 \right\rangle} = \frac{[\mathrm{A}]_\tau}{[\mathrm{A}]_0} = \frac{1}{2} . \tag{5.11}$$

Thus, as focusing on a relaxation process of concentration of a certain component, the interpretation of the MC/MD cycle as time t can be established by means of the rate law and the concentrations at each MC/MD cycle.

5.3. Reaction System and its Computational Treatment

5.3.1. Reaction System: $H_2 + I_2 \rightleftharpoons 2HI$

As a reaction system, I treated a gaseous system consisting of H_2, I_2 and HI molecules. In the present chapter, it was assumed that in the system the reversible second-order reaction occurs simply in one-step reaction for both forward and backward ones. The initial structures including H_2 and I_2 molecules without an HI molecule were prepared, as the typical structure shown in Figure 5.1(a). In such situation, as HI molecules are formed by the forward reaction, the backward reaction to H_2 and I_2 molecules starts to occur competing with the forward reaction. As a result, this reaction system reaches chemical equilibrium in which all of the molecules spatially uniformly distribute, as its typical structure shown in Figure 5.1(b) [1-3]. Accordingly, the property of the system at the equilibrium state shows a certain concentration distribution of them with temperature dependence, and therefore the equilibrium constant K_{eq} expressed by the ratio of their equilibrium concentrations also has the same dependence [1-3].

For the simulation setting, 125 molecules of H_2 and I_2, 250 molecules as a whole, were arranged in the simulation box. The cubic unit cell of which each side length is 250 Å was used for the box, and then the initial concentrations of both H_2 and I_2 were 0.013 mol/L (denoted as $[H_2]_0$ and $[I_2]_0$). To reproduce the temperature dependence of K_{eq}, the hybrid MC/MD reaction simulations were performed at three temperatures 300 K, 500K and 700K. Moreover, to obtain statistically meaningful results, the ten different initial structures were prepared at each temperature for the simulations. The Lennard-Jones (LJ) parameters were set to the previous experimentally and theoretically estimated values [23,24] for H_2 and I_2 molecules, while those for an HI molecule were evaluated using those LJ parameters for H_2 and I_2 molecules by the Berthelot rule. Atomic point charges for HI molecule were determined using restricted electrostatic potential (RESP) charge, calculated at M062X/MidiX level of theory in gas phase.

5.3.2. Computational Treatment

For the present H_2-I_2 system, in order to obtain the experimentally observed equilibrium concentrations of all components [3], it should be reproduced by the hybrid MC/MD reaction method that the rates of the forward and backward reactions are equal each other in chemical equilibrium. Thus, according to the correspondence between "$N_{\mathrm{cand}}^{\mathrm{R}i}$" in the method and "$A[\mathrm{A}]^a[\mathrm{B}]^b\cdots$" (the principle of chemical kinetics) (see subsection 5.2.1), I define the criterial distances for the reactions so as to prescribe the collisions between H_2 and I_2 molecules, and between HI molecules.

In the reaction formula of Eq. (5.4), each rate law for the forward and backward reactions is described [1-3],

$$\begin{cases} v^{\mathrm{R}_1} = A^{\mathrm{R}_1}[\mathrm{H}_2][\mathrm{I}_2]\exp\left(-\beta\Delta E_{\mathrm{a}}^{\mathrm{R}_1}\right) \\ v^{\mathrm{R}_2} = A^{\mathrm{R}_2}[\mathrm{HI}]^2\exp\left(-\beta\Delta E_{\mathrm{a}}^{\mathrm{R}_2}\right) \end{cases}, \tag{5.12}$$

where the subscripts R_1 and R_2 mean the forward and backward reactions, respectively, v^{R_1} and v^{R_2} are their reaction rates, A^{R_1} and A^{R_2} are their frequency factors, and $\Delta E_{\mathrm{a}}^{\mathrm{R}_1}$ and $\Delta E_{\mathrm{a}}^{\mathrm{R}_2}$ are their activation energies. From the estimation by the Arrhenius plot with the experimental values of rate constants and temperatures for R_1 and R_2 [2], A^{R_1} and A^{R_2} were obtained as 2.27×10^{11} $(\mathrm{mol/L})^{-1}\cdot\mathrm{s}^{-1}$ and 3.39×10^{10} $(\mathrm{mol/L})^{-1}\cdot\mathrm{s}^{-1}$, respectively. ($\Delta E_{\mathrm{a}}^{\mathrm{R}_1}$ and $\Delta E_{\mathrm{a}}^{\mathrm{R}_2}$ were obtained as 41.23 kcal/mol and 44.16 kcal/mol, respectively.)

From those A^{R_1} and A^{R_2} obtained, the pre-exponential parameters for R_1 and R_2 in Eq. (5.12) were calculated and shown as the ratio,

$$A^{\mathrm{R}_1}[\mathrm{H}_2]_0[\mathrm{I}_2]_0 : A^{\mathrm{R}_2}[\mathrm{HI}]_0^{\,2} = 1.673, \tag{5.13}$$

where $[H_2]_0$ and $[I_2]_0$ are the concentrations for the present H_2-I_2 system, $[HI]_0$ is the concentration of 0.026 mol/L in case that all the H_2 and I_2 molecules could transform to HI molecule. Then, I assumed that this ratio can be applied to the ratio as

$$N_{\mathrm{cand}}^{\mathrm{R}_1} : N_{\mathrm{cand}}^{\mathrm{R}_2} = 1.673, \tag{5.14}$$

where $N_{\mathrm{cand}}^{\mathrm{R}_1}$ and $N_{\mathrm{cand}}^{\mathrm{R}_2}$ are the numbers of the candidates obtained under the criterial distances for R_1 and R_2, respectively. When the criterial distances for R_2 were determined as the sums of vdW radii of the atoms involved ($D_{\mathrm{H-H}}$=1.610 Å, $D_{\mathrm{I-I}}$=4.176 Å), the distance for R_1 to reproduce the ratio 1.673 was estimated as $D_{\mathrm{H-I}}$=4.700 Å, which was larger than the sum of vdW radii for R_1 (2.893 Å). Specifically for the estimation, the average $\langle N_{\mathrm{cand}}^{\mathrm{R}_1} \rangle$ and $\langle N_{\mathrm{cand}}^{\mathrm{R}_2} \rangle$ were calculated with the criterial distance(s) $D_{\mathrm{H-I}}$ for H_2-I_2 system, and $D_{\mathrm{H-H}}$ and $D_{\mathrm{I-I}}$ for HI system, respectively, adjusting $D_{\mathrm{H-I}}$ to satisfy Eq. (5.14).

Thus, the chemical reaction process for the present H_2-I_2 system is simulated appropriately by using the relative weights w^{R_1} and w^{R_2} expressed by Eq. (5.1), i.e., $w^{\mathrm{R}_1} = N_{\mathrm{cand}}^{\mathrm{R}_1} \exp\left(-\beta \Delta E_{\mathrm{a}}^{\mathrm{R}_1}\right)$ and $w^{\mathrm{R}_2} = N_{\mathrm{cand}}^{\mathrm{R}_2} \exp\left(-\beta \Delta E_{\mathrm{a}}^{\mathrm{R}_2}\right)$, taking account of the collisions involving in reaction occurrence. The application of the criterial distance discussed here would mean to introduce a "reactive radius", which is similar to a reactive cross-section, i.e., the area for the chemical reaction to occur in collision and one of the components of the frequency factor *A* in collision theory [1-3].

5.3.3. Computational Details

All the MD simulations were executed by the SANDER module of AMBER 9 [25] under the periodic boundary condition in the NVT ensemble (constant volume and

temperature). The system temperature was controlled by the Berendsen thermostat [26]. The equations of motion were numerically solved using the velocity Verlet algorithm with a time step 1.0 fs. The particle-mesh Ewald (PME) method [27] was adapted to treat long-range electrostatic interactions. All covalent bonds were constrained at the equilibrium lengths by the SHAKE method [28].

The hybrid MC/MD reaction algorithm was implemented into some modules in the AMBER 9 program. The MD simulation time to search for a candidate pair for chemical reaction (in step 2-(ii) in subsection 5.2.1) in one MC/MD cycle, was set to 1 ps. On the other hand, the MD simulation time for relaxation in one MC/MD cycle for a trial of chemical reaction (in step 2-(iii) in subsection 5.2.1), was set to 5 ps. The temperature during MD simulations was kept at 300 K, 500 K and 700 K using different structures in order to reproduce the temperature dependence on equilibrium constant, which corresponds to the experimental conditions [3]. The total MC/MD cycles was 6000 ns and enough to reach equilibrium states for the present system. I used the heats of formation for the correction in Eq. (5.5), $\Delta U_0^{\mathrm{reac}}\left(=\Delta E_{\mathrm{a}}^{\mathrm{b}}-\Delta E_{\mathrm{a}}^{\mathrm{f}}=\Delta E_{\mathrm{a}}^{\mathrm{R_2}}-\Delta E_{\mathrm{a}}^{\mathrm{R_1}}\right)$ = 2.93 kcal/mol, obtained by Arrhenius plot (see subsection 5.3.2).

5.4. Results and Discussion

5.4.1. Reproduction of Equilibrium States with the Effective Treatment

In Figure 5.2(a), shown are the normalized concentrations of H_2 and HI by the initial concentration of H_2 obtained by the hybrid MC/MD reaction simulation at 500 K

as a function of the MC/MD cycle. The curves were obtained as the averages of the simulation results from ten different initial structures, and the curve of I_2 was not shown because it should show the same change as that of H_2. It was found the normalized concentration $[H_2]/[H_2]_0$ increased drastically by ~500 MC/MD cycles. Thereafter, its instantaneous rate of change became small gradually, and, later from ~2000 MC/MD cycles, $[H_2]/[H_2]_0$ fluctuated around a certain value. On the other hand, as the reaction formula of Eq. (5.4) shows, since a pair of one H_2 and one I_2 molecule turn to two HI ones, it was observed that the amount of change of $[HI]/[H_2]_0$ was twice that of $[H_2]/[H_2]_0$. In both cases of H_2 and HI, the observed convergences mean that the rates of the forward and backward reactions became equal in the MC/MD cycles. Accordingly, these facts indicate that the hybrid MC/MD reaction method works sufficiently well to simulate the chemical reaction process for the present H_2-I_2 system.

In Table 5.2, shown are the calculated equilibrium concentration of H_2, $[H_2]_{eq}(=[I_2]_{eq})$, and the equilibrium constants K_{eq} at each temperature 300 K, 500 K and 700 K with their corresponding experimental values [3]. It can be recognized that in Figure 5.2(a) the present systems reached its equilibrium state sufficiently after at least 4001 MC/MD cycle (the curves at 300 K and 700 K are not shown), so that $[H_2]_{eq}$s at all the temperatures were estimated by averaging $[H_2]$ from 4001 to 6000 MC/MD cycles over ten sample model systems. From the results, it was found that $[H_2]_{eq}$ at all the temperatures showed very good agreement with the experimental ones. Furthermore, K_{eq} estimated by the ratio $[HI]_{eq}{}^2/[H_2]_{eq}[I_2]_{eq}$ also sufficiently corresponded to the experimental ones, indicating that the temperature dependence of K_{eq} was reproduced by the present simulations.

It is considered, therefore, that such favorable results were brought about by the present effective treatment of the collision frequencies of reactants (H_2 and I_2 molecules) and products (HI molecules) (discussed in subsection 5.3.2).

5.4.2. Application of Time Interpretation of MC/MD Cycle

For an application of the present theoretical treatment, I denote each elementary reaction in the reaction formula of Eq. (5.4) separately as follows,

$$\begin{cases} \mathrm{R}_1: & \mathrm{H}_2 + \mathrm{I}_2 \xrightarrow{k^{\mathrm{R}_1}} 2\mathrm{HI} \\ \mathrm{R}_2: & 2\mathrm{HI} \xrightarrow{k^{\mathrm{R}_2}} \mathrm{H}_2 + \mathrm{I}_2 \end{cases}, \tag{5.15}$$

where k^{R_1} and k^{R_2} are the rate constants for the elementary reactions R_1 and R_2, respectively. According to the experimental results [3], their numerical values are 2.04×10^{-19} and 2.24×10^{-22} at 300 K, 2.14×10^{-7} and 1.66×10^{-9} at 500 K, and 3.02×10^{-2} and 5.50×10^{-4} at 700K, where the unit is $(\mathrm{mol/L})^{-1}\cdot\mathrm{s}^{-1}$, respectively.

As for the component H_2, the rate law is expressed by

$$\frac{\mathrm{d}[\mathrm{H}_2]}{\mathrm{d}t} = \frac{\mathrm{d}[\mathrm{H}_2^{\mathrm{R}_1}]}{\mathrm{d}t} + \frac{\mathrm{d}[\mathrm{H}_2^{\mathrm{R}_2}]}{\mathrm{d}t} = -k^{\mathrm{R}_1}[\mathrm{H}_2][\mathrm{I}_2] + k^{\mathrm{R}_2}[\mathrm{HI}]^2 . \tag{5.16}$$

As shown in Eq. (5.7), one can solve the equation for an infinitesimal time dt, and then it can be described as the difference equation with the differential time Δt_{H_2} for H_2,

$$\Delta t_{\mathrm{H}_2} = \frac{\Delta[\mathrm{H}_2]}{k^{\mathrm{R}_2}[\mathrm{HI}]^2 - k^{\mathrm{R}_1}[\mathrm{H}_2][\mathrm{I}_2]} . \tag{5.17}$$

Then, the average concentrations over ten sample model systems at the kth MC/MD cycle, $\langle[\mathrm{H}_2]_k\rangle$, $\langle[\mathrm{I}_2]_k\rangle$ and $\langle[\mathrm{HI}]_k\rangle$, and the average differential concentration of H_2 between the kth and k-1th MC/MD cycles, $\Delta\langle[\mathrm{H}_2]_k\rangle (= \langle[\mathrm{H}_2]_k\rangle - \langle[\mathrm{H}_2]_{k-1}\rangle)$, are

substituted for their corresponding variables in Eq.(5.17). Thereby, as shown in Eq. (5.8), the differential time between the *k*th and *k*-1th MC/MD cycles, $\Delta t_{\mathrm{H}_2,k}$, is obtained as

$$\Delta t_{\mathrm{H}_2,k} = \frac{\Delta\langle[\mathrm{H}_2]_k\rangle}{k^{\mathrm{R}_2}\langle[\mathrm{HI}]_k\rangle^2 - k^{\mathrm{R}_1}\langle[\mathrm{H}_2]_k\rangle\langle[\mathrm{I}_2]_k\rangle}. \tag{5.18}$$

In Figure 5.2(a), since $[\mathrm{H}_2]$ decreased almost monotonously to reach $[\mathrm{H}_2]_{\mathrm{eq}}$ with fluctuation owing to the statistically insufficient sampling, the average concentration changes of all the components were drawn by the fitting functions. (The fitting functions for all the components are shown at all the temperatures in APPENDIX A.) The curves of their functions, the fitted $[\mathrm{H}_2]/[\mathrm{H}_2]_0$ and the fitted $[\mathrm{HI}]/[\mathrm{H}_2]_0$, are shown in Figure 5.2(a) in which the curve of the function, fitted $[\mathrm{I}_2]/[\mathrm{H}_2]_0$, is not shown due to the same one of $[\mathrm{H}_2]$. With the concentrations obtained by their fitting functions and Eq. (5.18), the time *t* over the changes in the concentration of H_2 is estimated by summing $\Delta t_{\mathrm{H}_2,k}$ over the MC/MD cycle, i.e., Eq. (5.9). Then, since the relaxation process of the concentration of H_2 corresponds to the overall equilibration process for the system, its change depending on *t* shows the relaxation process for the system to reach the equilibrium state from the initial nonequilibrium one.

In Figure 5.2(b), shown are the normalized concentration changes obtained by the fitted $[\mathrm{H}_2]/[\mathrm{H}_2]_0$ and the fitted $[\mathrm{HI}]/[\mathrm{H}_2]_0$ as functions of the time *t* instead of the MC/MD cycle, and their analytically calculated ones described by

$$t = a\ln\frac{b\left(c-1+[\mathrm{H}_2]/[\mathrm{H}_2]_0\right)}{\left(b-1+[\mathrm{H}_2]/[\mathrm{H}_2]_0\right)c} = a\ln\frac{b\left(c-[\mathrm{HI}]/[\mathrm{H}_2]_0\right)}{\left(b-[\mathrm{HI}]/[\mathrm{H}_2]_0\right)c}, \tag{5.19a}$$

where

$$a=\frac{1}{2\sqrt{k^{\mathrm{R}_1}k^{\mathrm{R}_2}}}, b=1-[\mathrm{H}_2]_{\mathrm{eq}}/[\mathrm{H}_2]_0, c=1+[\mathrm{H}_2]_{\mathrm{eq}}/[\mathrm{H}_2]_0+2/\left(K_{\mathrm{eq}}-1\right). \tag{5.19b}$$

From these results, it was recognized that the normalized concentration changes of H_2 and HI with t are numerically accurate because they coincide enough with analytical ones. Actually, the half-lives τ's of $[H_2]$ at 300 K, 500 K and 700 K could be estimated by Eq. (5.10) as ~1.0×10^{17} h, ~9.8×10^{4} h and ~6.9×10^{-1} h, respectively, which reproduce well the analytic values (~1.0×10^{17} h at 300 K, ~9.8×10^{4} h at 500 K and ~7.0×10^{-1} h at 700 K). It can be concluded, therefore, that the present theoretical treatment is sufficiently valid to translate an MC/MD cycle as an effective time, and thus could provide the time-dependent information of structural change at the atomistic level.

5.5. Concluding Remarks

In this chapter, I proposed a theory to interpret the chemical reaction process along the MC/MD cycle base in the hybrid MC/MD reaction method as the process along the time axis. For its first application, I treated a gas reaction system in which the reversible second-order reaction $H_2+I_2\rightleftharpoons2HI$ occurs. Towards analyzing time evolution of the system, the chemical reaction process was atomistically simulated by the present method from the initial states consisting of a mixture of H_2 and I_2 molecules at 300 K, 500 K and 700 K. In order to reproduce the chemical equilibrium for the system, it was assumed that the collision frequencies for the reactions should be taken into consideration in the theoretical treatment. Therefore, with the experimental values of the frequency factors [3], the criterial distances for both forward and backward reactions were adjusted, so that the relative weights of the reactions correspond to the actual relative reaction rates in chemical equilibrium. As a result, the calculated equilibrium concentrations $[H_2]_{eq}$ and equilibrium constants K_{eq} at all the temperatures were in good agreements with their corresponding experimental values [3]. It was shown, therefore,

that the present method is sufficiently applicable to the gas reaction system. In addition, such criterial distances can be regarded as “reactive radius” similar to the reactive cross section, which is the area for the chemical reaction to occur in collision and one of the components of the frequency factor *A* in collision theory [1-3].

In the present method, a series of elementary reactions (or elementary steps), i.e., chemical reaction processes, can be treated by a cycle of computational procedure consisting of several steps, as the MC/MD cycle [13-16]. To analyze time evolution for the chemical reaction processes, I proposed the theoretical treatment to estimate a change in time corresponding to a change in a concentration obtained by the present simulation. With the concentrations of H_2, I_2 and HI components at each MC/MD cycle and the rate law that shows the instantaneous rate of consumption of H_2, the time was numerically estimated as a function of the MC/MD cycle. As a result, the concentration changes of H_2 and HI were successfully obtained as time evolution with the atomistic information of the whole system. It is concluded, therefore, that the present theoretical treatment becomes a useful methodology to interpret the chemical reaction process of the hybrid MC/MD reaction method as a virtual realistic dynamic process depending on the time.

In fact, for demonstration, I have shown the application of the present theoretical treatment to the H_2-I_2 gas reaction system. However, if only the rate constant(s) of an assumed reaction mechanism for some combination of chemical components can be set up by the experiments or theoretical calculations, the theoretical treatment would be applied not only in gas phase but also in other phases. Thus, by applying the theoretical treatment to such systems, the time evolution of coupled chemical reactions would make it possible to understand an instantaneous state of the whole system at the atomistic level

in accordance with the reaction progress. In real applications, it is useful to reveal any unknown reaction mechanism by comparing our calculated results in the assumed reaction mechanism, e.g., half-life τ, with their experimental ones. Furthermore, for the synthetic process, such temporal and structural information would provide some guiding principles in designing catalysts, e.g., the mutation of the active site, and optimizing their selection, leading to improve the yield of an important component.

References

[1] R. H. Petrucci, W. S. Harwood, G. E. Herring, J. Madura, GENERAL CHEMISTRY: Principles and Modern Application, 9th ed.; Prentice-Hall, Inc.: New Jersey, 2006.

[2] P. Atkins, J. de Paula, Atkins' Physical Chemistry, 9th ed.; Oxford University Press: Oxford, 2009.

[3] W. J. Moore, BASIC PHYSICAL CHEMISTRY; Prentice-Hall, Inc.: New Jersey, 1983.

[4] A. V. Hesketh, S. Nowicki, K. Baxter, R. L. Stoddard, J. S. McIndoe, Organometallics 34 (2015) 3816.

[5] T. Friščić, I. Halasz, P. J. Beldon, A. M. Belenguer, F. Adams, S. A. J. Kimber, V. Honkimäki, R. E. Dinnebier, Nat. Chem. 5 (2013) 66.

[6] G. X. Chen, C. F. Xu, X. Q. Huang, J. Y. Ye, L. Gu, G. Li, Z. C. Tang, B. H. Wu, H. Y. Yang, Z. P. Zhao, Z. Y. Zhou, G. Fu, N. F. Zheng, Nat. Mater. 16 (2016) 564.

[7] E. Harder, D. E. Walters, Y. D. Bodnar, R. S. Faibish, B. Roux, J. Phys. Chem. B 113 (2009) 10177.

[8] Y. Luo, E. Harder, R. S. Faibish, B. Roux, J. Membr. Sci. 384 (2011) 1.

[9] Z. E. Hughes, J. D. J. Gale, Mater. Chem. 20 (2010) 7788.

[10] Z. E. Hughes, J. D. J. Gale, Mater. Chem. 22 (2012) 175.

[11] H. Ebro, Y. M. Kim, J. H. J. Kim, Membr. Sci. 438 (2013) 112.

[12] K. Moorthi, K. Kamio, J. Ramos, D. N. Theodorou, AIP Conf. Proc. 1518 (2013) 455.

[13] M. Nagaoka, Y. Suzuki, T. Okamoto, N. Takenaka, Chem. Phys. Lett. 583 (2013) 80.

[14] Y. Suzuki, Y. Koyano, M. Nagaoka, J. Phys. Chem. B 119 (2015) 6776.

[15] N. Takenaka, Y. Suzuki, H. Sakai, M. Nagaoka, J. Phys. Chem. C 118 (2014) 10874.

[16] N. Takenaka, H. Sakai, Y. Suzuki, P. Uppula, M. Nagaoka, J. Phys. Chem. C 119 (2015) 18046.

[17] J. Tomasi, M. Persico, Chem. Rev. 94 (1994) 2027.

[18] N. Okuyama-Yoshida, M. Nagaoka, T. Yamabe, Int. J. Quantum Chem. 70 (1998) 95.

[19] M. Nagaoka, N. Okuyama-Yoshida, T. Yamabe, J. Phys. Chem. A 102 (1998) 8202.

[20] M. P. Allen, D. Tildsley, J. Computer Simulation of Liquids; Clarendon Press: Oxford, 1987.

[21] D. W. Heerman, Computer Simulation Methods in Theoretical Physics, 2nd ed.; Springer: Berlin, 1990.

[22] N. Metropolis, A. W. Rosenbluth, M. N. Rosenbluth, A. H. Teller, E. J. Teller, Chem. Phys. 21 (1953) 1087.

[23] E. Wilhelm, R. Battino, Chem. Phys. 55 (1971) 4012.

[24] J. Vrabec, J. Stoll, H. Hasse, J. Phys. Chem. B 105 (2001) 12126.

[25] D. A. Case et al., AMBER 9, University of California, San Francisco, 2006.

[26] H. J. C. Berendsen, J. P. M. Postma, W. F. van Gunsteren, A. DiNola, J. R. Haak, J. Chem. Phys. 81 (1984) 3684.

[27] T. Darden, D. York, Pedersen, Chem. Phys. 98 (1993) 10089.

[28] J. P. Ryckaert, G. Ciccotti, H. J. C. Berendsen, J. Comput. Phys. 23 (1997) 327.

FIGURES

(a)

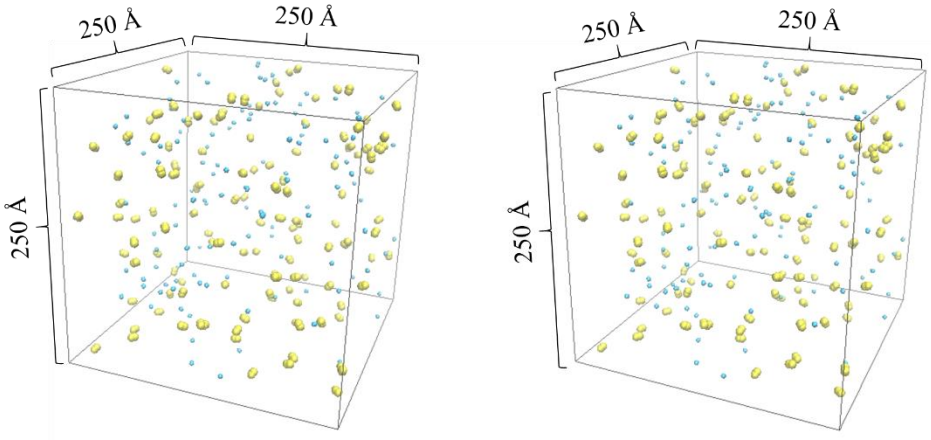

(b)

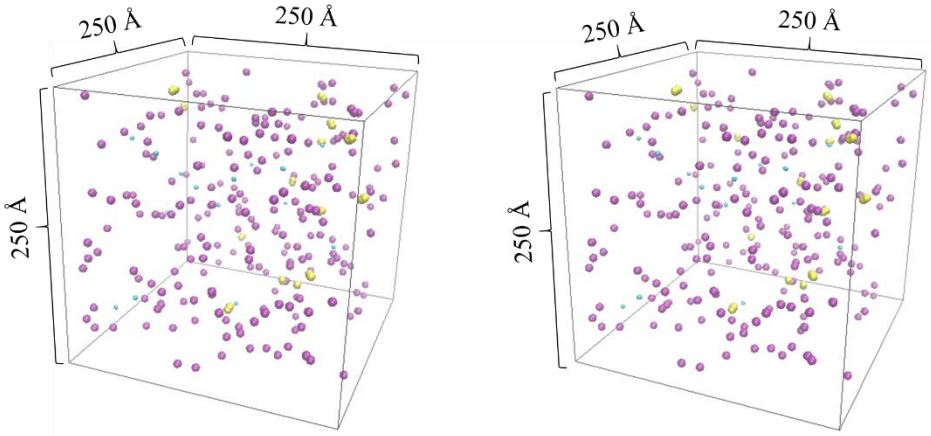

Figure 5.1. Side-by-side stereoview snapshots of the typical structures at (a) initial and (b) final states in gas phase (cyan, molecular hydrogen; yellow, molecular iodide; purple, hydrogen iodide molecule).

(a)

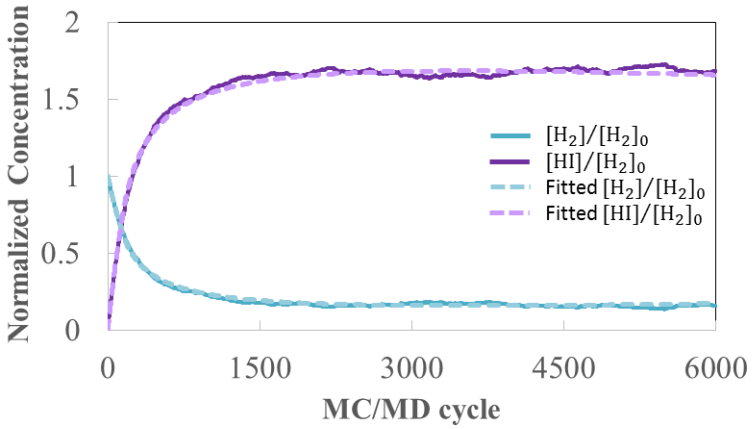

(b)

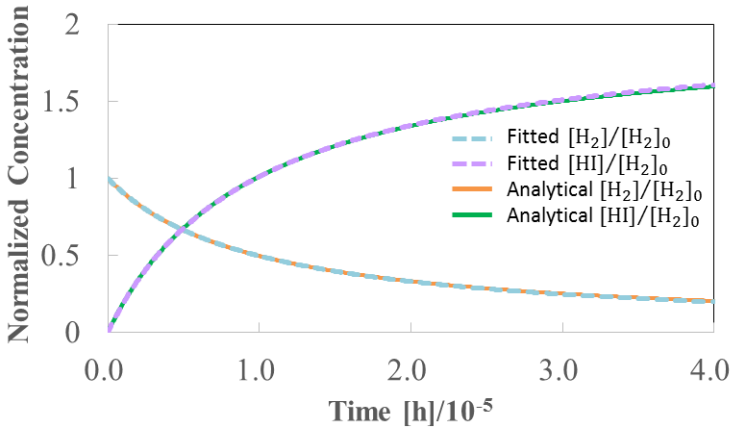

Figure 5.2. (a) Normalized concentrations of H_2 and HI relative to the initial concentration of H_2, obtained by the averages of the simulation results from 10 different initial structures at temperature 500K ($[H_2]/[H_2]_0$ and $[HI]/[H_2]_0$ are drawn by sky blue and purple solid lines, respectively), and their fitted ones as a function of the MC/MD cycle (drawn by washy sky blue and purple dash lines, respectively), (b) the fitted concentrations of H_2 and HI and their analytically estimated ones (shown as green and orange solid lines, respectively) as functions of the time. The present and analytical results were obtained under the condition of the temperature 500 K.

TABLES

Table 5.1. Concentrations of the component A among all the components with respect to the sample number and MC/MD cycle, and the sets of $\langle[\mathrm{A}]_k\rangle$, $\Delta[\mathrm{A}]_k$, $\Delta t_{\mathrm{A},k}$ and time *t*.

		MC/MD Cycle									
		0	1	…	k-1	k	…	N_τ	…	N_{eq}	…
Sample Number	S_1	$[\mathrm{A}]_0^{\mathrm{S}_1}$	$[\mathrm{A}]_1^{\mathrm{S}_1}$	…	$[\mathrm{A}]_{k-1}^{\mathrm{S}_1}$	$[\mathrm{A}]_k^{\mathrm{S}_1}$			…		
	S_2	$[\mathrm{A}]_0^{\mathrm{S}_2}$	$[\mathrm{A}]_1^{\mathrm{S}_2}$	…	$[\mathrm{A}]_{k-1}^{\mathrm{S}_2}$	$[\mathrm{A}]_k^{\mathrm{S}_2}$			…		
	⋮	⋮	⋮	…	⋮	⋮			…		
	S_i	$[\mathrm{A}]_0^{\mathrm{S}_i}$	$[\mathrm{A}]_1^{\mathrm{S}_i}$	…	$[\mathrm{A}]_{k-1}^{\mathrm{S}_i}$ [a]	$[\mathrm{A}]_k^{\mathrm{S}_i}$ [a]			…		
	⋮	⋮	⋮	…	⋮	⋮			…		
$\{\langle[\mathrm{A}]_k\rangle\}$ [b]		$\langle[\mathrm{A}]_0\rangle$	$\langle[\mathrm{A}]_1\rangle$	…	$\langle[\mathrm{A}]_{k-1}\rangle$	$\langle[\mathrm{A}]_k\rangle$	…	$\langle[\mathrm{A}]_{N_\tau}\rangle$	…	$\langle[\mathrm{A}]_{N_{\mathrm{eq}}}\rangle$	…
$\{\Delta\langle[\mathrm{A}]_k\rangle\}$ [c]			$\Delta\langle[\mathrm{A}]_1\rangle$	…		$\Delta\langle[\mathrm{A}]_k\rangle$	…	$\Delta\langle[\mathrm{A}]_{N_\tau}\rangle$	…	$\Delta\langle[\mathrm{A}]_{N_{\mathrm{eq}}}\rangle$	…
$\{\Delta t_{\mathrm{A},k}\}$ [d]			$\Delta t_{\mathrm{A},1}$	…		$\Delta t_{\mathrm{A},k}$	…	$\Delta t_{\mathrm{A},N_\tau}$	…	$\Delta t_{\mathrm{A},N_{\mathrm{eq}}}$	
t [e]		0	$\sum_{j=1}^{1}\Delta t_{\mathrm{A},j}$	…	$\sum_{j=1}^{k-1}\Delta t_{\mathrm{A},j}$	$\sum_{j=1}^{k}\Delta t_{\mathrm{A},j}$	…	$\tau\left(=\sum_{j=1}^{N_\tau}\Delta t_{\mathrm{A},j}\right)$	…	$t_{\mathrm{eq}}\left(=\sum_{j=1}^{N_{\mathrm{eq}}}\Delta t_{\mathrm{A},j}\right)$	

[a]Concentrations of the component A for the sample number S_i at the *k*-1th and *k*th MC/MD cycle. [b]The set of the average concentrations of A over all the samples at the *k*th MC/MD cycle. [c]The set of the differential concentrations of A by the difference of $\langle[\mathrm{A}]_k\rangle - \langle[\mathrm{A}]_{k-1}\rangle$. [d]The differential time for A between the *k*th and the *k*-1th MC/MD cycles shown in Eq. (5.8). [e]The time by the sum of $\Delta t_{\mathrm{A},k}$ over the MC/MD cycles shown in Eq. (5.9) and (5.10).

Table 5.2. The calculated values of the equilibrium concentration of H_2 and the equilibrium constants, and their corresponding experimental values.

	$[H_2]_{eq}$ /10^3 [molL^{-1}]		K_{eq}	
Temperature	calc. [a]	exp. [b]	calc. [a]	exp. [b]
300 K	0.86	0.83	834.0	912.0
500 K	1.93	1.99	119.6	129.0
700 K	2.80	2.82	56.0	54.9

[a]The calculated results at each temperature were obtained as the averages of ten sample model systems. [b]Experimental values from ref 3.

APPENDIX A: FITTING FUNCTIONS

The fitting functions $f_{H_2}(k)$ for the average concentration changes of the component H_2 using a variable *k* (denotes MC/MD cycle) are shown at (i) 300 K, (ii) 500 K and (iii) 700 K, respectively, as follows:

(i) 300 K

$$f_{H_2}(k) = \begin{cases} 1.001 - 3.598\times10^{-3}k + 6.290\times10^{-6}k^2 \\ (1 \le k \le 230) \end{cases} \quad \text{(A1.1)}$$

$$\begin{cases} 1.000 - 3.834\times10^{-1}\log(k/50) + 3.915\times10^{-2}\left(\log(k/50)\right)^2 \\ (231 \le k \le 6000) \end{cases}, \quad \text{(A1.2)}$$

(ii) 500 K

$$f_{H_2}(k) = \begin{cases} 1.000 - 3.112\times10^{-3}k + 4.219\times10^{-6}k^2 \\ (1 \le k \le 124) \end{cases} \quad \text{(A2.1)}$$

$$\begin{cases} 1.000 - 3.956\times10^{-1}\log(k/50) + 4.650\times10^{-2}\left(\log(k/50)\right)^2 \\ (125 \le k \le 6000) \end{cases}, \quad \text{(A2.2)}$$

and, (iii) 700 K

$$f_{H_2}(k) = \begin{cases} 1.000 - 3.358\times10^{-3}k + 5.359\times10^{-6}k^2 \\ (1 \le k \le 252) \end{cases} \quad \text{(A3.1)}$$

$$\begin{cases} 1.000 - 3.914\times10^{-1}\log(k/50) + 4.878\times10^{-2}\left(\log(k/50)\right)^2 \\ (253 \le k \le 6000) \end{cases}. \quad \text{(A3.2)}$$

Note that the fitting functions, $f_{I_2}(k)$ and $f_{HI}(k)$, of the components, I_2 and HI, are not shown at all the temperature because they can be described by the following expressions, $f_{I_2}(k) = f_{H_2}(k)$ and $f_{HI}(k) = 2\left(1 - f_{H_2}(k)\right)$.

Chapter 6

General Conclusion

In this thesis, I have aimed to computationally clarify chemical phenomena in complex chemical reaction systems at the atomistic level. For the purpose, I have proposed a new molecular simulation method, the hybrid MC/MD reaction method, that consists of a couple of MC and MD techniques. I would expect this method should play a significant role of a practical 'atomistic' simulation technique in order to treat complex chemical reaction systems.

In chapter 2, first I have shown the hybrid MC/MD reaction method in detail. The MC treatment stochastically manages such a rare event as activated processes of chemical reaction, whereas the MD one simply executes a common dynamical process in stable phase spaces for naturally searching candidate molecular configurations for reaction occurrence. Next, for the first application, I treated the 2-chlorobutane racemization in DMF solution. Actually, from the optical pure state (100% e.e.) of (*R*)-2chlorobutane molecules, this method succeeded in realizing a state with ~0% e.e. that is the expected purity of (*R*)- to (*S*)-enantiomers of the racemic mixture in chemical equilibrium. Thus, the hybrid MC/MD reaction method was shown to effectively promote the chemical reaction progress and to be useful in discussing its resulting chemical properties such as aggregation structures in chemical reaction systems and their stereo-chemistry.

In chapter 3, I next applied the hybrid MC/MD reaction method to the reverse osmosis membrane, called FT-30, an aromatic polyamide system that is very useful for the purpose of industrial applications and investigated the microscopic property of FT-

30. In the experiments, the polymer membrane FT-30 is synthesized by interfacial polycondensation (IP) reaction between *m*-phenylenediamine (MPD) and 1,3,5-tricarboxylyc acid chloride (TMC) monomers. For application of the hybrid MC/MD reaction method to polymer systems, its programmatic installation was modified to allow intercellular chemical bonds stretching over the periodic boundaries, i.e., minimum bond convention (MBC) method. Then, four bulk membrane models with different four MPD/TMC mixing ratios (1:4, 1:1, 3:2 and 4:1) were reasonably prepared from the four corresponding monomers assemblies, simulating a succession of condensation reactions. From the membrane models thus obtained, the degrees of polymer cross-linking (DPC) and the composition ratios of its constituent atoms were calculated. As a result, it was found the MPD/TMC mixing ratios in the near-surface active (NSA) and interior active (IA) regions associate with the reaction mechanism of IP. Further, water diffusion simulations using the membrane model of the IA region were executed. It was shown that the calculated values of the total mass density of the hydrated membrane and the partition coefficient K are in good agreement with the experimental ones. In conclusion, it can be said that the model polyamide membranes obtained computationally by the hybrid MC/MD reaction method, have sufficient fidelity to the actual membrane.

In chapter 4, third I applied the hybrid MC/MD reaction method to the solid electrolyte interphase (SEI) film formed on the anode surfaces in the lithium ion batteries (LIBs). Since the current performance of LIB with liquid electrolytes, e.g., ethylene carbonate (EC) and propylene carbonate (PC), depends strongly on a stability of the SEI films, I investigated their microscopic structures with the present method. Actually, I was able to demonstrate the formation processes and make the full atomistic

models of the SEI films from the EC or PC-based electrolytes with the graphite anode, stochastically treating some assumed elementary reactions. Further, both the SEI film models were found to reproduce successfully a number of structural characteristics reported experimentally, keeping the atomistic spatial heterogeneity. In addition, it was also clarified theoretically, for the first time, that the EC-based SEI film can play a role to protect the electrolyte from the excess reduction on the graphite surface. At the same time, the EC-based SEI film has dense property but some connective cavities which sufficient size for passing of Li cations. In contrast, the PC-Based SEI one showed sparser one, and is reasonably considered not to have the function for the protection of the electrolyte from reductive decomposition. This is because the presence of methyl groups of solvent PC molecules and their reaction products, which prevents the organic salts from their aggregation. It was concluded, from the microscopic view of point, that the long-term SEI film formation is highly influenced by such a small structural difference in solvent molecules.

Further, in chapter 5, I proposed a theory to translate as the time evolution such a stochastic process that is generated by the hybrid MC/MD reaction simulation. Then, I applied the theoretical method to the reversible second-order reaction $H_2+I_2 \rightleftharpoons 2HI$, a typical gaseous reaction. More specifically, in order to enable us to understand the atomistic progress of the hybrid MC/MD reaction simulation as the time evolution, I have proposed the theory to interpret “MC/MD cycle” as an effective time based on the chemical kinetics. The MC/MD cycle is a computational procedure consisting of several steps to generate chemical reaction occurrence. As a simple chemical reaction system, I have chosen the gas reaction system in which the reversible second-order reaction $H_2+I_2 \rightleftharpoons 2HI$ occurs. First, the progress of chemical reaction was simulated from the

configurational arrangement containing a number of H_2 and I_2 molecules, each at 300 K, 500 K and 700 K. To reproduce the chemical equilibrium for the system, the collision frequencies for the reactions were taken into consideration in the theoretical treatment. For that purpose, the criterial distances for both forward and backward reactions were adjusted for the relative weights of the reactions to correspond to the actual relative reaction rates in chemical equilibrium. Consequently, the calculated equilibrium concentrations $[H_2]_{eq}$ and equilibrium constants K_{eq} at all the temperatures agreed very well with their corresponding experimental values. Next, I applied the theoretical treatment for the time interpretation to the system, and have shown the calculated half-lives τ's of $[H_2]$ reproduce very well with the analytical ones at all the temperatures. It is, therefore, concluded that the application of the present theoretical treatment with the hybrid MC/MD reaction method makes it possible to analyze reasonably the time evolution of complex chemical reaction systems to chemical equilibrium at the atomistic level.

Finally, in this thesis, I proposed the hybrid MC/MD reaction method towards the realization of exploring rare events such as chemical reaction, diffusion in solids, rotation of polymer chain, etc., in chemical phenomena. However, I could only apply it to treat elementary reactions for some chemical reaction systems because of the difficulty of implementing its scheme. Accordingly, I have been still theoretically developing it and making its program to be capable of generating such all the rare events. As already mentioned, the method has a rare event-driving mechanism of our necessity. Thus, I have prepared an appropriate alternate name for the method, which is the "Red Moon" method (from Rare-Event Driving Mechanism Of Our Necessity). In future, I dream that my molecular simulation method would be well-known as the "Red Moon"

method and widely used to computationally clarify chemical phenomena by chemists all over the world. That gives me a great pleasure and is very meaningful especially for my study life.

Acknowledgements

This thesis is the summary of my researches in the Graduate School of Information Science, Nagoya University.

I would like to thank many people who supported me to complete this thesis by their invaluable assistance and discussions. First, I would like to express my deep gratitude to Prof. Masataka Nagaoka who gives me kind guidance and continuous encouragement for instructive discussions and initiation into the research publication. I would like to thank also Prof. Nobuaki Koga, Prof. Hedong Zhang, Prof. Satoru Iuchi and Prof. Koji Yasuda who instructed me in theories of electronic states and molecular dynamics. I gratefully acknowledge Dr. T. Yamazaki at Asahi Kasei Corporation for his fruitful discussion and helpful suggestion for the selection of appropriate polymer membrane from the industrial chemical standpoint. Further, I thank all of collaborators in Nagaoka's laboratory for their many important advices and discussions. Finally, I would like to thank my parents and brother for their "watching over" fondly and supporting me in my research life during the doctor's course.

This thesis was partially supported by a Grant-in-Aid for Scientific Research from the Ministry of Education, Culture, Sport, Science and Technology (MEXT) in Japan and also by the Core Research for Evolutional Science and Technology (CREST) "High Performance Computing for Multi-scale and Multi-physics Phenomena" and "Establishment of Molecular Technology towards the Creation of New Functions" from the Japan Science and Technology Agency (JST).

Publication List

1. Masataka Nagaoka, Yuichi Suzuki, Takuya Okamoto and Norio Takenaka, "A Hybrid MC/MD Reaction Method with Rare Event-driving Mechanism: Atomistic Realization of 2-Chlorobutane Racemization Process in DMF Solution", Chem. Phys. Lett. 524 (2013) 80.
DOI:10.1016/j.cplett.2013.08.017
(Chapter 2)

2. Yuichi Suzuki, Yoshiyuki Koyano and Masataka Nagaoka, "Influence of Monomer Mixing Ratio on Membrane Nanostructure in Interfacial Polycondensation: Application of Hybrid MC/MD Reaction Method with Minimum Bond Convention", J. Phys. Chem. B. 119 (2015) 6776.
DOI: 10.1021/jp512333h
(Chapter 3)

3. Norio Takenaka, Yuichi Suzuki, Hirofumi Sakai and Masataka Nagaoka, "On Electrolyte-Dependent Formation of Solid Electrolyte Interphase Film in Lithium-Ion Batteries: Strong Sensitivity to Small Structural Difference of Electrolyte Molecules", J. Phys. Chem. C. 118 (2014) 10874.
DOI: 10.1021/jp5018696
(Chapter 4)

4. Norio Takenaka, Hirofumi Sakai, Yuichi Suzuki, Purushotham Uppula and Masataka Nagaoka, "A Computational Chemical Insight into Microscopic Additive Effect on Solid Electrolyte Interphase Film Formation in Sodium-Ion Batteries: Suppression of Unstable Film Growth by Intact Fluoroethylene Carbonate", J. Phys. Chem. C. 119 (2015) 18046.
DOI: 10.1021/acs.jpcc.5b04206